

The University of Maine

DigitalCommons@UMaine

Electronic Theses and Dissertations

Fogler Library

Summer 8-7-2020

Fabrication of Silicon Microneedles for Dermal Interstitial Fluid Extraction in Human Subjects

Caleb A. Berry

University of Maine, caleb.a.berry@maine.edu

Follow this and additional works at: <https://digitalcommons.library.umaine.edu/etd>



Part of the [Biomedical Commons](#), [Biomedical Devices and Instrumentation Commons](#), [Chemical Engineering Commons](#), [Electronic Devices and Semiconductor Manufacturing Commons](#), and the [Semiconductor and Optical Materials Commons](#)

Recommended Citation

Berry, Caleb A., "Fabrication of Silicon Microneedles for Dermal Interstitial Fluid Extraction in Human Subjects" (2020). *Electronic Theses and Dissertations*. 3269.

<https://digitalcommons.library.umaine.edu/etd/3269>

This Open-Access Thesis is brought to you for free and open access by DigitalCommons@UMaine. It has been accepted for inclusion in Electronic Theses and Dissertations by an authorized administrator of DigitalCommons@UMaine. For more information, please contact um.library.technical.services@maine.edu.

**FABRICATION OF SILICON MICRONEEDLES
FOR DERMAL INTERSTITIAL FLUID EXTRACTION
IN HUMAN SUBJECTS**

By

Caleb A. Berry

B.S. University of Maine, 2017

A THESIS

Submitted in Partial Fulfillment of the

Requirements for the Degree of

Master of Science

(in Chemical Engineering)

Office of Graduate Studies

University of Maine

August 2020

Advisory Committee:

Rosemary L. Smith, PhD., Professor of Electrical Engineering, Advisor

Scott D. Collins, PhD., Professor of Chemistry.

M. Clayton Wheeler, PhD., Professor of Chemical Engineering.

The project depicted is sponsored by the Department of the Defense, Defense Threat Reduction Agency (Award no. HDTRA1-17-1-0021). The content of the information does not necessarily reflect the position or the policy of the federal government, and no official endorsement should be inferred.

**FABRICATION OF SILICON MICRONEEDLES
FOR DERMAL INTERSTITIAL FLUID EXTRACTION
IN HUMAN SUBJECTS**

By Caleb Berry

Thesis advisor: Dr. Rosemary Smith

An Abstract of the Thesis Presented
in Partial Fulfillment of the Requirements for the
Degree of Master of Science
(in Chemical Engineering)
August 2020

The goal of this project is to design and develop a fabrication process for silicon microneedle arrays to extract dermal interstitial fluid (ISF) from human skin. ISF is a cell-free, living tissue medium that is known to contain many of the same, clinical biomarkers of general health, stress response and immune status as in blood. However, a significant barrier to adoption of ISF as a diagnostic matrix is the lack of a rapid, minimally invasive method of access and collection for analysis. Microfabricated chips containing arrays of microneedles that can rapidly and painlessly access and collect dermal ISF for bioassay could greatly facilitate point-of-care diagnosis and health monitoring, especially in times of crisis or in austere environments, where drawing venous blood poses an unnecessary infection or biohazard risk.

Two different fabrication methods were explored. The first method borrows from a previously reported dicing saw process, where a series of parallel and perpendicular cuts of partial depth are made into a thicker silicon wafer, creating arrays of square columns, which are subsequently sharpened into needles. The second method uses a new, entirely-

DRIE process to create the arrays of columns. The columns are sharpened into needles using an isotropic wet etch method (HNA etch) which preferentially enhances etching at the tips and diminishes etching at the base, creating remarkably sharp, conical shaped needles capable of piercing skin. The needles contain holes that pass through the wafer to the opposite side, where they connect to a series of microfluidic channels that lead to a reservoir. The back of the wafer is bonded to glass, providing a hydrophilic cap to the channels, as well as a way to see into the device to detect whether the channels are filling with liquid. The fabrication procedures for both methods are presented, along with 2D- and 3D-rendered schematics for the final devices.

Needle geometric shape is crucial to their ability to extract ISF. To determine the appropriate pre-sharpened etched shape, needle columns with a variety of different shapes were designed, produced, sharpened, and examined under a scanning electron microscope. The most promising shapes were selected for further processing and testing. Resulting chips were first bench tested to ensure capillary filling capability, and then tested for ISF collection from human skin. Microneedle arrays which were successfully demonstrated to extract ISF are presented, and the unsuccessful shapes are also shown in the interest of completion. Potential means for improving performance and future research directions are discussed.

ACKNOWLEDGMENTS

First, I would like to thank my advisor and rock star scientist, Dr. Rosemary Smith. Thank you for taking me in as a master's student when I was just a 9th semester undergraduate who only stayed for that 9th semester because I didn't know what I wanted to do with my degree yet. Thank you for showing me the joys of microfabrication. Thank you for training, and mentoring me from near zero-experience to master's-level competency. Thank you for placing your faith in me, and for all your time. I hope to do great things with this knowledge, and make you proud.

Thank you, Dr. Collins for your patience in the lab, for always being there to show me a new procedure, or help me with some random equipment malfunction when I couldn't find the manual. Thank you for your immense knowledge, your sense of humor, and your Doors CD you left in the lab CD player.

I would also like to thank Mike Call for your many hours training me in the cleanroom and for tirelessly fixing equipment when it would go down.

Thank you to Dr. George Bernhardt for your safety and materials assistance.

Thank you to Tracy, for your help with purchase orders, shipping, paperwork, and your cheerful demeanor.

Thank you, Dr. Clay Wheeler, for your help in being my undergraduate advisor, and for serving on my graduate committee.

Thank you to my lab colleagues, Jon Bomar, Phaneendra Chennampally, Matt Moyet, Zachary Smith, and Mick Small for various trainings, assistance at conference presentations, and - most of all – camaraderie.

My wonderful friends – Alex & Sam, Fred & Dani & Vinny & the Riggs family, Jacob & Madison, Ryder, Powell, Lucas, Mikayla, Matt & Sasha, Danny, Jonny, Lucy. You've given me a lifetime worth of memories and I'm not even 25.

Lastly, my loving family – Mom and Dad, for raising me, and the tireless financial support throughout undergrad – my sister Cam, and my beautiful partner, Brittany.

I love you all.

TABLE OF CONTENTS

ACKNOWLEDGMENTS.....	iii
LIST OF TABLES.....	viii
LIST OF FIGURES.....	ix
LIST OF ABBREVIATIONS	xiii
CHAPTER 1 – INTRODUCTION	1
1.1 Motivation and background.....	1
1.2 Project goals.....	4
1.3 Thesis organization	4
CHAPTER 2 – SILICON MICRONEEDLES PRIOR ART	6
2.1 Pioneering work: 1990s	6
2.1.1 The Normann group – intracortical stimulation, 1991.....	6
2.1.2 The Prausnitz group – skin permeability for drug delivery, 1998.....	7
2.2 Microneedles for diagnostics.....	8
2.2.1 Wound potential.....	8
2.2.2 Blood glucose monitoring	8
2.2.3 Interstitial fluid (ISF) extraction	9
2.3 Other applications.....	10
2.3.1 Drug and vaccine delivery.....	10
CHAPTER 3 – DESIGN FEATURES	13
3.1 Design.....	13
3.1.1 DRIE column frames.....	14
3.2 Starting points.....	17
3.2.1 Needle spacing.....	17

3.2.2 Sharpening	19
3.2.3 Glass bonding.....	19
3.2.4 Capillary fill	19
3.3 Modifications and improvements.....	20
CHAPTER 4 – MICROFABRICATION METHODS & RESULTS	22
4.1 The backside: microchannels and reservoir.....	22
4.1.1 Microfluidic channel and reservoir fabrication	22
4.1.2 Anodic bonding to glass.....	25
4.2 The frontside: DRIE column fabrication	27
4.2.1 Needle shape	27
4.2.2 Testing a variety of shapes	29
4.2.3 The center slot problem	35
4.2.4 Success – a diagonal slot.....	37
4.3 The frontside: dicing saw fabricated columns	38
4.3.1 Design parameters.....	39
4.3.2 The in-house dicing saw.....	41
4.3.3 DISCO DAD 3240, Andover, MA.....	43
4.4 Dicing from wafer to individual chips	46
4.5 Microneedle sharpening and oxidation.....	46
4.5.1 Thinning	47
4.5.2 Sharpening	49
4.5.3 Oxidation.....	50
4.6 Cost analysis.....	50
CHAPTER 5 – TESTING METHODS & RESULTS.....	54

5.1 Water draw	54
5.2 ISF collection from human subjects.....	54
5.3 Depth of penetration	57
CHAPTER 6 – CONCLUSIONS & FUTURE WORK	59
6.1 Conclusions	59
6.2 Future considerations	60
References	62
APPENDIX A – COMPLETE FABRICATION PROCESS FLOW	66
A.1 Backside fabrication.....	66
A.2 Frontside fabrication, DRIE design.....	69
A.3 Frontside fabrication, dicing saw design	72
APPENDIX B – RECIPES	76
B.1 STS DRIE	76
B.2 HNA ETCH.....	76
B.2.1 Thinning	77
B.2.2 Sharpening.....	77
APPENDIX C – DEVICE FABRICATION SCHEMATIC	79
C.1 BACKSIDE FABRICATION, BOTH DESIGNS	79
C.2 DRIE COLUMN FABRICATION PROCESS.....	81
C.3 SAW COLUMN FABRICATION PROCESS	82
APPENDIX D – PHOTOMASKS.....	85
D.1 Backside: Channels, Mask #1.....	85
D.2 Backside: 30-micron holes, mask #2.....	86
D.3 Frontside – Saw: 10-micron holes, mask #3	87

D.4 Frontside – DRIE: columns, mask #4.....	87
D.5 Alignment marks.....	87
APPENDIX E – WAFER SPECIFICATIONS	89
APPENDIX F – EQUIPMENT	90
APPENDIX G – STOCK SOLUTIONS.....	91
G.1 Chemicals.....	91
G.2 Developers.....	91
G.3 Etchants	92
G.4 Photoresists	92
BIOGRAPHY OF THE AUTHOR	93

LIST OF TABLES

Table 3-1 – Design improvements	21
Table 4-1 – Two-step DRIE etch for microchannel and borehole fabrication	23
Table 4-2 – Process rates from a variety of universities	51
Table 4-3 – Cost analysis	52
Table 4-4 – Cost analysis, hypothetical 12-inch scaleup.....	52
Table 4-5 – Cost analysis, hypothetical 12-inch scaleup with 2x faster DRIE	52
Table E-1 – Dicing saw wafer specifications	89
Table E-2 – DRIE-only wafer specifications	89
Table E-3 – Extra-thick test wafer specifications	89
Table F-1 – Equipment	90
Table G-1 – Chemical Concentration Table	91

LIST OF FIGURES

Figure 1.1 – A basic timeline for infection ¹	1
Figure 1.2 – Composition of total body water in humans ²⁻⁴	2
Figure 1.3 – Anatomy of the layers of human skin. Dermal ISF is found in the dermis. ⁹	3
Figure 2.1 – Two of the first silicon microneedle designs published	8
Figure 2.2 – SEM micrographs of different needle shapes achieved with changing hole position.	9
Figure 2.3 – Gardeniers, et al. Wedged shaped microneedles fabricated with KOH etching. ¹¹	11
Figure 2.4 – Grisse & Stemme’s side-opened microneedles. ²⁸	12
Figure 3.1 – 3D CAD-rendered images of a single chip for both designs – DRIE (left) and dicing saw (right).....	13
Figure 3.2 – 3D CAD-rendered images of the backside of a single chip.	14
Figure 3.3 – SEM images of unsharpened columns for both designs – DRIE (left) and dicing saw (right).....	14
Figure 3.4 – SEM images of needles after sharpening for both designs – DRIE (left) and dicing saw (right).....	14
Figure 3.5 – Base undercut in the DRIE visualized.	16
Figure 3.6 – Small openings typically lead to etch termination.....	17
Figure 3.7 – Column tapering in the DRIE-fabricated columns is nearly eliminated with the inclusion of a frame around each column.	17
Figure 3.8 – The skin will stretch and deform around a single needle	18
Figure 3.9 – Each needle stretches the skin nearby it, preventing deformation and facilitating skin piercing.	19
Figure 3.10 – Placement of the borehole along a microchannel side-wall allows capillary forces to draw liquid into the channel.....	20
Figure 4.1 – The wafer backside features microfluidic channels for ISF transport, and is anodically bonded to glass containing a series of predrilled holes which are aligned to the reservoir of each chip	23

Figure 4.2 – 3D CAD images of a single chip, showing the microchannels and reservoir with the bonded glass layer.	23
Figure 4.3 – Image of a single chip, bonded to glass	27
Figure 4.4 – SEM images of needles whose tip-shape is not sufficient to extract ISF.....	28
Figure 4.5 – A hole was required to extract ISF from SAW-fabricated chips. ¹⁶	29
Figure 4.6 – The holes were unacceptably widened in the DRIE, if a two-step DRIE etch was used.	29
Figure 4.7 – 16 cropped optical microscope images showing a top-down view of all 16 column shapes tested	30
Figure 4.8 – Two SEM images showing column shapes for the test mask, pre-thinning and -sharpening	31
Figure 4.9 – SEM images showing some of the failed column shapes.	31
Figure 4.10 – Optical microscope image of colors produced by differing SiO ₂ film thickness mid-BOE etch	33
Figure 4.11 – Optical microscope images of undercutting seen with SiO ₂ etch.....	33
Figure 4.12 – Optical microscope images showing the degradation of the frame around the columns as the DRIE etch progresses.....	34
Figure 4.13 – Final SEM results show unacceptable levels of column undercut from DRIE.....	34
Figure 4.14 – Two SEM images showing the two successful-looking designs employed for further testing.....	34
Figure 4.15 – Two SEM images showing hole from backside, after sharpening.	35
Figure 4.16 – Different slot orientations.....	36
Figure 4.17 – SEM images of successful DRIE-fabricated devices.	37
Figure 4.18 – CAD-rendered images of the final DRIE chip.	38
Figure 4.19 – A dicing saw in action. Image courtesy of DISCO Corporation.	39
Figure 4.20 – the dicing saw cuts columns into the silicon surface with many equally-spaced parallel and perpendicular cuts.	40
Figure 4.21 – columns produced by dicing saw after removal of the field.....	41

Figure 4.22 – SEM images of the first attempt to fabricate columns with the dicing saw.....	42
Figure 4.23 – SEM images from a couple of the four salvageable chips from the run.....	43
Figure 4.24 – SEM images showing needle tips of Mukerjee 2004 (dubbed the “snake fang”) ¹³	43
Figure 4.25 – Columns showing proper placement of the 10 μ m hole, obtained using DISCO DAD3240.	44
Figure 4.26 – Results from the first round of sharpening of the DISCO-fabricated wafer.	45
Figure 4.27 – SEM image of sharp needles, which extract ISF.....	46
Figure 4.28 – Columns are thinned in a beaker of HNA.	48
Figure 4.29 – An example of what some columns look like mid-thinning.....	48
Figure 4.30 – Columns are sharpened in a beaker of HNA.	49
Figure 4.31 – Columns after sharpening for both designs – DRIE (left) and dicing-saw (right).	49
Figure 5.1 – Six still frames from a 24 fps video showing water filling the microfluidic channels.	54
Figure 5.2 – Top and bottom left: A chip being applied to a human hand.....	56
Figure 5.3 – Image results showing the needles’ penetration into the skin at (L to R) 0, 30, 50, and 100 microns.....	58
Figure 5.4 – Image results showing the needles’ penetration, after contrast stretching, into the skin at (L to R) 132, and 164 microns.	58
Figure B.1 – Curves of constant rate of change of die thickness (mils/min) as a function of etchant composition in the system 49% HF, 70% HNO ₃ and diluent. ³⁸	77
Figure B.2 – The thinning procedure utilizes an up/down motion of the chip and a stir bar to minimize the effects of diffusion.	77
Figure B.3 – The sharpening procedure is quiescent.....	78
Figure D.1 – The first mask level patterns the microchannels, reservoirs and first level alignment marks.	85
Figure D.2 – Closeup of a single chip, with a further closeup of some individual channels.....	86
Figure D.3 – closeup of microchannels, from Figure D.2.....	86

Figure D.4 – The 30-micron boreholes are aligned to the microchannels.	86
Figure D.5 – 10-micron holes.....	87
Figure D.6 – DRIE columns.....	87
Figure D.7 – Mask #1 alignment marks.....	87
Figure D.8 – Mask #2 aligns to marks left by mask #1.....	88
Figure D.9 – Mask #3 (saw only) aligns to marks left by mask #1	88
Figure D.10 – Mask #4 (DRIE only) aligns to marks left by mask #1	88

LIST OF ABBREVIATIONS

§ - section

°C – degrees Celsius

AcOH – acetic acid

BOE – buffered oxide etch

DI, DIW – deionized water

DRIE – deep-reactive ion etch

ECF – extracellular fluid

HCl – hydrochloric acid

HF – hydrofluoric acid

HNA – hydrofluoric/nitric/acetic acid, wet isotropic silicon etch

HNO₃ – nitric acid

ICF – intracellular fluid

IPA – isopropyl alcohol

ISF – interstitial fluid

MeOH – methanol

micron - micrometers

mL – milliliters

mm – millimeters

PECVD – plasma-enhanced chemical vapor deposition

resist – photoresist

SiO₂, SiO₂ – silicon dioxide

SEM – scanning electron microscope/microscopy

μL – microliters

μm – micrometers

CHAPTER 1 – INTRODUCTION

1.1 Motivation and background

Shown in Figure 1.1 is a basic timeline for infection. After exposure to a pathogen or infectious agent, there begins an incubation period, before one begins to show symptoms. This period can last anywhere from hours to years, depending on the agent. Without other tests, it is essentially impossible to conclude that a person has been infected before they show symptoms. Testing for the presence of antibodies or other biomarkers in blood is typically done to diagnose disease during incubation or even after the symptomatic period begins. However, blood drawing is invasive, opening the host up to additional infection risks, especially in non-sterile environments. Also, most on-site analysis methods require blood sample preparation, minimally to remove cells (plasma) and add anti-coagulant. In some austere environments, such as a military field setting, blood analysis can therefore be impractical or outright impossible. Although there have been recent advances in some continuous blood monitoring capabilities, e.g. glucose monitoring for diabetics, the extension to early indicators of exposure to infectious or toxic agents are still under investigation. Dermal interstitial fluid (ISF) has been proposed as a substitute analyte for blood, which may be accessed continuously or with high intermittent frequency in a minimally invasive manner. It is also a cell-free, non-clotting fluid, that eliminates or reduces pre-analysis processing.

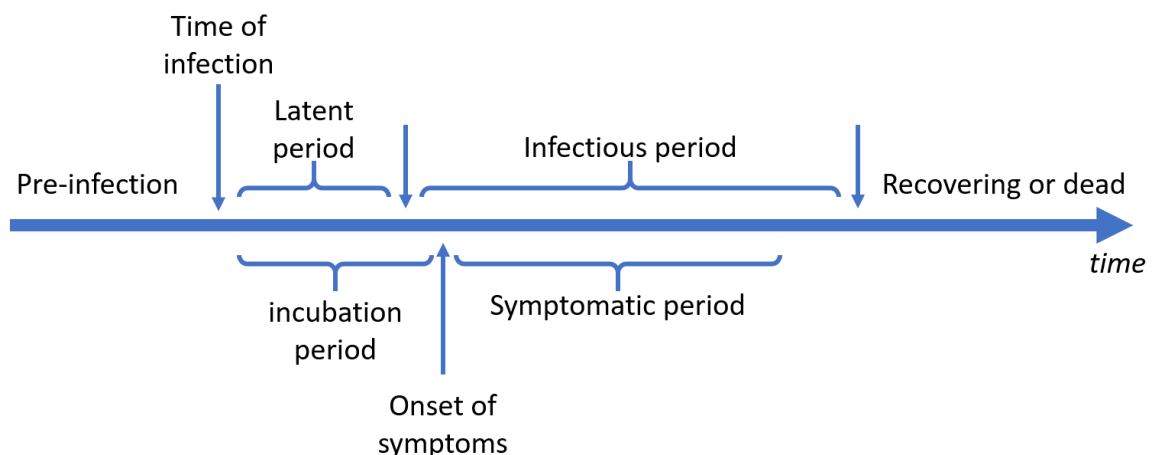


Figure 1.1 – A basic timeline for infection¹

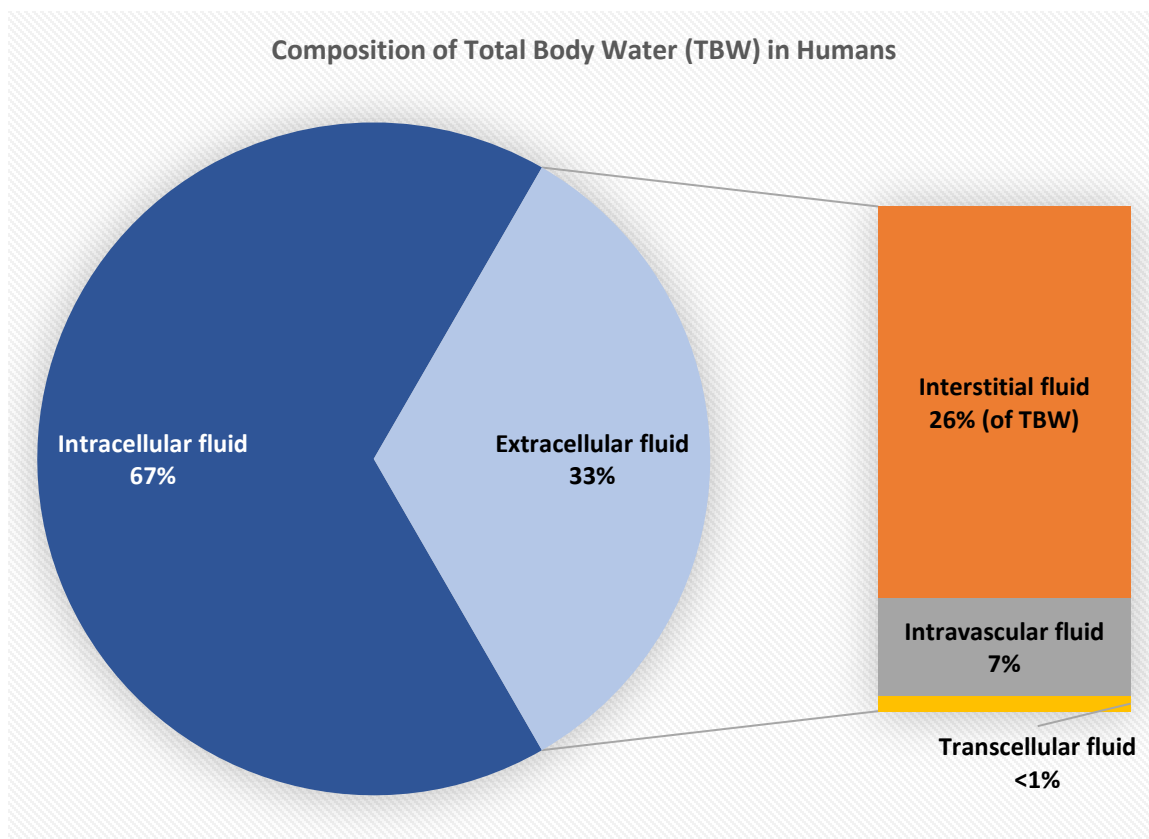


Figure 1.2 – Composition of total body water in humans²⁻⁴

The distribution of total body water (TBW) in humans (Figure 1.2) is divided into two main compartments: intracellular fluid (ICF), or all fluid inside cells, which makes up around two-thirds of body fluid; and extracellular fluid (ECF), all fluid outside the cells, comprising the remaining one-third.² ECF is further divided into subcomponents. Interstitial fluid (ISF) and intravascular fluid (blood plasma) compose at least 97% of the ECF (~33% TBW), of which lymph composes a small portion of ISF.³ The remaining approximately 2.5% of ECF (<1% TBW) includes the transcellular fluid: cerebrospinal fluid, aqueous humor, serous fluid, joint fluid, and others.⁴ ISF has recently been a target of interest as an alternative to blood, due to its comparability to blood plasma. Several reports have shown a high degree of overlap in protein, cytokine and metabolic molecule composition between ISF and blood serum.⁵⁻⁸ Nonetheless, a barrier of entry to adoption of ISF as a diagnostic matrix is the lack of a rapid, minimally invasive method of access and collection for analysis. Blisters provide the volume of fluid needed for investigative compositional analysis, but

they are a level greater than *minimally* invasive, and are not amenable to a wearable diagnostic device. Additionally, a blister is a wound, and therefore blister fluid may have a different composition compared to ISF residing in intact, normal skin.

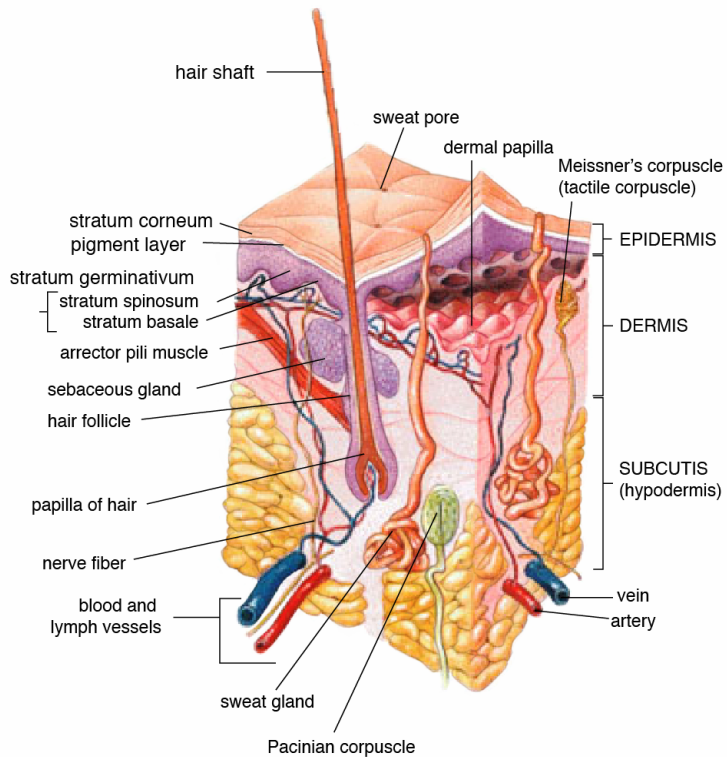


Figure 1.3 – Anatomy of the layers of human skin. Dermal ISF is found in the dermis.⁹

Enter microneedle arrays: minimally-invasive devices that can painlessly penetrate the skin's *stratum corneum*, the principal physical barrier, found in the epidermis, which separates what would be considered the body's inside and outside.¹⁰ Microneedle instruments have been the subject of a great deal of excitement and research for nearly three decades, having current and developing applications in minimally invasive transdermal drug and vaccine delivery, disease diagnostics, immunobiological administration, and even cosmetics. Using microneedles to access, extract and analyze dermal ISF, in lieu of venous blood, could greatly improve point-of-care diagnosis and health monitoring in austere environments, pandemic situations, and any case where blood monitoring is inconvenient or dangerous to the patient or doctor. However, despite

several previously published microneedle chip designs,¹¹⁻¹⁴ very few have been demonstrated to successfully collect ISF from human skin *in vivo*. In our work, presented here, and by others,^{13,14} skin penetration and ISF collection was achieved only in microneedles possessing a specific geometric shape. In the course of this research, a reliable and robust microneedle geometry for accessing and collecting dermal ISF has been fabricated and experimentally verified *in vivo*. Fabrication can be realized with relative ease in silicon, and is fully explained in subsequent chapters.

The primary focus of this thesis is the development of fabrication methods for microfabricated silicon microneedle arrays intended for dermal-ISF extraction in human subjects. Two avenues of fabrication are presented. The first method borrows from a previously reported dicing saw process,^{13,15} where a series of parallel and perpendicular cuts of partial depth are made into a thicker silicon wafer, creating arrays of square columns. The second method uses a new, entirely-DRIE process to create the arrays of columns. The columns are sharpened into needles using an isotropic wet etch method (HNA etch) which preferentially enhances etching at the tips and diminishes etching at the base, creating remarkably sharp, conical shaped needles capable of piercing skin.

1.2 Project goals

The specific aim of this project is to design and develop a fabrication process for silicon microneedle arrays that successfully extract dermal interstitial fluid (ISF) from human skin *in vivo*. The sub aims are a) to increase ISF collection volume and b) to achieve a high throughput, high yield process of manufacture, which may be scaled up for mass production.

1.3 Thesis organization

The organization of this thesis is summarized below.

Chapter 2 presents silicon microneedle device prior art.

Chapter 3 describes the key design features of the devices. It presents the starting point for the design, based on prior work by Mukerjee *et al.*,^{13,16} and lists the explicit improvements made to the design and fabrication, to optimize throughput and performance, over the course of the research.

Chapter 4 contains microfabrication process development, discussing the methods and designs attempted along the path to achieving a working device. In the interest of completion, and to inform future endeavors, failures are analyzed. First, the fabrication for the backside of the chip is presented, which is common to both designs. The backside contains the microchannels and reservoir where ISF is collected, and is covered by a transparent layer of glass, covalently bonded to the silicon surface. Then, two methods are presented for fabrication of the needles columns on the front side of the chip: one that uses DRIE, and another where they are formed with partial-depth cuts by a precision dicing saw.

Chapter 5 details the methods and results used in testing the devices.

Chapter 6 concludes the main body, summarizing the thesis and presents avenues of future research potential.

Appendices A and B contain a full microfabrication recipe for both designs. With that information, this project should be fully repeatable.

Appendix C contains a step-by-step pictorial representation of the process flow.

Appendix D presents the photomasks layouts, and details how alignment was performed.

Appendix E lists wafer specifications, Appendix F lists equipment makes/models used, and Appendix G lists stock solutions and notable dangers.

CHAPTER 2 – SILICON MICRONEEDLES PRIOR ART

Modern medicine has seen continuous growth of hypodermic needles for venous blood collection for laboratory analyses due to its high efficiency and low cost. However, phlebotomy can present problems¹⁷: (1) reuse of un- or inappropriately sterilized needles is common in developing countries, posing serious transmission risk of blood-borne pathogens like HIV,¹⁸ (2) 3.5%-10% of the world's population have trypanophobia, a fear of needles, which may cause them to avoid treatment,¹⁹ (3) hypodermic needles are difficult to use by untrained persons, and the imposed infection risks are unacceptable in austere environments, such as military field, pandemic situations, and other unsafe or unsanitary domains.

In contrast to traditional hypodermic needles, the microneedles developed for this project cause little to no pain sensation due to fewer interactions with Meissner's corpuscles, Pacinian corpuscles, and large nerve endings.²⁰ The microneedles are short (< 0.5 mm), very sharp, and thin enough that they evoke little to no sensation upon insertion, and therefore provide a minimally invasive approach to facilitate bidirectional transport of molecules (drugs, ISF, etc.) that normally would not be able to permeate the *stratum corneum*.²¹ While the initial use case for transdermal microneedles was predominantly for transdermal delivery of drugs and vaccines,²² there has been an increased interest in extracting interstitial fluid from the dermis, and on the development of lab-on-a-chip (LoC) technologies using microneedle devices equipped with on-chip diagnostic sensors.

2.1 Pioneering work: 1990s

2.1.1 The Normann group – intracortical stimulation, 1991.

Perhaps the earliest demonstration of silicon microneedle devices was in 1991 by Campbell *et al.*¹⁵ from the University of Utah. They created an array of electrically isolated, solid silicon microneedles to be used for chronic intracortical stimulation of feline cortex. They fabricated the

microneedles by using a computer-controlled dicing saw to transform a silicon wafer into a 10 x 10 array of rectangular columns by making deep orthogonal cuts into the wafer. The columns were subsequently sharpened into needles with a biphasic wet etch. The saw process substantially informed our saw-fabricated design, and the wet etch formulation and process is similar to the sharpening procedure used here, as discussed in future sections (§ 3.2.2, § 4.5.1, & § 4.5.2).

2.1.2 The Prausnitz group – skin permeability for drug delivery, 1998.

The first published study on the use of silicon microfabricated microneedles to enhance drug delivery across skin was in 1998 by Henry *et al.*²² from Georgia Institute of Technology. This paper detailed a fabrication method for an array of solid needles produced and sharpened with reactive-ion-etch (RIE) technology, using chromium dots as a mask for the individual needles. The conditions of the etch allowed for deep vertical etching with slight lateral underetching, which naturally produced sharp needles as the etch was allowed to persist until the masks fell off due to the underetching. The needles were used to increase skin permeability after insertion and removal of the needles; results showed several orders-of-magnitude increase in skin permeability, indicating promise for drug-coated solid microneedles to be used as a delivery mechanism.

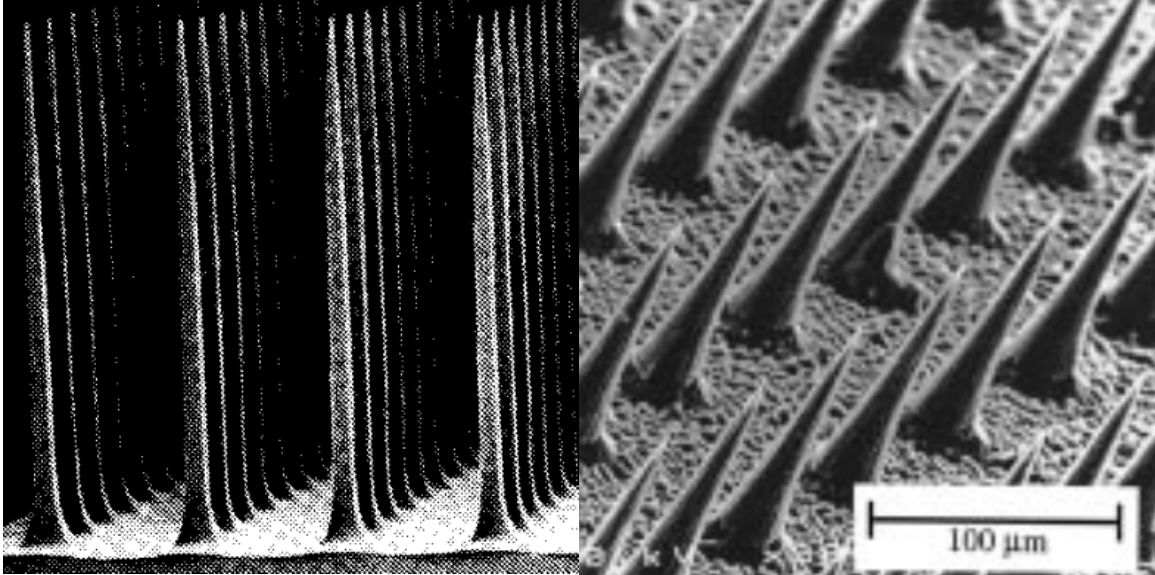


Figure 2.1 – Two of the first silicon microneedle designs published. Left: The Normann group.¹⁵ Right: The Prausnitz group.²²

2.2 Microneedles for diagnostics

2.2.1 Wound potential

In 2000, silicon microneedles were gaining in popularity. Mukerjee *et al.*,²³ from the University of California at Davis, developed a microfabricated instrument for transdermal wound potential measurements which employed an array of silicon microneedles with platinum coated tips. The completed device was used to measure the endogenous electric fields generated at the edge of superficial skin wounds. The microfabrication technique to form the columns and etch to needles was borrowed from Campbell *et al.*,¹⁵ using a dicing saw to form columns and wet silicon etch to sharpen to needles.

2.2.2 Blood glucose monitoring

In 2000, an article was published in *Diabetes Technology & Therapeutics* on the use of silicon microneedles in painless monitoring of blood glucose. Smart, *et al.*,²⁴ developed devices which featured a single, disposable out-of-plane silicon microneedle which punctures any skin surface, contrary to traditional lancets which use the tip of the finger. The microneedle is advanced and withdrawn by a microprocessor and draws less than 200 nanoliters of blood into a microcuvette. The attached instrument performs an assay and displays blood glucose concentration. The

microneedle and microcuvette are then disposed of, and a new chip can be loaded into the instrument for later use. Most subjects tested reported the pain as “barely noticeable” or “can’t feel.” In comparison to a conventional lancet, the microneedle device was perceived as significantly less painful.

2.2.3 Interstitial fluid (ISF) extraction

In 2004, a silicon array for biological fluid extraction was published by Mukerjee *et al.*¹³ in *Sensors and Actuators*. This design also employed a dicing saw for column creation and wet silicon etch to sharpen the needles. However, this time the needles were hollow, containing integrated microchannels on the backside, and through-wafer boreholes facilitating flow from the needles to a collection point on the backside. The boreholes were drilled with DRIE prior to column creation with the dicing saw. It was found that final needle shape was critically dependent on the placement of the borehole relative to the top of the column. A “volcano-like” needle was formed if the 10-micron borehole was placed in the geometric center of the square column, prior to sharpening. A “micro-hypodermic” needle was formed if the borehole was shifted 25 microns from the column’s center. Lastly, a “snake-fang” needle was formed if the borehole was shifted an additional 25 microns from center (50 microns total). All shapes are displayed in Figure 2.2.

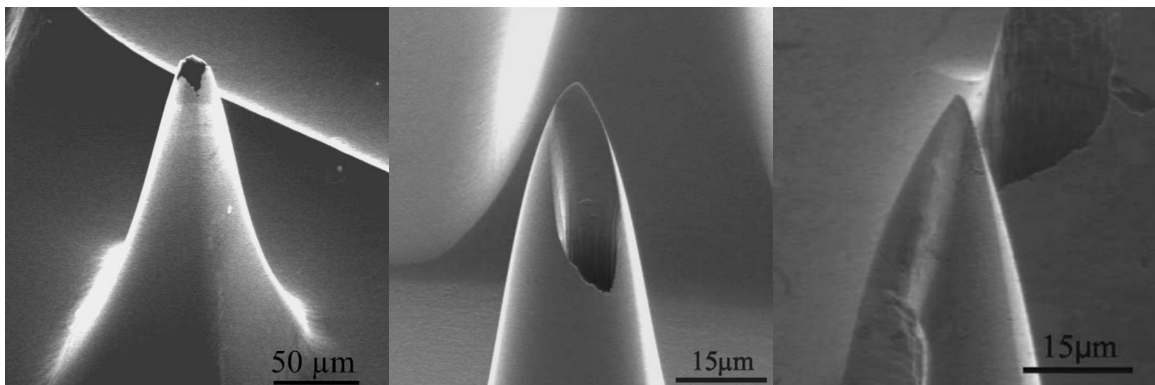


Figure 2.2 – SEM micrographs of different needle shapes achieved with changing hole position. Left: volcano-shaped; center: hypodermic-shaped; right: “snake-fang”-shaped.¹³

The “snake-fang” design was shown to extract ISF from skin. The other two designs were susceptible to blockage due to plugging of the holes with tissue, preventing flow of ISF, but the “snake-fang” design was capable of pushing the skin to the side, allowing unobstructed flow from tip to base. This design has informed much of the fabrication techniques and initial development for the devices detailed in this thesis, especially the saw-fabricated design (§ 4.3).

2.3 Other applications

2.3.1 Drug and vaccine delivery

The vast majority of hollow microneedle literature, employing a variety of materials and manner of fabrication, is focused on drug delivery. This thesis is concerned with diagnostics, and as such a literature review of microneedles for drug delivery is outside the scope of this document. Many review articles can be found on the subject.^{25,26,27} However, I include a brief description of two silicon microneedle designs intended for drug and vaccine delivery, as I find their shapes and manner of fabrication interesting and results informative.

Developments by Gardeniers *et al.*¹¹ (van den Berg group) were published in a 2003 article in the *Journal of Microelectromechanical Systems*. These needles were wedge-shaped, between 150 and 350 microns in height, and 250 microns wide at the base (Figure 2.3). Drug delivery was increased by a factor of 750 in microneedle patch applications compared to diffusion through the *stratum corneum* alone.¹¹ Also in 2003, Griss & Stemme²⁸ published “side-opened” microneedle arrays which contained an opening in the shaft rather than an orifice at the tip (Figure 2.4). They were fabricated using DRIE, and the side-opened hole was intended to eliminate tissue clogging at the tip during insertion (see § 2.2.3). However, they observed issues in fabrication which led to a high degree of uncertainty and reliability of the structure and strength of the needles. At random times, the top mask used in the process may fall off and stick to a side-wall which lead to errors in fabrication of the side-ports. A future group, Zhang *et al.*, from the University of Calgary, was

able to improve this uncertainty, and simulated drug delivery through the needles via computer modeling.^{29,30}

These results were interesting to me mainly due to their odd shapes (Figure 2.3 and Figure 2.4). However, they also did not require a separate wet sharpening etch as do the microneedles presented in this thesis (see § 4.5). Instead, the needles were sharpened with either a dry etch, or during initial formation; in Gardeniers' needles, the photomask was designed with a small radius of curvature at the tip, naturally creating a sharp point; and in the Griss & Stemme needles, the needles were sharpened with an isotropic (dry) plasma etch. In both cases, this likely reduces variability between devices, and even between needles of the same array, as the wet etch I currently use attacks needles on the edge of the array slightly faster than those in the center. Eventually, a wafer scale sharpening etch should be implemented to reduce chip-to-chip variability, which could be accomplished with the current wet etch (again, see § 4.5). However, a dry etch or a more-controllable wet etch would be preferable.

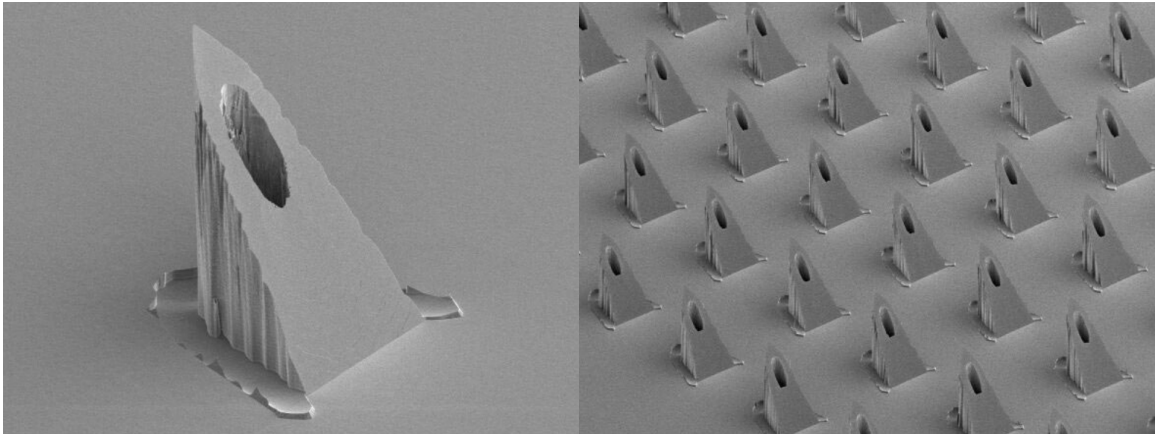


Figure 2.3 – Gardeniers, et al. Wedged shaped microneedles fabricated with KOH etching.¹¹

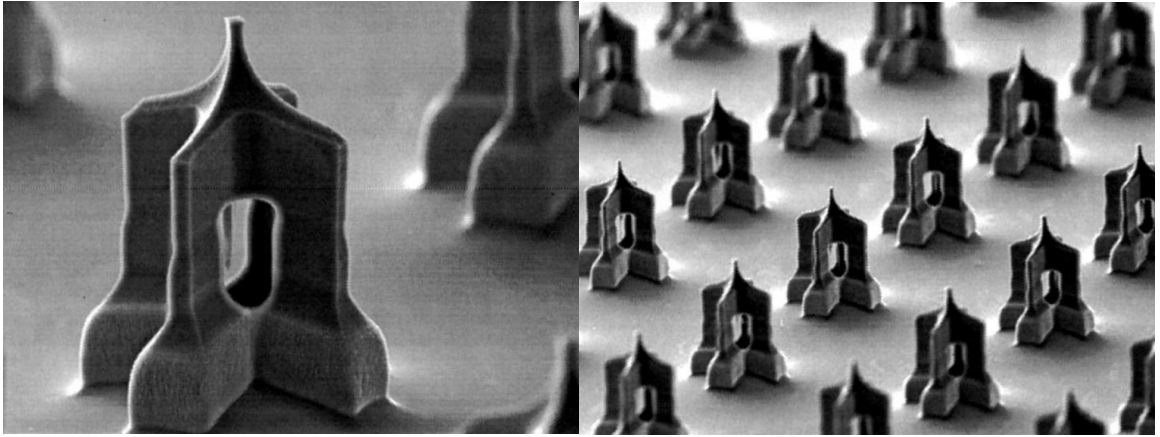


Figure 2.4 – Grisse & Stemme's side-opened microneedles.²⁸

CHAPTER 3 – DESIGN FEATURES

3.1 Design

Main design features:

- A 22x22 array of needles (484 total) on frontside
 - 300 μm center-to-center spacing between needles
 - 400-420 μm needle height
 - Notch that travels from the tip to a borehole, facilitating ISF flow from the tip
- 30 μm -diameter boreholes on every other needle (162 out of 484), which travel through the wafer
- Microfluidic channels and a reservoir that stores collected fluid on the backside, connecting with the boreholes

To create the microneedle arrays, columns are formed first (Figure 3.3), which are then sharpened into needles (Figure 3.4). Two different fabrication processes for column formation are presented:

- Columns formed by deep-reactive ion etching (DRIE), a highly anisotropic etch process used to create deep, high aspect-ratio holes and trenches in a substrate. Dimensions (LWH): 120 μm \times 120 μm \times 400 μm .
- Columns formed by making many equally-spaced parallel and perpendicular cuts at partial depth, with a dicing saw (borrowed from Mukerjee *et al.*¹³). Dimensions (LWH): 135 μm \times 135 μm \times (400-420 μm).

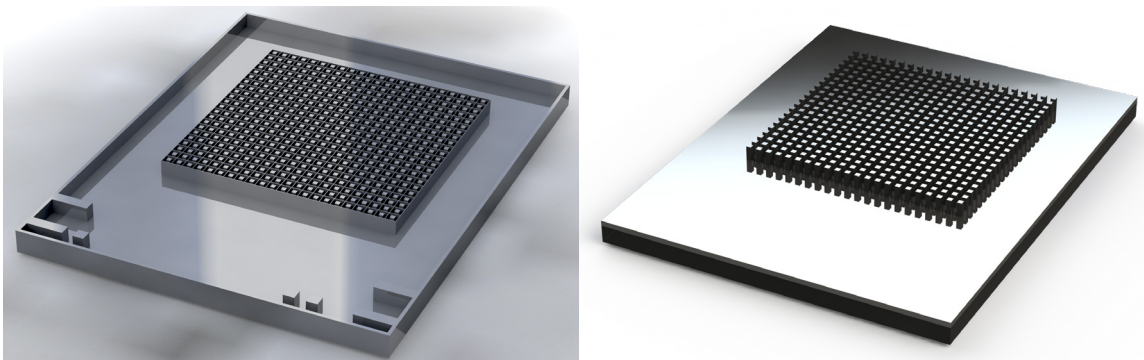


Figure 3.1 – 3D CAD-rendered images of a single chip for both designs – DRIE (left) and dicing saw (right).

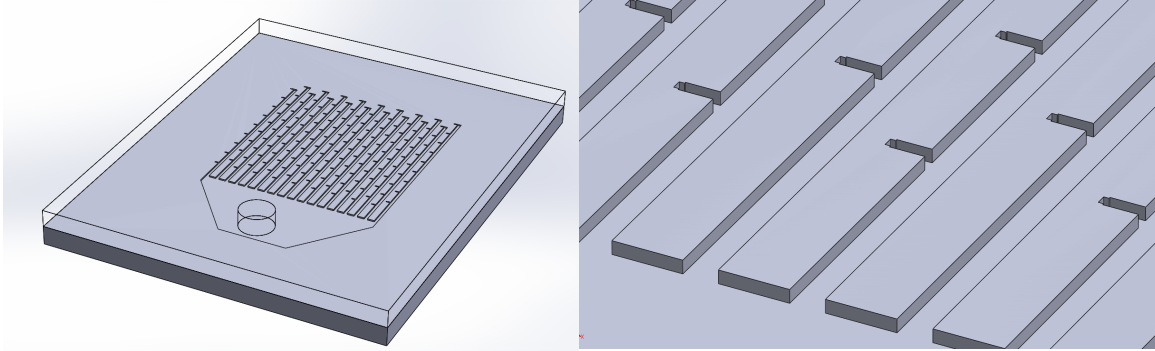


Figure 3.2 – 3D CAD-rendered images of the backside of a single chip. The microchannels are the same for both DRIE and dicing saw designs.

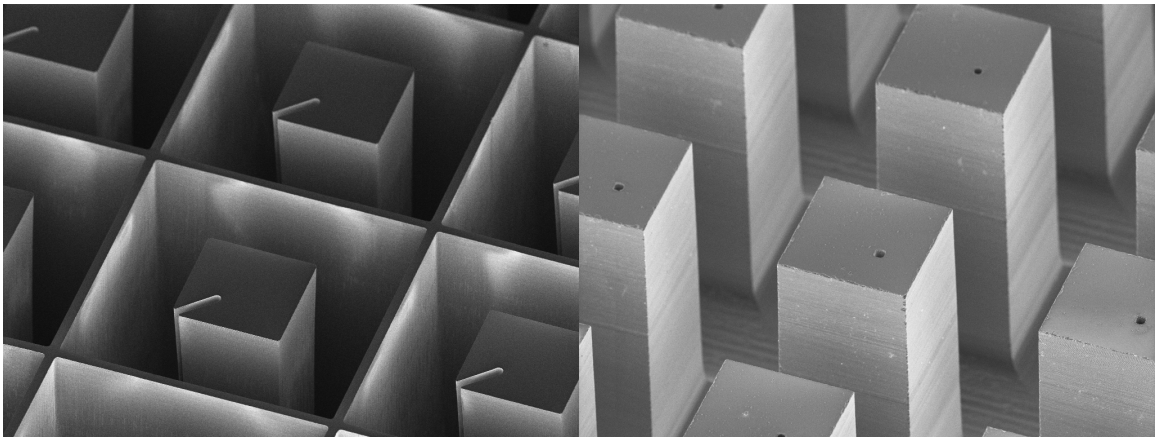


Figure 3.3 – SEM images of unsharpened columns for both designs – DRIE (left) and dicing saw (right).

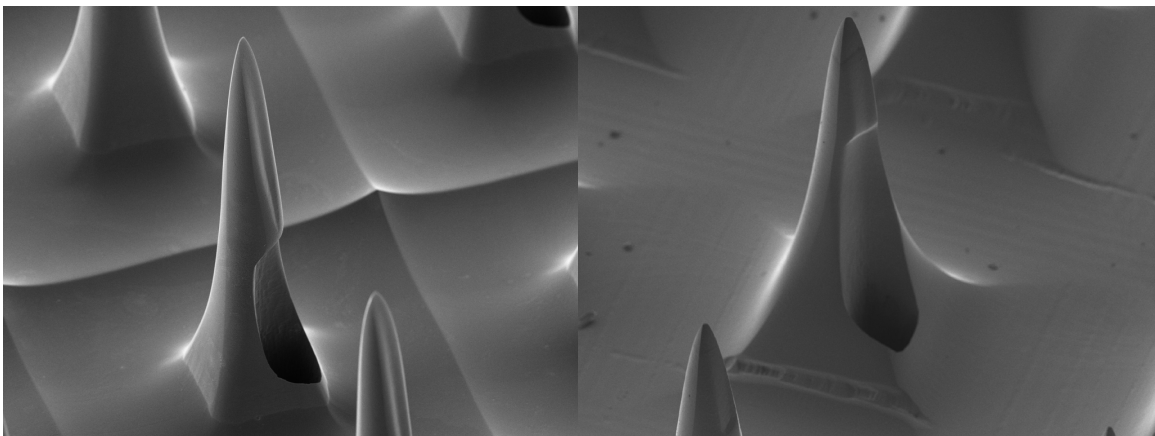


Figure 3.4 – SEM images of needles after sharpening for both designs – DRIE (left) and dicing saw (right).

3.1.1 DRIE column frames

The frames around the columns created by the DRIE (Figure 3.3, left) are an effort to maintain vertical etching in the DRIE when used to achieve etch depths of more than a few hundred microns. An optimized DRIE recipe can achieve nearly vertical etching (90 ± 3 degrees). Etch aspect ratios (vertical/lateral) of 22-30 are typical for the Bosch DRIE process for etch depths of

100-300 μm , corresponding to 87-88° sidewalls. Relatively large etch openings permit rapid mass transport of reactants and byproducts to/from the bottom of the etch openings. But, large openings also mean higher ion flux density inside the etched regions, which can interact. Charge repulsion results in deviation of ion path from vertical, resulting in > 90-degree sidewalls (Figure 3.5). The deeper the etch, the more pronounced this effect has on ion trajectory. Other factors, such as ion “bouncing” off the bottom, and changes in heat transfer with etch depth contribute to enhanced etching at the base of the columns. If the mask opening is very small, then the etch will terminate for a sidewall angle less than 90 degrees. The aspect ratio (sidewall angle) of the DRIE recipe, diffusion limitations, and feature tolerances (overetch) will determine the maximum depth one can achieve for a given opening size. For a typical etch aspect ratio of 30 (88 degrees), a 10 μm hole can only achieve a maximum hole depth of 150 μm (Figure 3.6). “Large” and “small” here are unquantifiable, and will depend on the application, materials, and DRIE recipe used. For this purpose, I will define “small” as *less than ten microns*, and “large” as *a few hundred microns or more*. Certain parameters (bias power, step times, chamber pressure, among others) can be adjusted to change the sidewall angle.³¹ However, optimizations to a DRIE recipe are time-, and resource-consuming. In this situation, it was far easier to modify the photomask, in a way which would maintain a sidewall angle \approx 90 degrees. This was achieved through the inclusion of a thin frame around each column, thereby reducing the opening between columns. The frame does not impede sharpening the columns into needles, as it is thin enough that it etches away quickly. It is nearly completely successful at maintaining a near vertical etch (Figure 3.7).

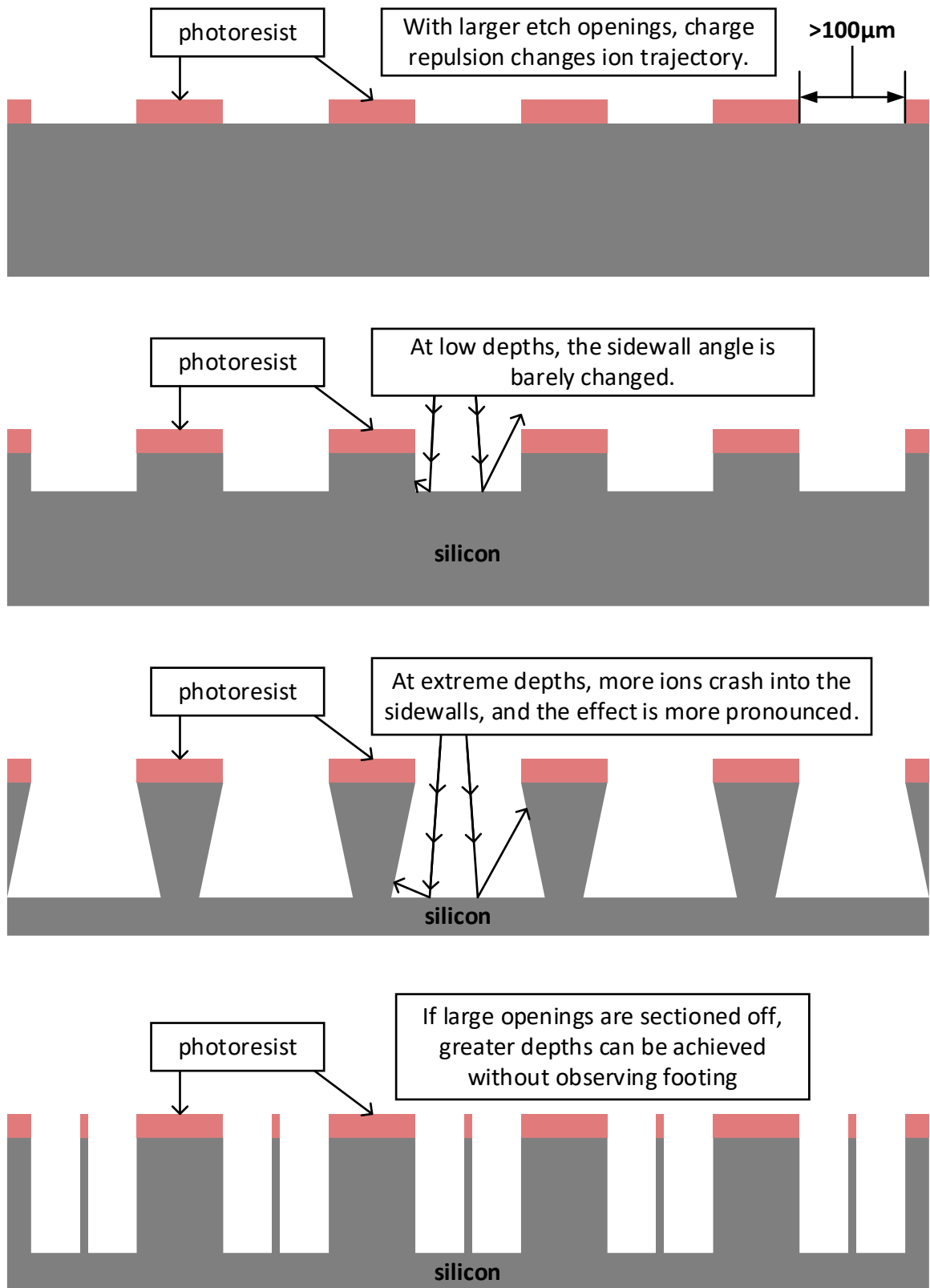


Figure 3.5 – Base undercut in the DRIE visualized.

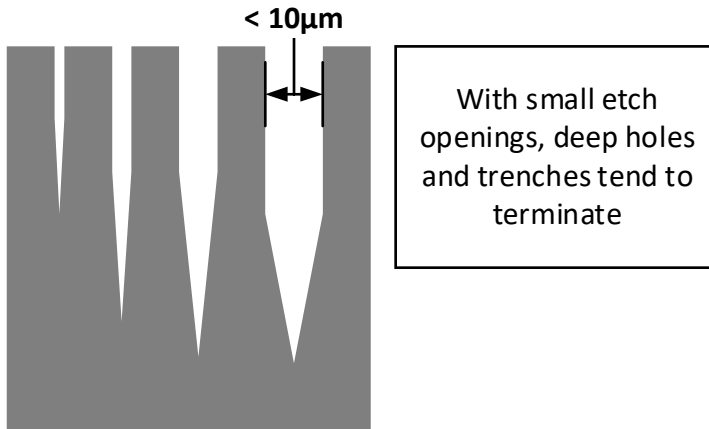


Figure 3.6 – Small openings typically lead to etch termination.

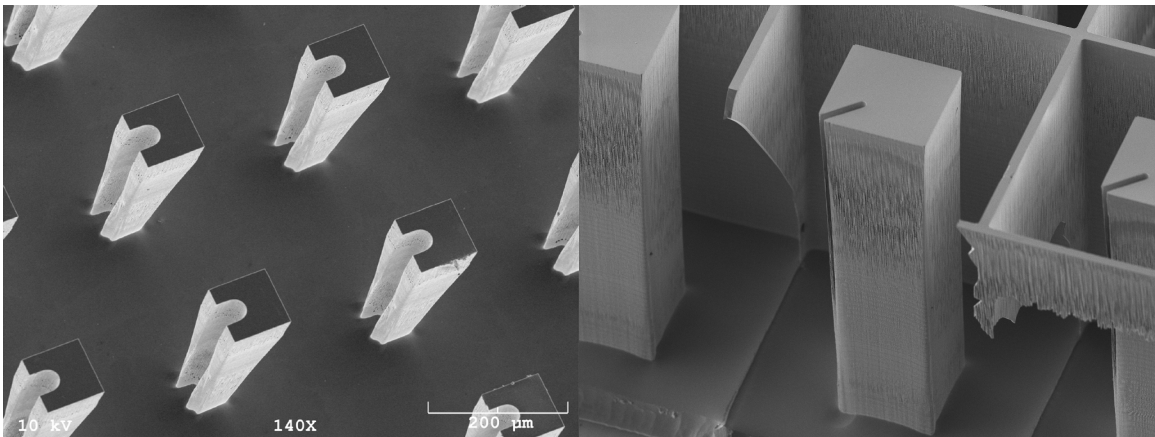


Figure 3.7 – Column tapering in the DRIE-fabricated columns is nearly eliminated with the inclusion of a frame around each column.

3.2 Starting points

My work on microneedle devices was heavily influenced by the work of Mukerjee *et al.*^{13,16} at the University of California at Davis, published in Mukerjee's doctoral thesis in 2003, and in the peer-reviewed *Sensors and Actuators* in 2004. I am very grateful for the starting point this work provided, and note several problems that were solved by Mukerjee *et al.*, and therefore implemented in the design and fabrication of devices presented here (Figure 3.1). My specific design modifications and fabrication improvements are detailed in the following section (§ 3.3).

3.2.1 Needle spacing

The center-to-center spacing of each microneedle is important. If the needles are too far apart, the elasticity of the skin will prevent piercing. For example, take a single tack or nail and lightly

press it to your finger. Even though it is very sharp, the tack will not immediately pierce the skin, which deforms around it (Figure 3.8). It takes significant force and height, which microneedles do not have, for a single needle to pierce the skin.

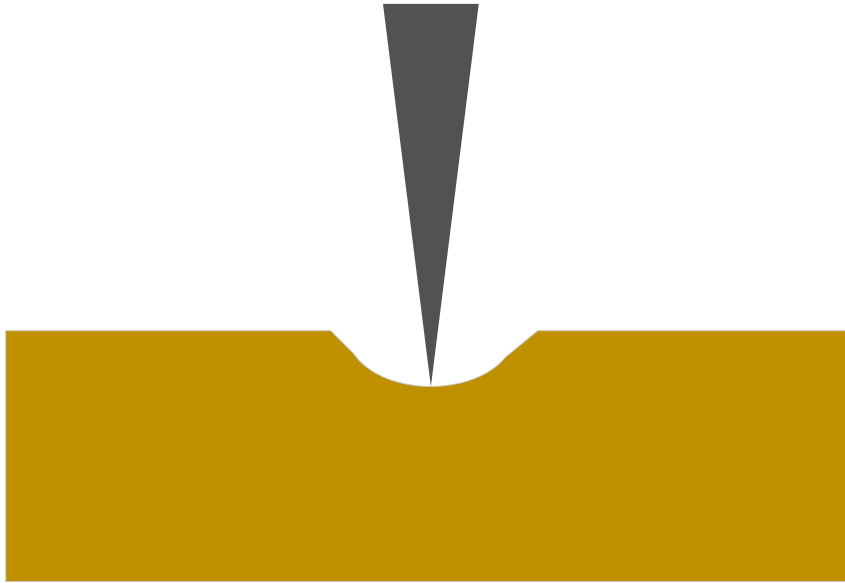


Figure 3.8 – The skin will stretch and deform around a single needle

Placing the microneedles close together, like a bed of nails, stretches the skin, preventing the skin from just deforming around each needle, and facilitates insertion. The work published by Mukerjee *et al.* used a 300 μm spacing between each needle, which was found to be very effective. Thus, it was incorporated into the designs for this project.

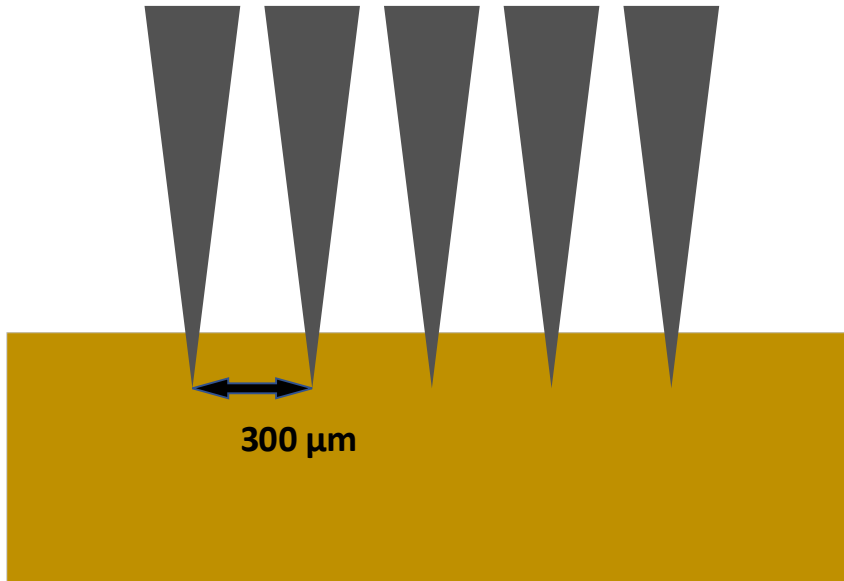


Figure 3.9 – Each needle stretches the skin nearby it, preventing deformation and facilitating skin piercing.

3.2.2 Sharpening

After producing columns (Figure 3.3), they must be sharpened into needles (Figure 3.4). The needles produced by Mukerjee *et al.* were demonstrably sharp enough to pierce human skin. The biphasic sharpening procedure, including temperatures, chip orientation, and stir bar spin speeds, was used in the fabrication of my devices (see § 4.5 for full explanation of sharpening procedure).

3.2.3 Glass bonding

Mukerjee *et al.* found that bonding the backside microchannels to a layer of glass provided mechanical strength to the device, allowing pressure to be applied for insertion into the skin without breaking. It also provides a window into the device to observe if the channels are being filled, and glass is very hydrophilic, assisting with capillary fill.

3.2.4 Capillary fill

Mukerjee *et al.*¹³ additionally solved the problem of getting the devices to fill via capillary action alone. It was found that the boreholes must be placed adjacent to the microchannel wall, rather than sitting in the center of a microchannel, where the force required to overcome the boundary at the hole edges is too great for capillary forces. If the hole is instead placed along a wall, the

fluid will keep traveling up the wall until it reaches the glass surface which will pull the fluid along the channel.

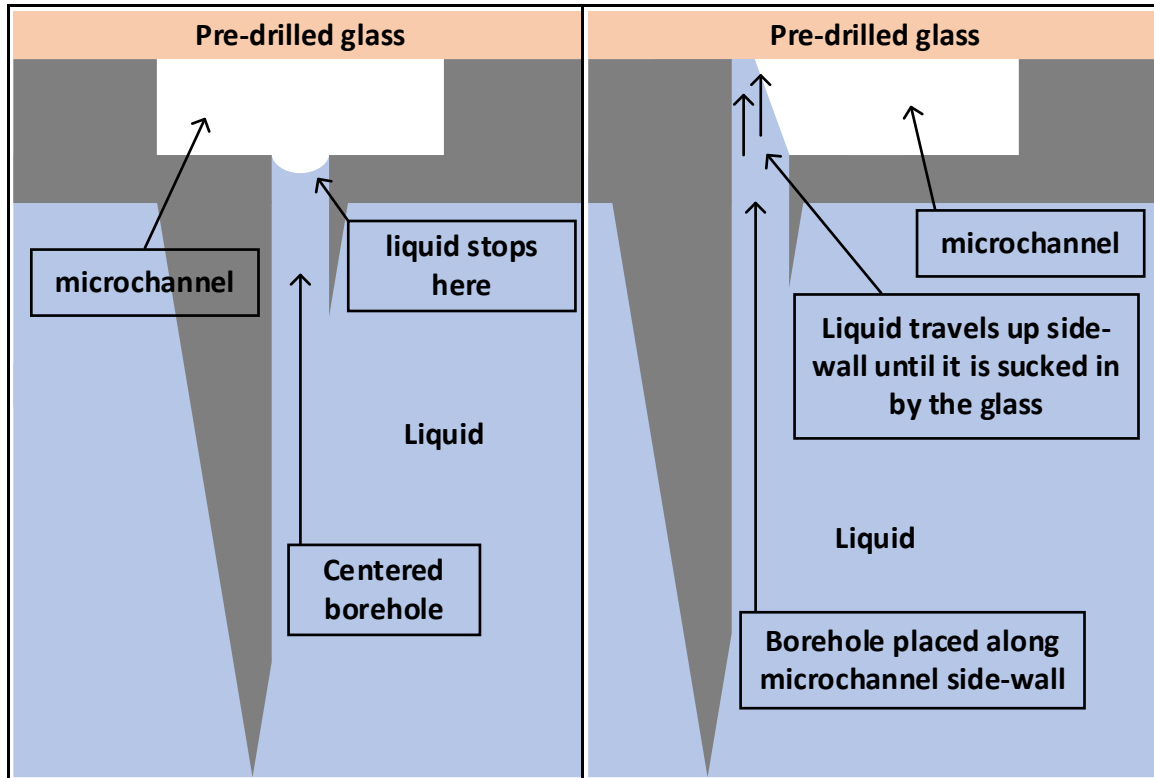


Figure 3.10 – Placement of the borehole along a microchannel side-wall allows capillary forces to draw liquid into the channel.

3.3 Modifications and improvements

Many modifications were made to the design and fabrication published by Mukerjee *et al.*,¹³ to increase ISF collection capacity, and to increase the throughput and yield of the manufacturing process. Mukerjee's devices were tedious to manufacture, due to process, wafer and equipment limitations. The columns, formed with a dicing saw, required precise alignment that was not possible at the time without re-aligning after nearly every cut (poor optics and positioning accuracy). Regardless, the resulting devices were successful in extracting a miniscule volume ($\approx 0.15 \mu\text{L}$) of dermal ISF. My research aimed to improve on extraction, volume, and microfabrication yield, both of which were successfully achieved. The improvements are summarized in the table below.

Table 3-1 – Design improvements

Improvement	Mukerjee <i>et al.</i>	My devices
Fluid capacity	≈0.2 microliters	≈0.7-1 microliters
# of collecting needles	18	162
# of collecting channels	7	18
Surface area of collection	≈3.6 mm ²	≈36 mm ²
Fabrication time, yield	>120 hours (non-published estimate), yielding a couple of chips	Roughly 40 process hours, yielding 36 chips per 4-inch wafer
Wafer thickness (which enabled the following, needle height and channel depth improvements)	500 μm	550 μm (dicing saw design) 650 μm (DRIE design)
Needle height	250-350 μm	400-420 μm
Microchannel depth	15 μm	40-50+ μm

CHAPTER 4 – MICROFABRICATION METHODS & RESULTS

This chapter describes in detail the trial-and-error that went into developing a working design for both methods of fabrication, saw and DRIE. SEM, optical, and CAD-rendered images are shown to assist comprehension. Complete microfabrication flows for the final process sequences are provided in APPENDIX A.

4.1 The backside: microchannels and reservoir

The fabrication process begins with the backside of the wafer, which contains a series of microfluidic channels (microchannels) which connect the holes of the collecting needles to a reservoir – with opening for air escape and access for collection off-chip. Borofloat® glass (Schott) of half-millimeter thickness is anodically bonded to the silicon, creating a hydrophilic cap for the channels, and a transparent window through which ISF collection may be visualized.

4.1.1 Microfluidic channel and reservoir fabrication

The fabrication method employs a two-step etch method.¹⁶ First, virgin, double-side polished silicon wafers are thermally oxidized to a thickness of roughly 500 nm. Then photolithography is performed, exposing the resist to the first level mask, which patterns the microchannels and reservoir shapes. After development of the photoresist layer, the exposed oxide area is removed with a buffered oxide etch (BOE). (Note: before the BOE etch, wafer tape is applied to the *frontside*, to protect the oxide layer on that side during the BOE etch. That oxide layer exists to prevent scratching on the silicon surface during processing.) After BOE, the wafer tape and photoresist are removed, revealing mask #1's pattern in the oxide layer. Another photolithography step is subsequently executed, this time with a 10 micron-thick SPR-220 photoresist, which completely covers the pattern in the oxide. This is exposed to the second level mask, which contains an array of 30-micron boreholes. The boreholes are then etched in the DRIE to a depth of 400-microns. These holes will enable fluid to travel from the needles on the frontside

(patterned in future steps), through the wafer, to the microchannels. After the photoresist is stripped, the microchannel oxide pattern is again revealed. This oxide pattern is used to mask the channel etch with DRIE to an approximate 40-micron depth, carving the channels and reservoir into the silicon. For enhanced comprehension, cross-sections are shown in Table 4-1. A cross-section schematic for the entire fabrication process can be found in APPENDIX C.

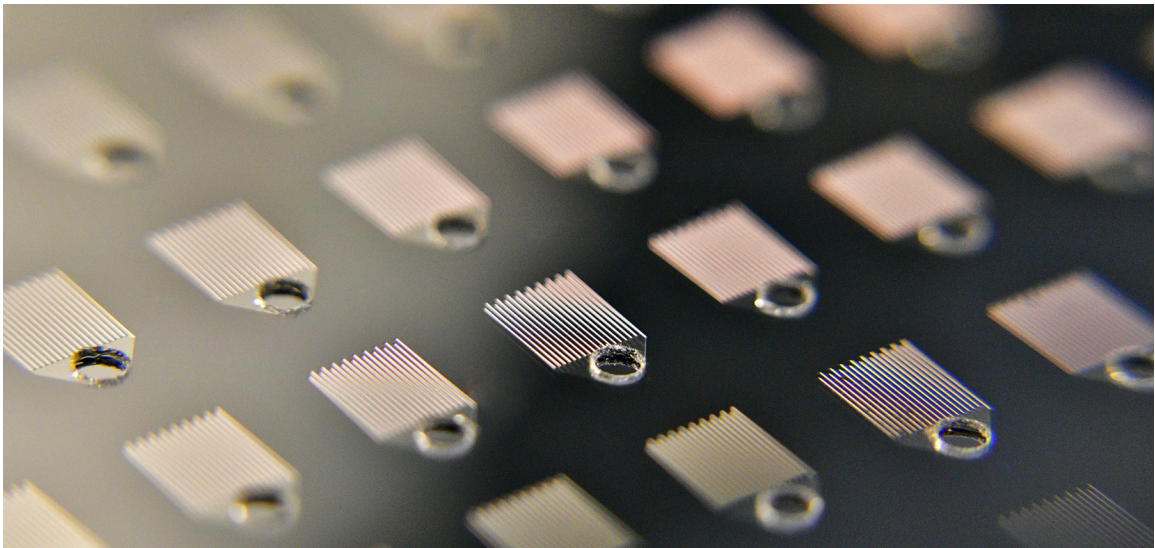


Figure 4.1 – The wafer backside features microfluidic channels for ISF transport, and is anodically bonded to glass containing a series of predrilled holes which are aligned to the reservoir of each chip

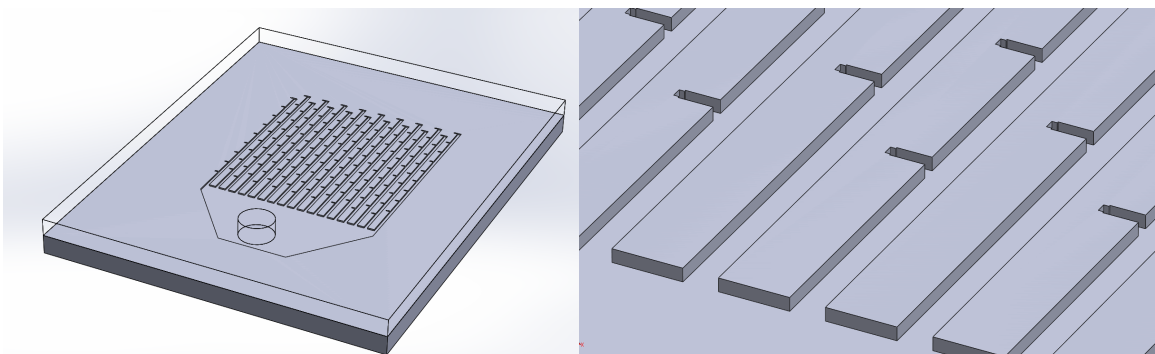


Figure 4.2 – 3D CAD images of a single chip, showing the microchannels and reservoir with the bonded glass layer.

Table 4-1 – Two-step DRIE etch for microchannel and borehole fabrication

<p>Step 1 – Silicon, double-side polished. Wafer thickness varies between column designs. (see § 4.2, and § 4.3)</p>	 <p>**THESE DRAWINGS ARE NOT TO SCALE**</p>
--	--

Table 4-1 (Continued)

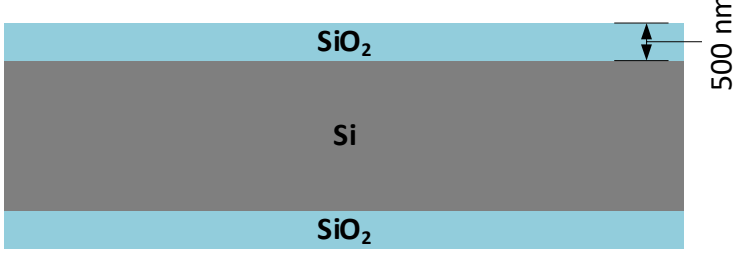
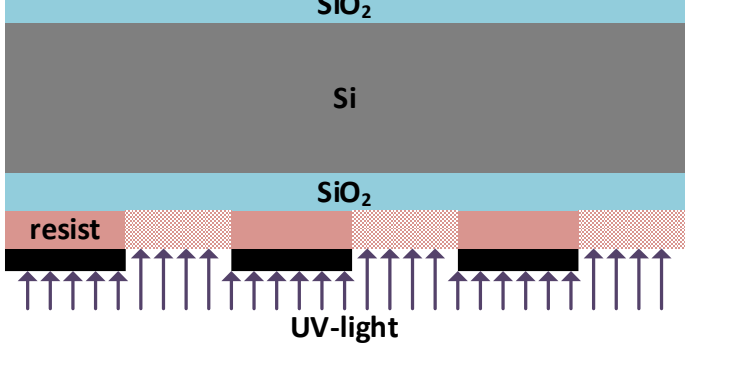


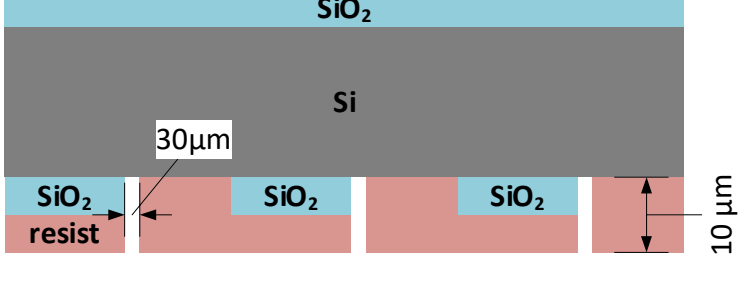
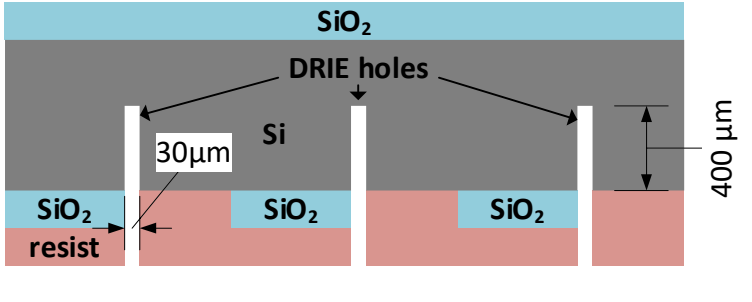
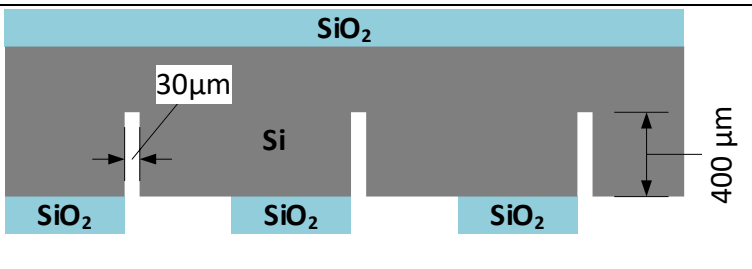
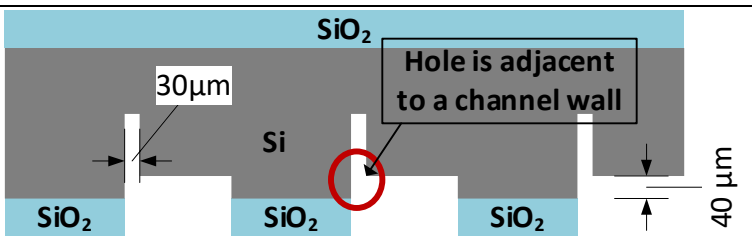
<p>Step 2 – Thermal steam oxidation, 500nm thickness</p>	 <p>A cross-sectional diagram showing a central grey layer labeled 'Si'. Above and below this layer are light blue layers labeled 'SiO₂'. A vertical double-headed arrow on the right side of the top SiO₂ layer is labeled '500 nm'.</p>
<p>Step 3 – Photolithography for channel-side oxide etch</p>	 <p>A cross-sectional diagram showing the same structure as Step 2, but with a red layer labeled 'resist' on top of the SiO₂ layer. Below the resist, there are black rectangular regions. Purple arrows labeled 'UV-light' point upwards from these black regions through the resist.</p>
<p>Step 4 – Channel oxide etch</p>	 <p>A cross-sectional diagram showing the result of etching. The top SiO₂ layer is gone, leaving three light blue rectangular islands labeled 'SiO₂' on the surface of the grey 'Si' substrate. The bottom SiO₂ layer remains.</p>
<p>Step 5a – Spin photoresist for channel-side 30μm hole arrays. <i>Note: mask/UV-light not shown</i></p>	 <p>A cross-sectional diagram showing the same structure as Step 4, but with a red layer labeled 'resist' spun on top of the SiO₂ islands. A vertical double-headed arrow on the right side of the resist layer is labeled '10 μm'.</p>
<p>Step 5b – Develop 30μm hole arrays</p>	 <p>A cross-sectional diagram showing the result of developing the resist. The red resist has been patterned into rectangular blocks. A horizontal double-headed arrow between two resist blocks is labeled '30μm'. A vertical double-headed arrow on the right side of the resist blocks is labeled '10 μm'.</p>

Table 4-1 (Continued)

<p>Step 6 – DRIE 30μm hole arrays 400μm deep</p>	
<p>Step 7 – Remove photoresist, revealing oxide pattern. DRIE channels 40μm deep using the patterned oxide as an etch mask</p>	
<p>Step 8 – DRIE channels 40μm deep using the patterned oxide as an etch mask</p>	

4.1.2 Anodic bonding to glass

This section describes the procedure by which the backside microchannels and reservoir are sealed by a layer of glass.

4.1.2.1 Anodic bond concepts

Anodic bonding is a wafer bonding process where glass is fused to silicon or metal without an intermediate layer, i.e. adhesive or eutectic. This process requires clean, polished wafers of low surface roughness, allowing intimate contact between the glass and silicon. A DC voltage is applied such that the glass is negative (cathode) with respect to the silicon (anode). Borosilicate glass is used due to its high alkali ion (sodium ion) concentration. The thermal expansion coefficients between the two substrates must be closely matched, as the process takes place at temperatures between 250 and 500 degrees Celsius to increase sodium ion mobility in the glass.³²

When voltage is applied, the sodium ions in the borosilicate glass migrate towards the cathode and electrons in the silicon move towards the anode, away from the silicon-glass interface. This charge separation results in an electric field at the glass-silicon interface and an electrostatic force that pulls the surfaces together. Under the high electric field, oxygen anions at the glass surface electrochemically react with the silicon (anodic oxidation) creating a chemical bond.³³ This bond is irreversible, and persists after the electric field is removed and the substrates return to room temperature. The anodic bond between glass and silicon produces a hermetic seal, that not only acts as an effective fluidic seal, but can also be used to create a reference pressure or vacuum in MEMS devices, such as absolute pressure sensors and resonators.

In the microneedle devices, the bonding is performed after all DRIE steps have been realized. Glass is not permitted in the UMaine DRIE due to contamination concerns, and because its insulating properties prevent adequate heat transfer between the helium-cooled chuck and the silicon, necessary for maintaining control over etch rate and selectivity.

4.1.2.2 Glass hole design

The glass wafer, containing predrilled holes, is aligned and bonded to the channel-side of the wafer. The holes are aligned to the reservoir of each chip. The holes are intended to allow for air escape, and removal of the fluid collected by the chip.

The holes for our first-generation devices were mechanically drilled (Schott Glass – Elmsford, New York) to a 2-mm diameter. The holes were spaced to be aligned to the center of the reservoir. In order to increase the ISF capacity on the chip, the hole diameter was reduced to 1-mm for future designs, currently in development. Schott Glass could not mechanically drill the smaller diameter holes; therefore, they were shipped to another company (AdValue Technology – Tucson, Arizona) for laser-drilling.

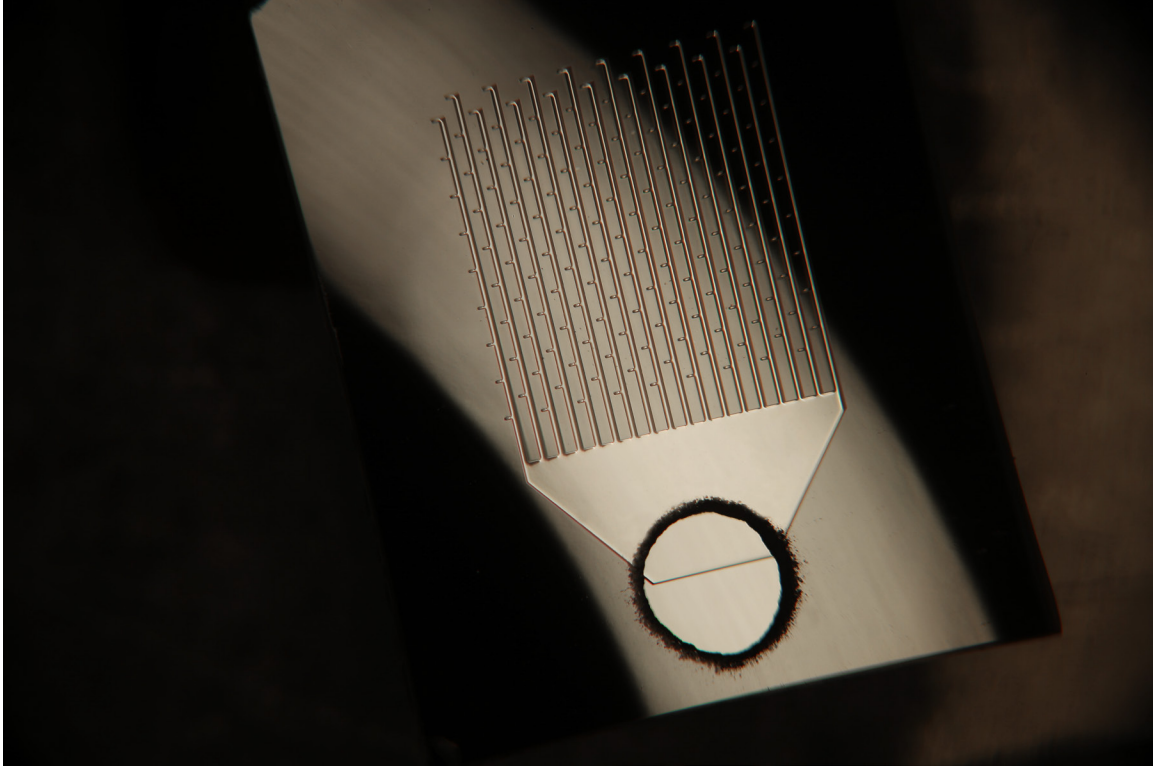


Figure 4.3 – Image of a single chip, bonded to glass

4.2 The frontside: DRIE column fabrication

Much effort was expended on the design of a fabrication process by which hollow microneedles could be made at the wafer scale, using DRIE instead of a dicing saw to create the columns. The primary reasons for this were: a) the required, high-precision alignment of the dicing saw to the via hole is not reliably feasible using the dicing saw at UMaine; and b) future integration of a dry sharpening etch at the wafer scale is more compatible with a DRIE approach. It was also anticipated, at the start of this project, that the DRIE column formation would be more economical. An assessment of this is provided in § 4.6 - Cost analysis. As of the publication of this thesis, there are no published methods for making hollow microneedle devices in silicon, capable of extracting ISF, except for those previously made using a dicing saw.

4.2.1 Needle shape

Research by us and others^{13,16,34} has determined that needle shape is a paramount characteristic of microneedle devices that successfully extract ISF from human skin. Upon joining this project,

some chips had been fabricated that were incapable of extracting ISF (Figure 4.4). One wafer was saw-fabricated (left) and one was DRIE-fabricated (right). These wafers shared a common feature: both had rectangular columns, without any hole or grooves, before sharpening. It was hypothesized, based on prior art success,^{13,16} that a path for ISF flow from the microneedle tip to the borehole was necessary. For the saw design, this would require inclusion of a hole connecting to the borehole, prior to dicing (Figure 4.5). For the DRIE design, a slot or hole would need to be incorporated.

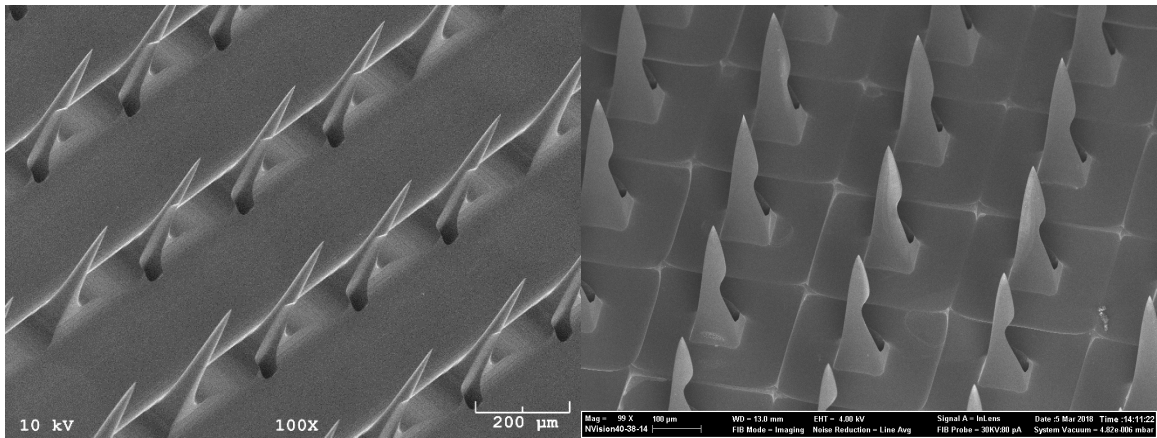


Figure 4.4 – SEM images of needles whose tip-shape is not sufficient to extract ISF.

This proved to be challenging with an all-DRIE design. Previous saw-based needle arrays were designed with a small hole at the top of the column (Figure 4.5). I found it impossible to employ the same design in two DRIE steps, as the holes are too deep for subsequent spin-on photoresist application. Attempts to fill the holes with resist, clear the wafer surface, and spin-coat were unsuccessful, leaving a bubble or a depression in the resulting surface which would open at some point during DRIE, severely widening the holes and ruining the columns (Figure 4.6). Given currently available technology at UMaine, it was concluded a single DRIE step is required for the formation of the columns.

Additionally, the same hole design is very difficult to be created by a single DRIE step, due to the effect of feature size on etch rates. It would have to be designed so that the small topside hole

would meet the backside 30 μm borehole at some point during the etch. This would require bonding the wafer to a carrier wafer after the holes opened, to prevent damage to the DRIE chuck from open holes. After the topside holes open to the backside, DRIE reactants would still enter the holes causing indeterminable levels of damage to the holes themselves (widening). Thus, it was decided to avoid this approach, but could prove to be successful in the future.

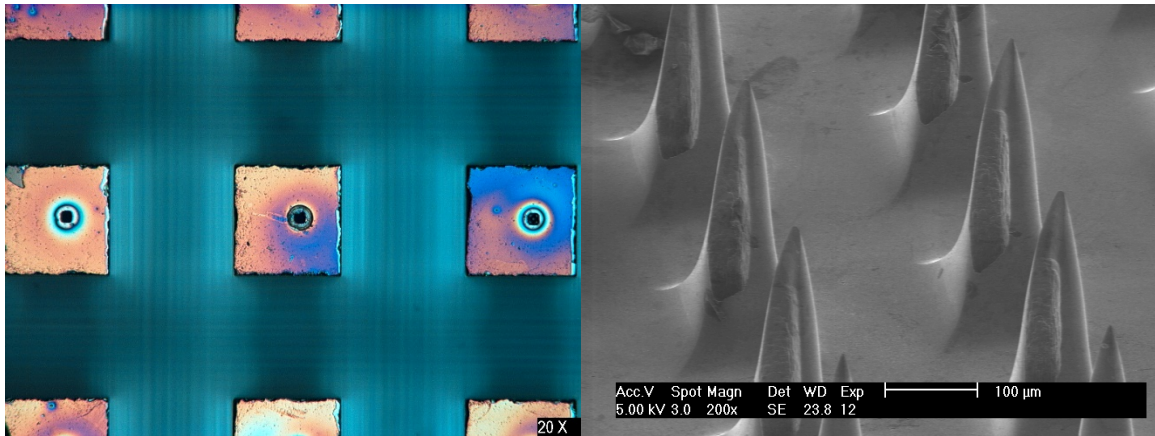


Figure 4.5 – A hole was required to extract ISF from SAW-fabricated chips.¹⁶

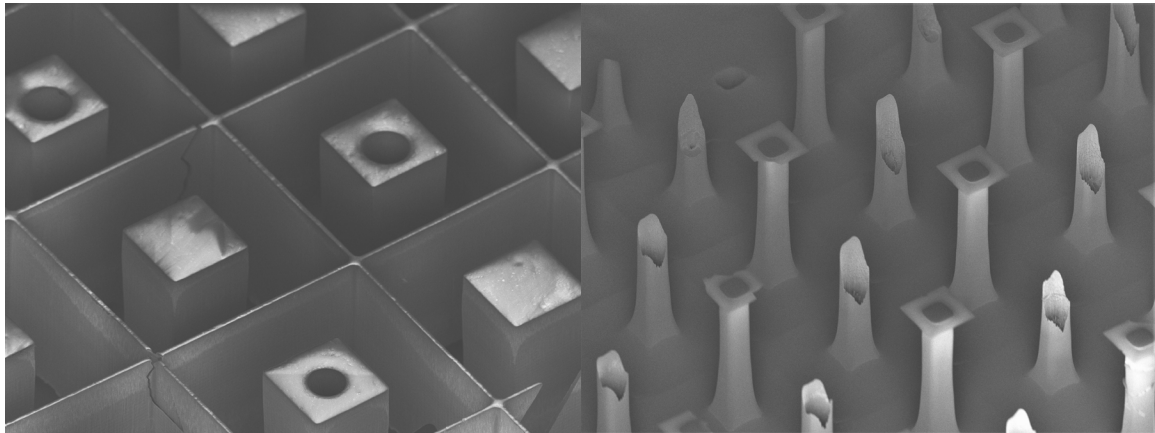


Figure 4.6 – The holes were unacceptably widened in the DRIE, if a two-step DRIE etch was used.

4.2.2 Testing a variety of shapes

Given the requirement for a single DRIE step to form the columns, and the likely impossibility of just including a hole in the column, a special, new, column design needed to be created which would lead to forming needles that were of similar shape to those created by the dicing saw (Figure 4.5). For efficiency, a single mask was designed that incorporated a variety of different column shapes on the same chip, so all of the potential designs could be made on the same chip

at the same time (Figure 4.7), to facilitate comparison using SEM imaging. Each chip featured 4x4 needles of each of the 16 designs (Figure 4.8). These shapes included slots, cuts, boxes and holes of varying sizes. The fabrication process purposely excluded any backside processing, as I was only concerned with realizing needle shape. A 750- μm thick wafer was used for rigidity. An 800-nm thick layer of PECVD silicon nitride was deposited to the column-side before DRIE to act as an etch-mask during the future HNA wet etch used to thin and sharpen the needles (§ 4.5).

4.2.2.1 – SPR-220 photoresist as DRIE etch mask

The first round of column shape testing with the mask employed MEGAPOSIT SPR-220-7.0 photoresist as an etch mask for the DRIE process. SPR-220 i-Line photoresist is a general-purpose, multi-wavelength resist designed to cover a wide range of film thicknesses.³⁵ The “7.0” stands for a nominal film thickness of 7.0 microns. However, the lengthy, 400 μm DRIE etch required by this project requires greater thickness. At slower spin speeds (1.8-2.0 krpm), thicknesses of approximately 10 microns are reliably achieved. Optical microscope results are displayed in Figure 4.7. Note that these depict column shape post-DRIE, before any thinning or sharpening.

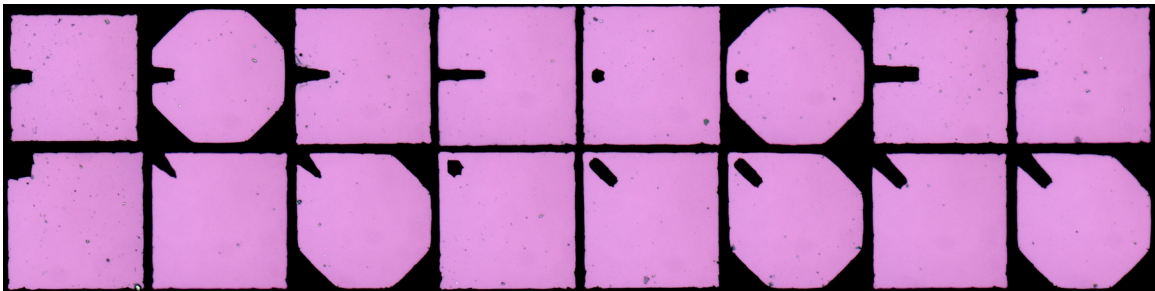


Figure 4.7 – 16 cropped optical microscope images showing a top-down view of all 16 column shapes tested

After thinning and sharpening, the needles were examined with scanning-electron microscopy. Results were mostly unsatisfactory. For nearly all column shapes tested, the hole or groove feature sizes were too small, becoming smoothed out during the sharpening etches (Figure 4.9). This approach was consequently set aside in favor of trying SiO_2 as an etch mask for DRIE instead

of photoresist (§ 4.2.2.2). However, there were two promising results that were initially missed, which were subsequently pursued and will be discussed in a later section (§ 4.2.2.3).

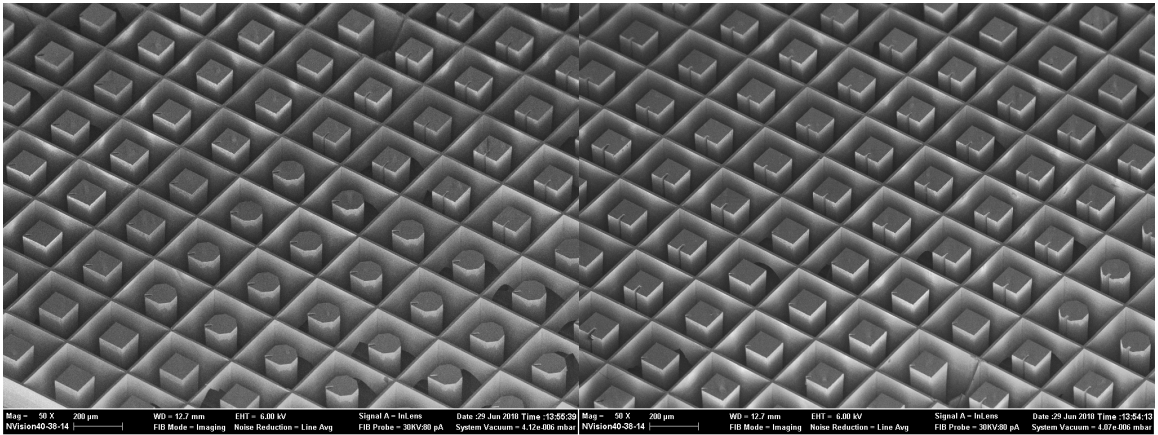


Figure 4.8 – Two SEM images showing column shapes for the test mask, pre-thinning and -sharpening

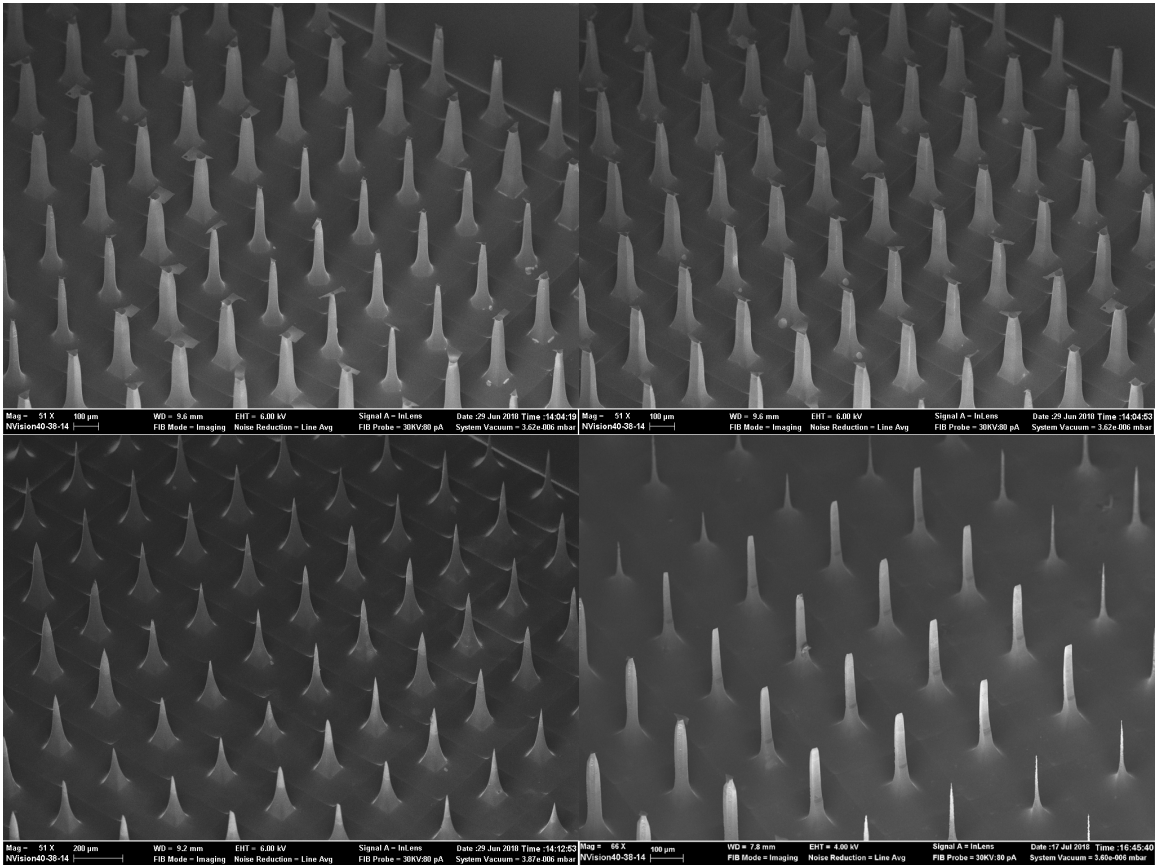


Figure 4.9 – SEM images showing some of the failed column shapes. The two top images are post-thinning step, but before sharpening. The two bottom images are post thinning and sharpening.

4.2.2.2 – PECVD SiO_2 as DRIE etch mask

Upon obtaining initial, disappointing results with the various column geometries, it was decided that the feature sizes of the cuts, slots, holes, etc. were too small, or did not protrude far enough

into the columns. Redesigning the photomask would have been time consuming considering I had little experience with the pattern generator and mask software at the time. So instead, I wanted to try silicon dioxide as the mask for DRIE, since oxide has an etch selectivity 3-10x higher than photoresist.³⁶ This meant that a SiO_2 thickness of 1-2 μm could be used as the etch mask (as opposed to 10 μm with resist), enabling smaller feature size patterning by using a thin resist to pattern the oxide. Additionally, the isotropic BOE etch would help undercut the features so the original photomask could be used while trying out larger feature sizes. The idea was also that this would serve more than one purpose: if the SiO_2 had turned out to be a viable solution, it would have minimized defects that occur from particulates in the photoresist or on the wafer surface.

Plasma-enhanced chemical vapor deposition (PECVD) silicon dioxide had to be used in lieu of higher-quality thermal oxide, because a thin film of silicon nitride must exist on the silicon surface to serve as the HNA etch mask for the thinning and sharpening steps. Without it, the tips of the columns would also etch, significantly reducing final shank height and/or tip sharpness. HNA attacks silicon nitride far slower than silicon, with a selectivity of more than 2200.³⁷ SiO_2 is attacked too rapidly by the hydrofluoric acid in HNA and therefore cannot be used as the sharpening etch mask.

Aiming to increase the isotropic undercutting effect of the BOE etch as much as possible, I used an SiO_2 thickness of 3 μm . The results were far worse than the SPR-220. Significant undercutting did occur, thanks entirely to the 21-minute BOE etch time required to get through the thick oxide layer. The photoresist frame around each column (to prevent footing in DRIE) created pockets where the BOE was allowed to etch inconsistently, producing some stunningly beautiful colors mid-etch due to film thickness differences (Figure 4.10).



Figure 4.10 – Optical microscope image of colors produced by differing SiO₂ film thickness mid-BOE etch

After completion of the BOE etch, the undercut bias was very pronounced. Figure 4.11 shows a few notable examples, after stripping the photoresist and approximately 50 μ m of DRIE.

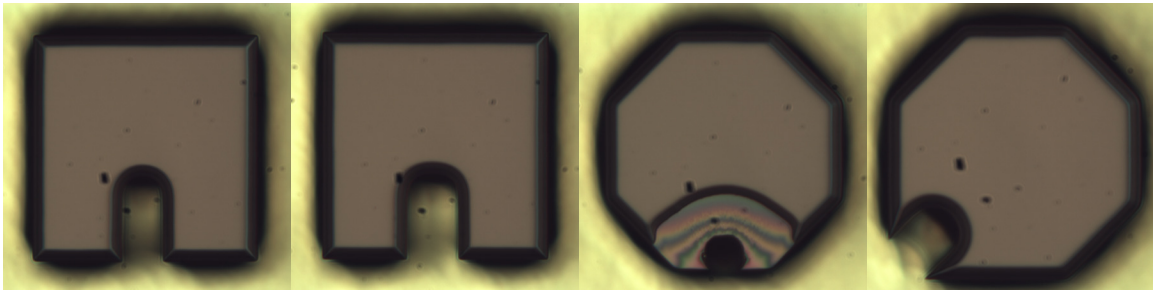


Figure 4.11 – Optical microscope images of undercutting seen with SiO₂ etch.

I did not consider the effects that undercut would have on the column frames. As mentioned previously, the 14 μ m-thick frames around each individual column reduces unacceptable levels of footing (base undercut) that occurs in the DRIE when used to achieve etch depths of >200 μ m. When present, they satisfactorily reduce footing, and if thin enough, they disappear quickly during the thinning etch, so as to not cause issues with needle sharpening. Here, they were almost completely etched away due to the BOE etch undercut of the oxide mask. The walls are visible for the first \approx 125 μ m of DRIE etch; they start to break through starting at \approx 150 μ m, and become completely removed by the end of the etch (Figure 4.12 and Figure 4.13). The result was footing that created columns that were too small at the base due to the footing to make viable needles.

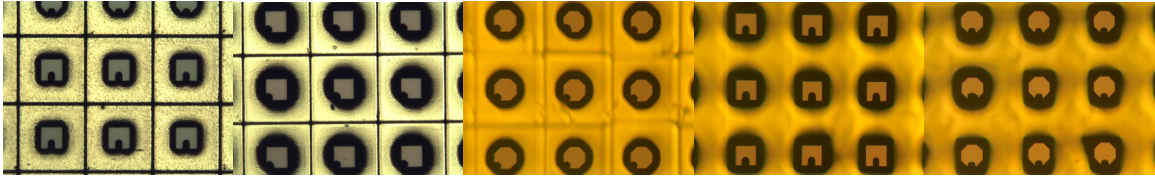


Figure 4.12 – Optical microscope images showing the degradation of the frame around the columns as the DRIE etch progresses. DRIE depths from L to R: 50μm, 113μm, 168μm, 340μm, 400μm

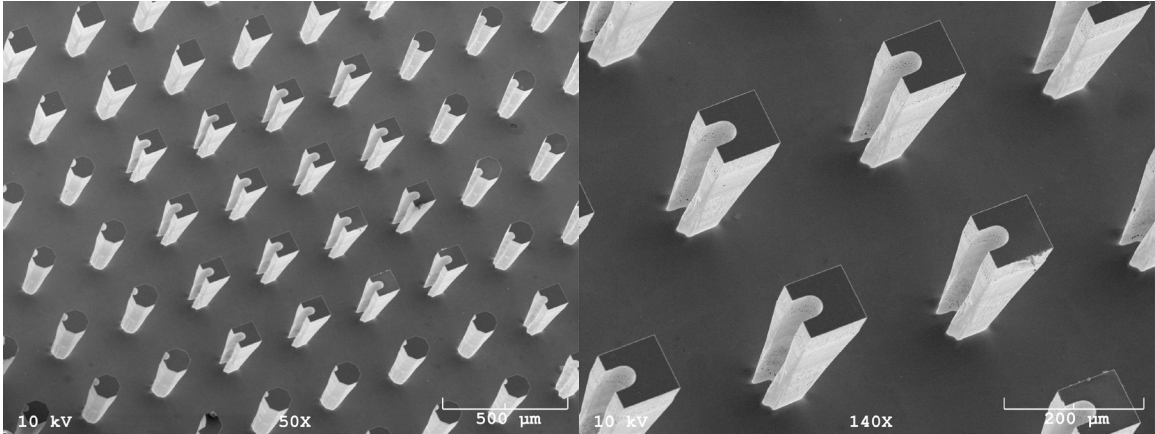


Figure 4.13 – Final SEM results show unacceptable levels of column undercut from DRIE. This left the bases too small to make viable needles

4.2.2.3 – SPR-220 results revisited

There were two promising results from the initial SPR-220 photoresist mask that produced final needle tip shapes similar to the saw-fabricated needles with the topside 10μm holes: the long, center slots, one slightly thinner than the other (Figure 4.14).

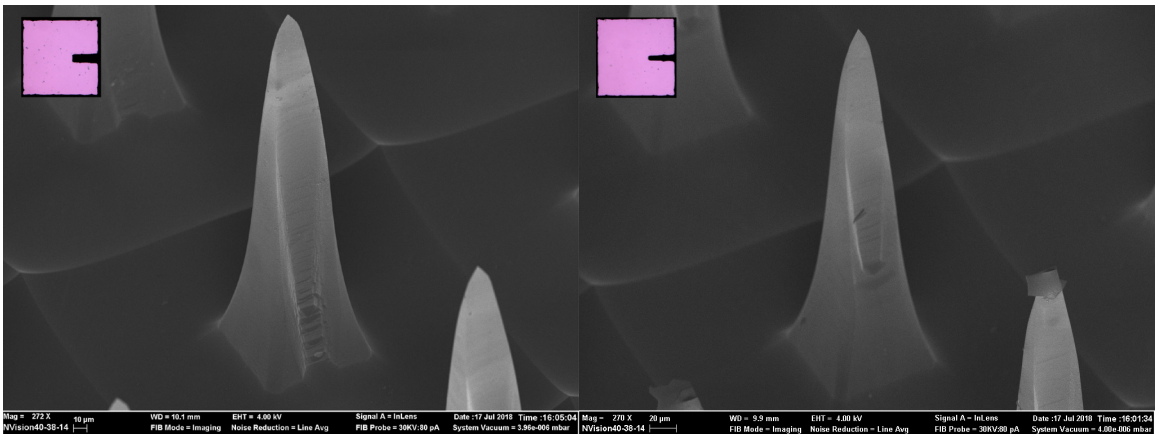


Figure 4.14 – Two SEM images showing the two successful-looking designs employed for further testing

After seeing positive results from the deep center slot designs, the thinner one was selected for the next round of testing. The thinner one was more desirable, because it did not continue all the way to the base of the column. When DRIE etching, large open areas etch more quickly and footing

at the bottom of walls produces undercut, while walls inside small openings slope in the opposite direction, closing themselves off. In the final design, the needles have a 30 μ m hole coming from the backside which is intended to protrude around 100-150 μ m beyond the silicon floor, into the columns (Figure 4.15). If the slot were to continue all the way to the bottom of the column, it would meet the 30 μ m backside hole before the column etch was complete, causing a backside leak of the helium used to cool the wafer. This would stop the etch, and a carrier wafer would need to be attached to plug the holes. This is inconvenient, and severely reduces etch rate, so it is wise to avoid when possible. It is also preferred for the interior hole to become opened and connected to the exterior groove during the HNA sharpening etch, not during the DRIE column etch. Additionally, it is desired that the hole opens as late in that sharpening step as possible, to minimize exposure of the interior holes to HNA, which would unpredictably widen them. HNA will etch any exposed silicon it touches.

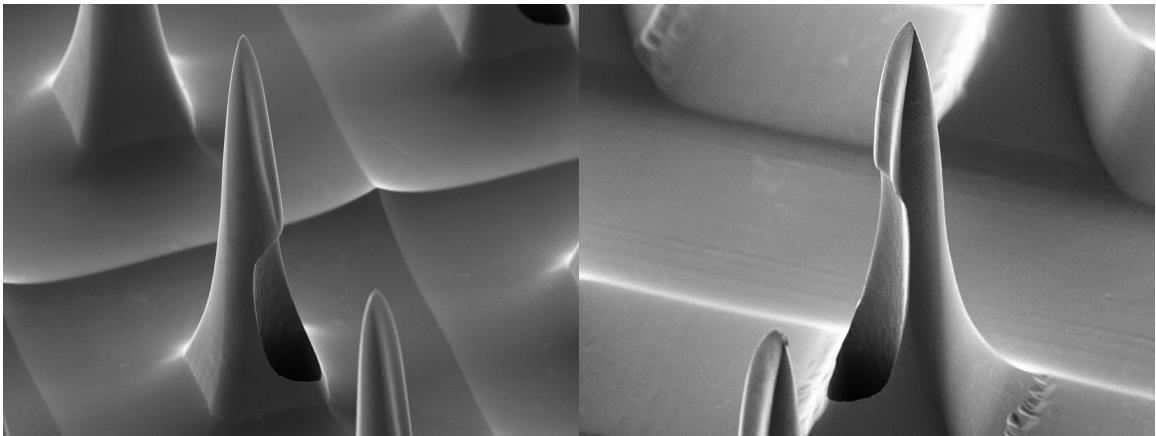


Figure 4.15 – Two SEM images showing hole from backside, after sharpening. (Left): DRIE design. (Right): Saw design.

4.2.3 The center slot problem

As promising as the center slot appeared, it was not in the correct spot. Having it positioned along the center of a side of the column, as opposed to facing a corner (Figure 4.16), created a shovel-shaped needle often with a blunt tip (Figure 4.14). I discovered that the shovel-shaped needle shape was ineffective for ISF-collection during development of the dicing-saw fabricated devices

(§ 4.3). In that case, the 10 μ m hole was being placed along a line perpendicular to a side and passing through the center. The resulting tip shape was blunt (Figure 4.22), much like was appearing in this DRIE case, and those devices were unsuccessful at ISF extraction. In response, I placed the hole along a diagonal on the dicing-saw design, which created a scoop-like needle shape which did extract ISF. Attempting to emulate that successful design in the DRIE process, I placed the slot facing a corner of the column instead of a side (Figure 4.16). Consequently, a DRIE device with a slot facing the side of the column was never fully fabricated, i.e. with via hole and collecting microchannels for *in vivo* collection testing.

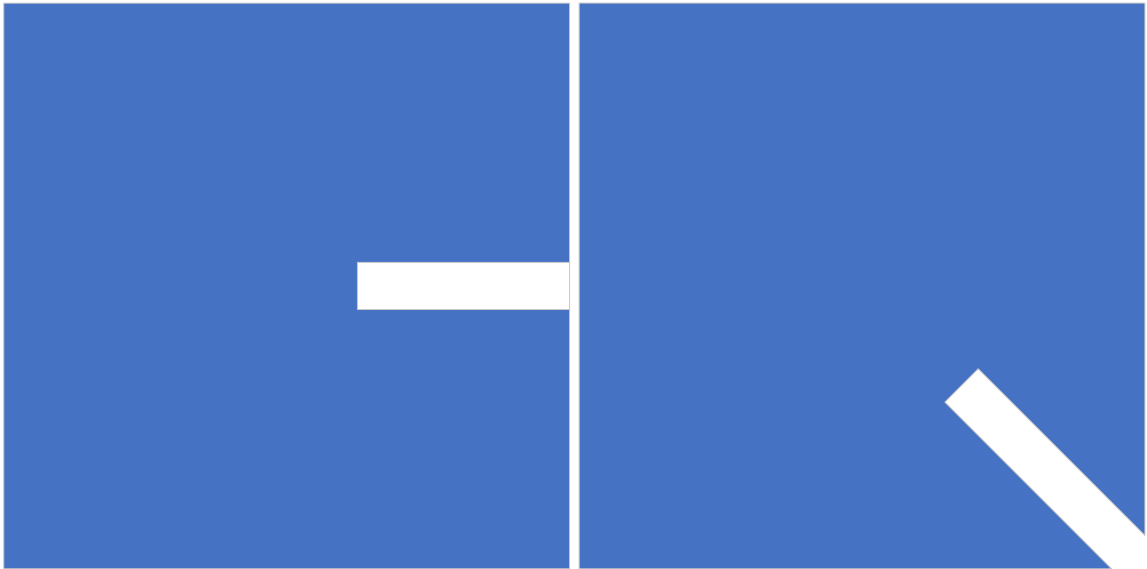


Figure 4.16 – Different slot orientations. Left: along the center of a side. Right: facing a corner.

4.2.4 Success – a diagonal slot

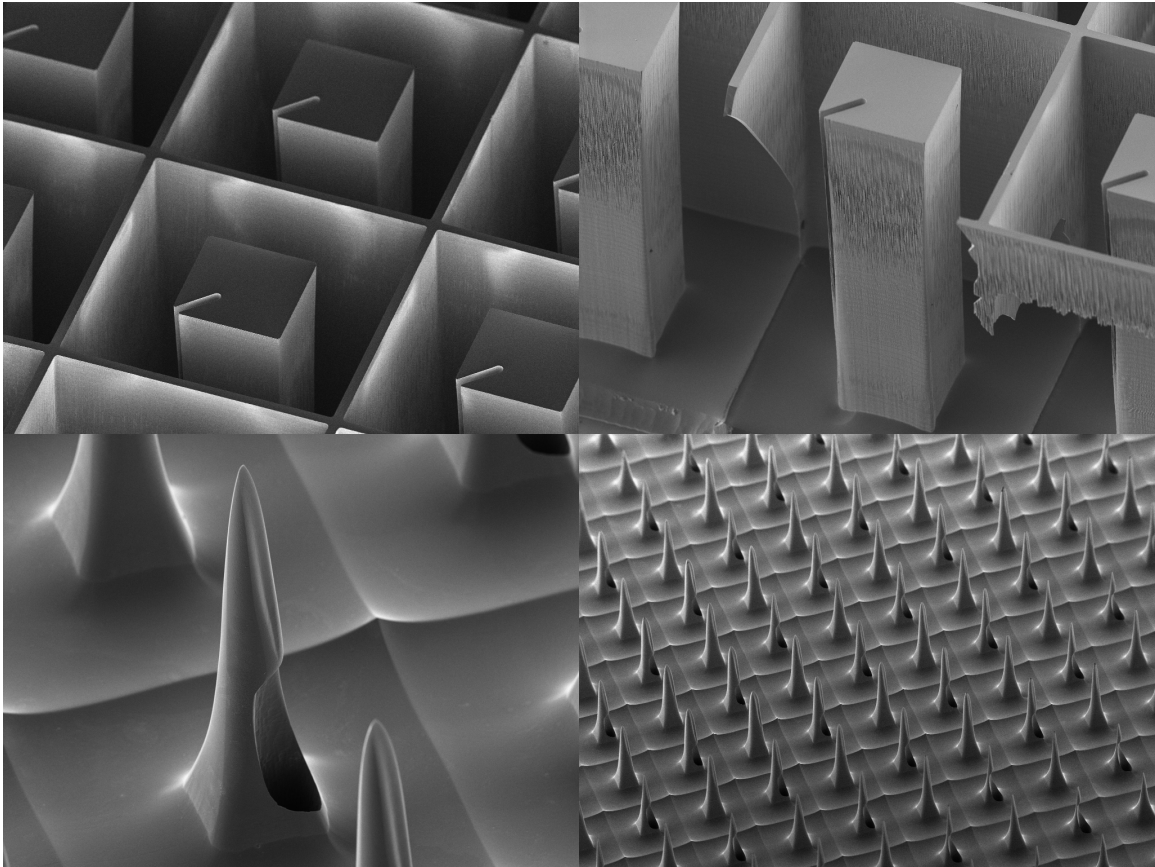


Figure 4.17 – SEM images of successful DRIE-fabricated devices. Top left: unsharpened, straight out of the DRIE. Top right: A view of a column after breaking the frame around, giving a clear view of a beautiful, minimally-tapered base. Bottom left: A sharpened needle. The slot didn't quite make it to the backside 30 μ m hole, but this device is still capable of ISF extraction. Bottom right: a view of many needles in the array.

When the slot was placed on the diagonal, facing a corner, a nice “scoop-like” shape was produced at the tip. This shape was successful in collecting dermal ISF. It is hypothesized that this shape, which is similar to the snake fang shape created by Mukerjee, is necessary for flow of ISF from tip to base, where it is drawn by capillary action through to the backside microchannels. Bench tests results revealed that all designs were capable of drawing water into the microchannels, even those with an opening only at the base of the needle. However, in skin, only those needles with a groove along the side that extends to the tip were successful in extracting ISF. It is hypothesized that the groove prevents skin from completely sealing to the surface of the needle, at the tip, providing a channel for ISF to flow into the via hole.

Although the design in Figure 4.17 worked, the slot did not quite connect with the 30 μ m via hole. This could pose an impediment to collecting ISF. Therefore, I redesigned the mask to widen the slot, which would not taper as quickly and would meet the backside hole. This redesign is in fabrication, at the time of publication of this document.

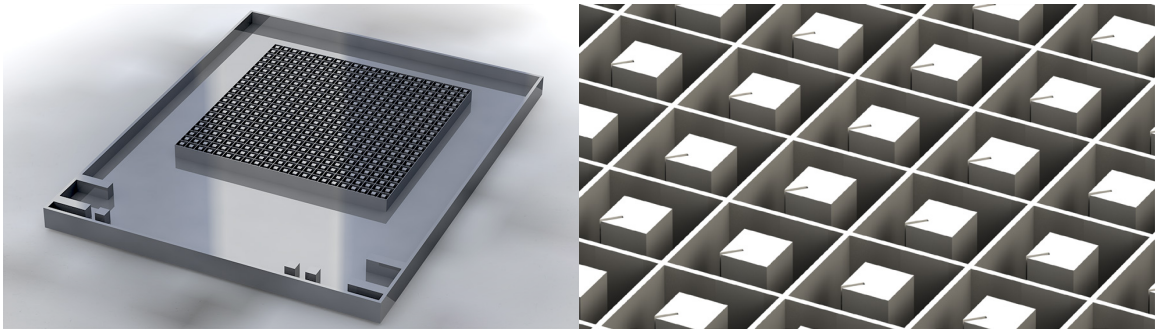


Figure 4.18 – CAD-rendered images of the final DRIE chip.

4.3 The frontside: dicing saw fabricated columns

An initial aim for this project was to develop a working, all-DRIE process for microneedle fabrication. Saw-fabricated devices were not initially considered, as they had been previously developed and demonstrated, but had low throughput and yield.¹³ However, in the face of all the hardship incurred in the early stages of the DRIE design, a sawed column design was added to development. Some elements of the previous design were incorporated, although significant changes have been made, with the aim of increasing the collected ISF volume:

- a) The number of hollow, collecting microneedles was increased from 20 to 162 per chip
- b) The depth of the microchannels and reservoir was doubled
- c) The opening in the glass covering the reservoir was decreased to reduce evaporation and to increase reservoir fill volume

Additionally, valuable insight into requisite needle shape was gained from repeating this design.

4.3.1 Design parameters

A wafer dicing saw (Figure 4.19) is a type of saw which uses a high-speed spindle and circular diamond dicing blades to cut silicon and other solid-state materials into rectangular pieces, or die. It is typically used in the semiconductor packaging industry post-fabrication to cut silicon wafers into hundreds to thousands of individual chips. Usually, it is intended to cut nearly or entirely through a wafer, but this process can be exploited to form grooves by making many equally-spaced parallel cuts at a specified depth. Columns are created after rotating the wafer 90 degrees and repeating the cuts.

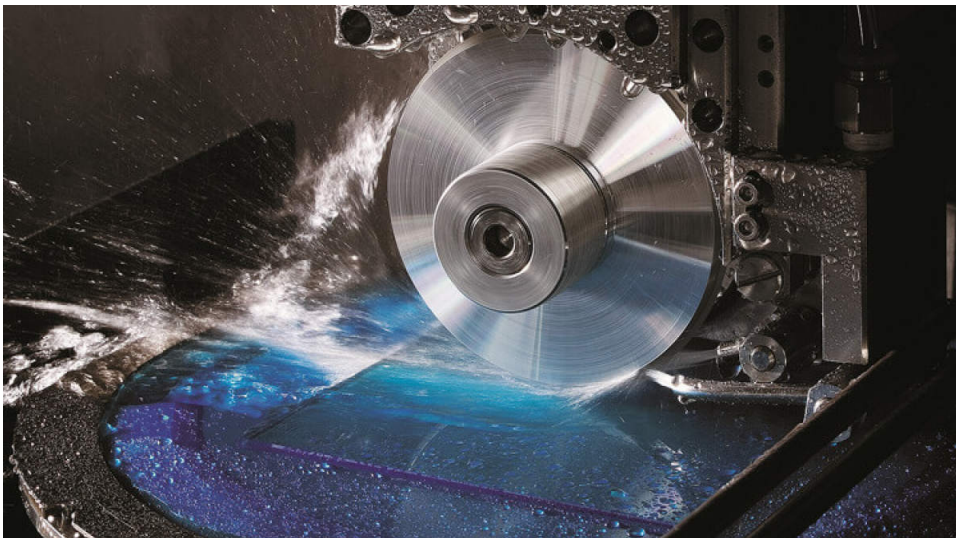


Figure 4.19 – A dicing saw in action. Image courtesy of DISCO Corporation.

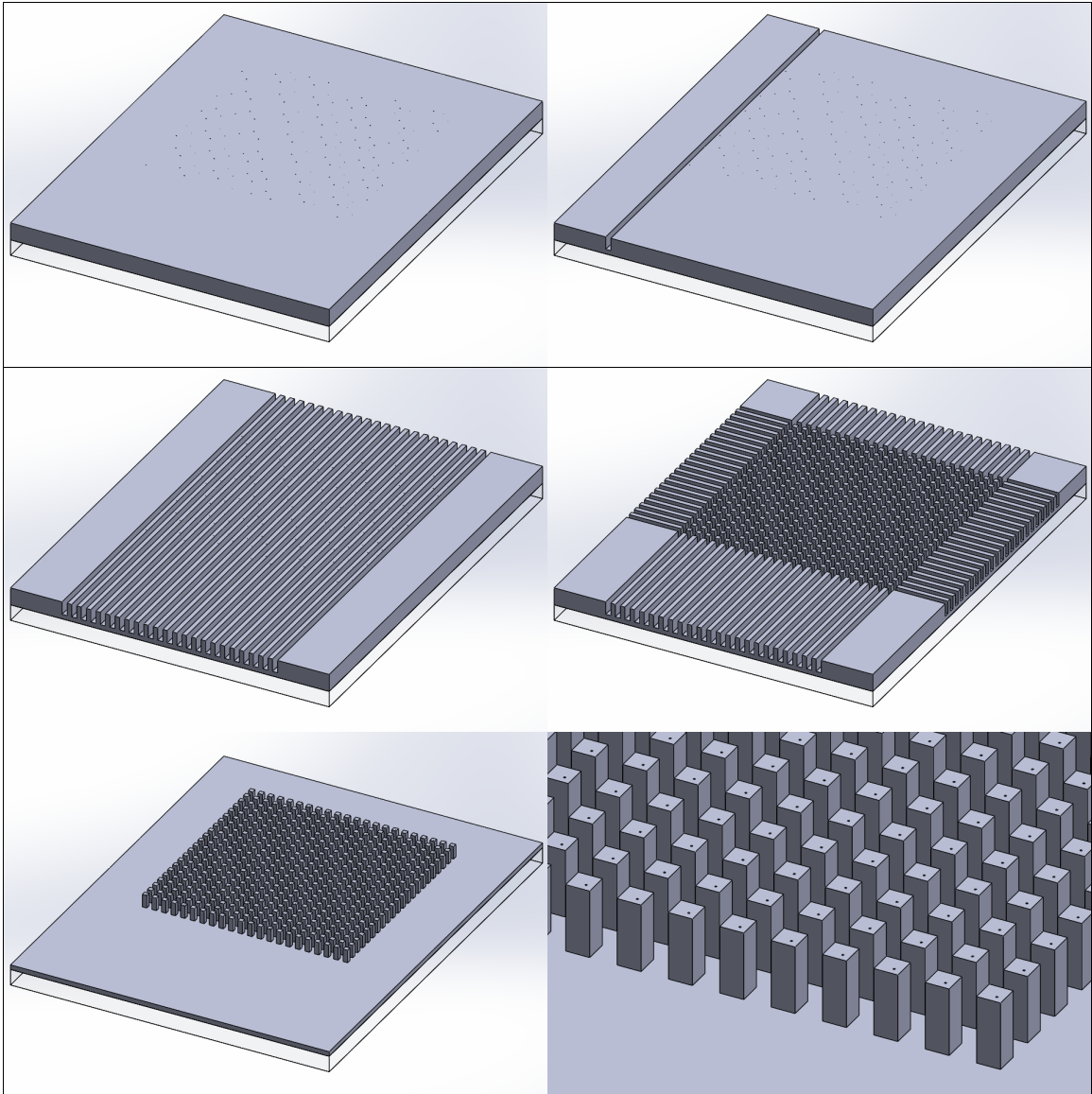


Figure 4.20 – the dicing saw cuts columns into the silicon surface with many equally-spaced parallel and perpendicular cuts. The cuts' diameter is equal to the width of the blade. After the columns are formed, remaining silicon surrounding them is removed with a wider blade. This leaves only the columns on the wafer. Shown in the figure is one single chip. The process is performed with an entire wafer at once, but the resulting document possesses too many faces for SolidWorks to handle.

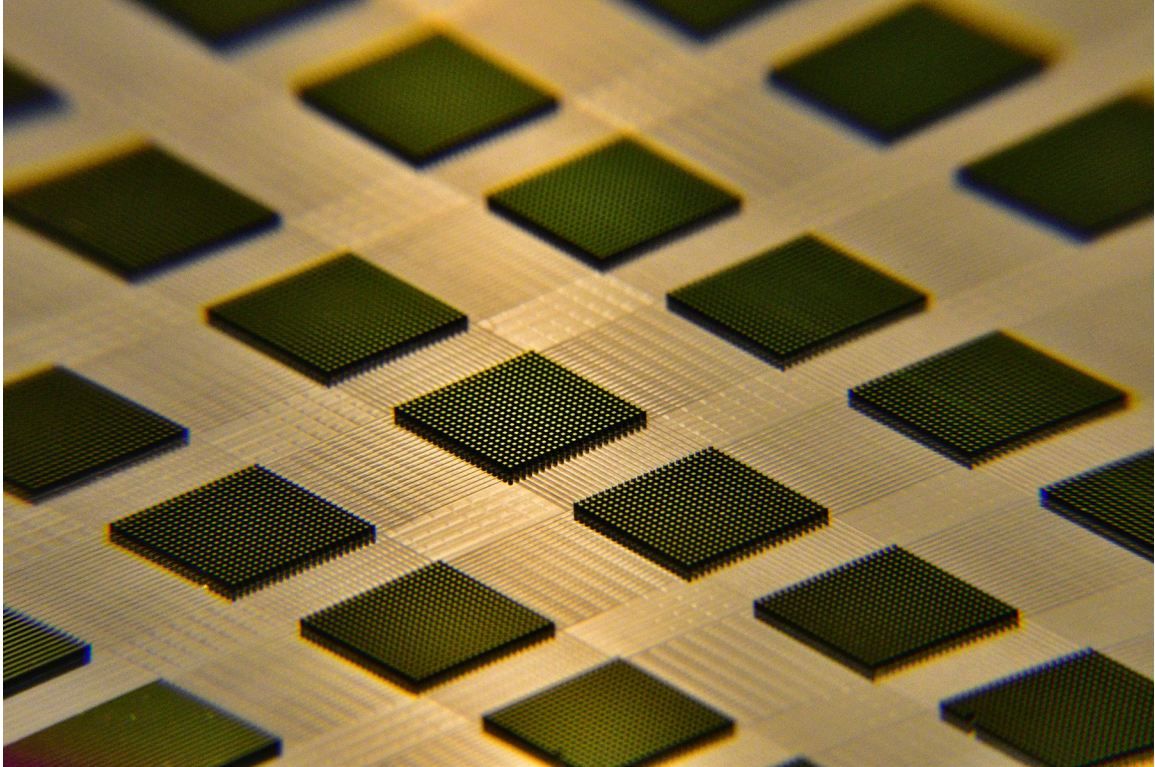


Figure 4.21 – columns produced by dicing saw after removal of the field

The column shape produced by the saw (Figure 4.21) is very similar to the ones produced by DRIE. The main differences between the two designs are, a) the lack of a surrounding frame (Figure 4.17), b) the surfaces are rougher, c) the saw kerf produces a column that is wider at the base than at the top, and d) some chipping at the top edge of the columns is inevitable. However, the roughness and chipping is much reduced or removed during the sharpening etch.

4.3.2 The in-house dicing saw

The first attempt to saw-fabricate these columns was with the Kulicke & Soffa 775 (circa 1990s) saw in the lab at the University of Maine. The stage of this “old” saw is not completely level, and the optics are too poor to reproducibly and accurately align to the 10 μ m hole that must be positioned precisely off-center within the columns. I attempted to highlight the holes by spinning photoresist and letting it drain through them before a hard bake. This did create visible rings around each hole, but still required me to estimate the centers and as a result, alignment was not accurate enough and for much of the wafer, hole placement ended up being off-spec enough

to cause significantly different needle tip shapes (Figure 4.22). If the hole is placed too near the geometric center of the column, it produces volcano-like needle tips (Figure 4.22, bottom left).

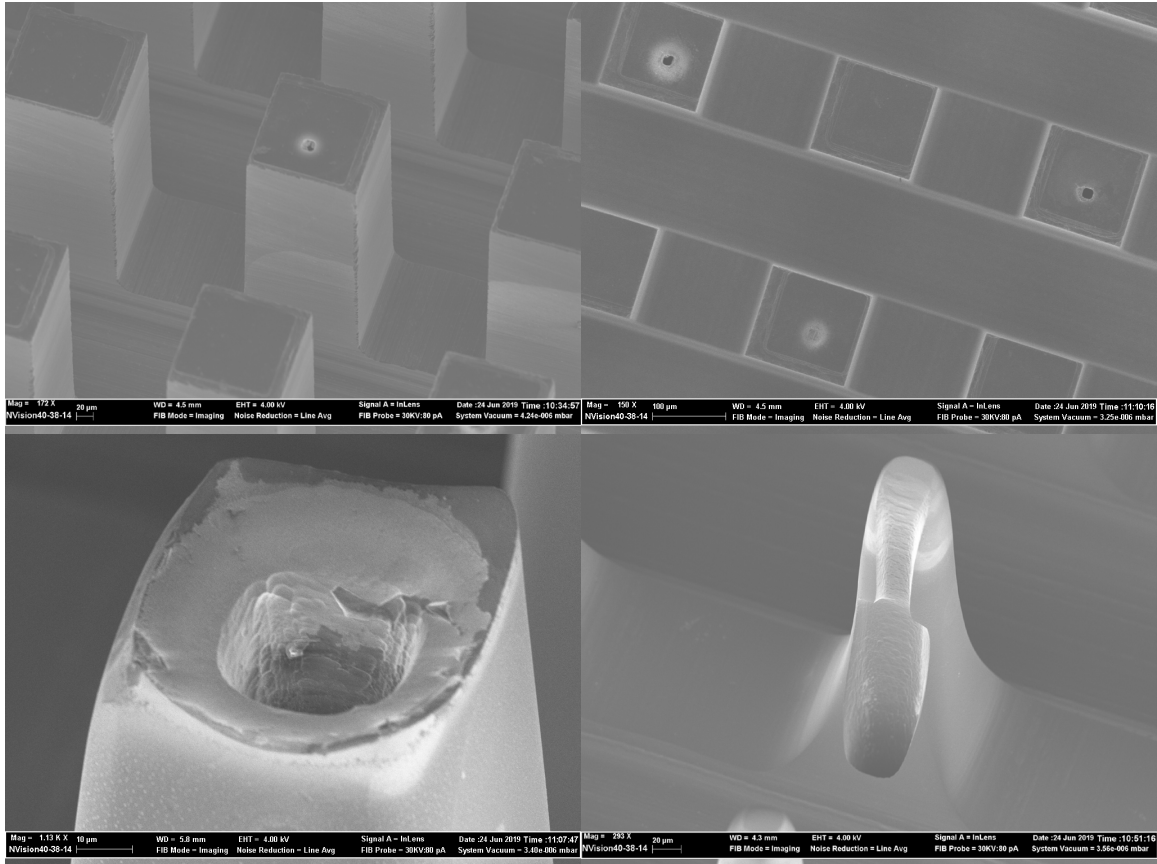


Figure 4.22 – SEM images of the first attempt to fabricate columns with the dicing saw. Major inconsistencies in alignment produced a variety of different shapes as the columns were sharpened into needles. The successfully-aligned needles looked satisfactory (bottom right), but they were rare.

A few chips from the run were salvageable, as they had accurate hole placements along enough of the columns on the chip to create a potentially-working device (Figure 4.23). Alas, they did not work. This was quite confusing, because based on what was known, they *should* have worked. This was the same design published in 2004, which successfully extracted ISF.¹³ Several ideas were mused upon, including 10 μ m hole DRIE slopes, wafer resistivity differences affecting etching, and etchant temperature. There was a slight difference between Mukerjee’s chips and these: the slope of the groove in the chip was much steeper in these chips compared to Mukerjee (Figure 4.24). The direction that the groove was pointing was also different – the prior devices had the

groove aligned with a corner, rather than the side of the column. In future designs, using the DISCO DAD 3240 (§ 4.3.3), the hole (saw design) and groove (DRIE design – § 4.2.4) position were changed to face the column corner. Additionally, the importance that needle tip design has on the ability to extract dermal ISF was again revealed.

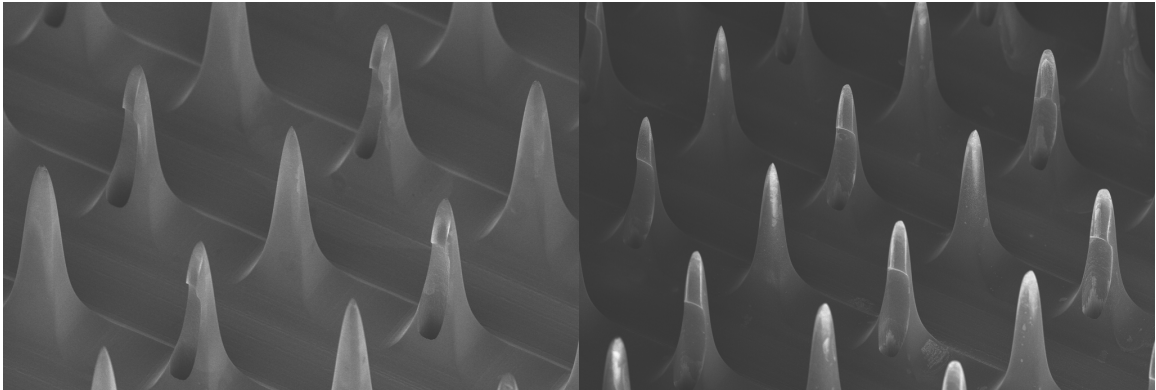


Figure 4.23 – SEM images from a couple of the four salvageable chips from the run

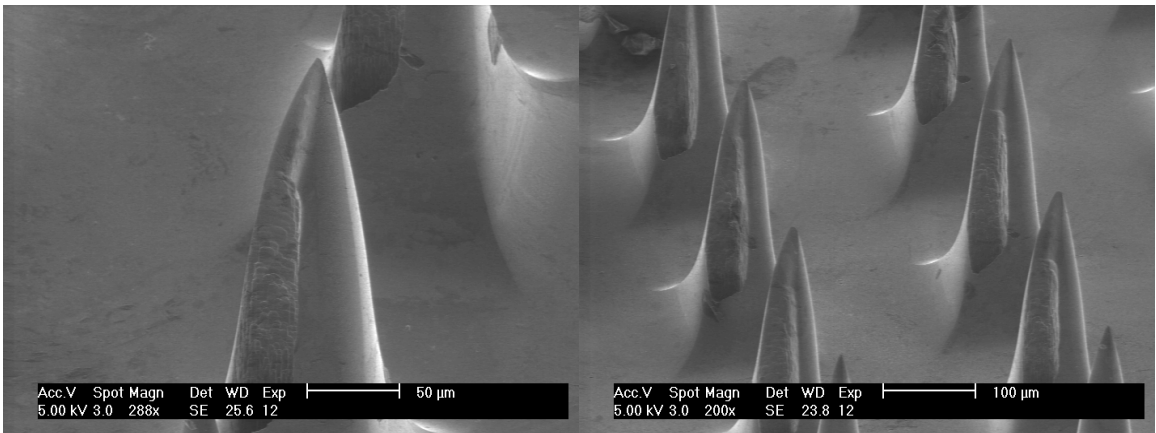


Figure 4.24 – SEM images showing needle tips of Mukerjee 2004 (dubbed the “snake fang”)¹³

4.3.3 DISCO DAD 3240, Andover, MA

Advances in dicing saw technology since the release of the Kulicke & Soffa 775 have been significant. For the IC industry, high throughput is of paramount importance for maximizing profits. Automation and machine learning are means for achieving high throughput, with high precision and minimal loss or error, compared to strictly-human operators. Major advancements of relevance to this project include the far improved imaging and alignment capabilities, high positional precision, and dynamic control of cut depth. DISCO Hi-Tec, an advanced dicing saw

manufacturer out of Japan, has a sales facility in Andover, MA, where they also perform contracted work for university projects and startups. I visited the facility twice to work closely with the staff who taught me how to operate the DAD3240 machine, and to design a recipe for column formation. Results obtained with the DAD3240 were extremely positive, and I am very thankful to the crew at Disco for their assistance.

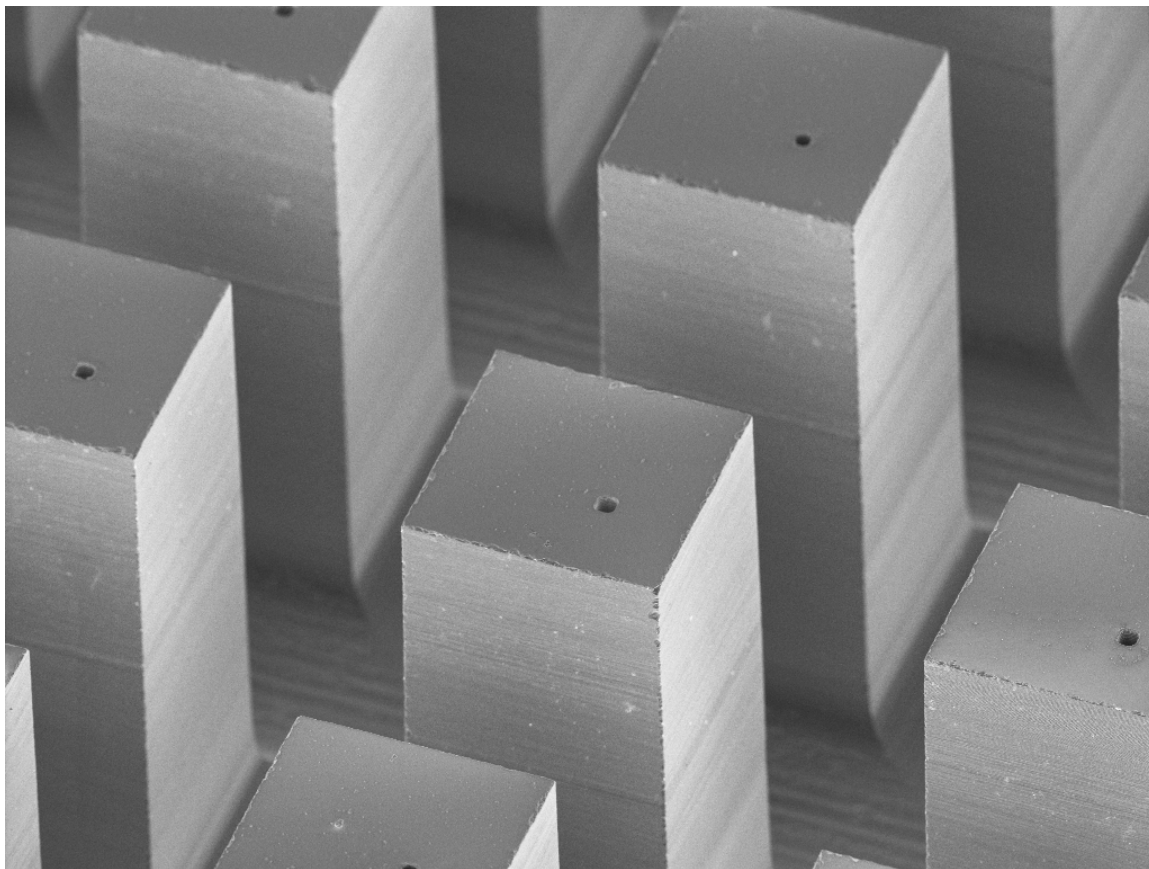


Figure 4.25 – Columns showing proper placement of the 10 μ m hole, obtained using DISCO DAD3240.

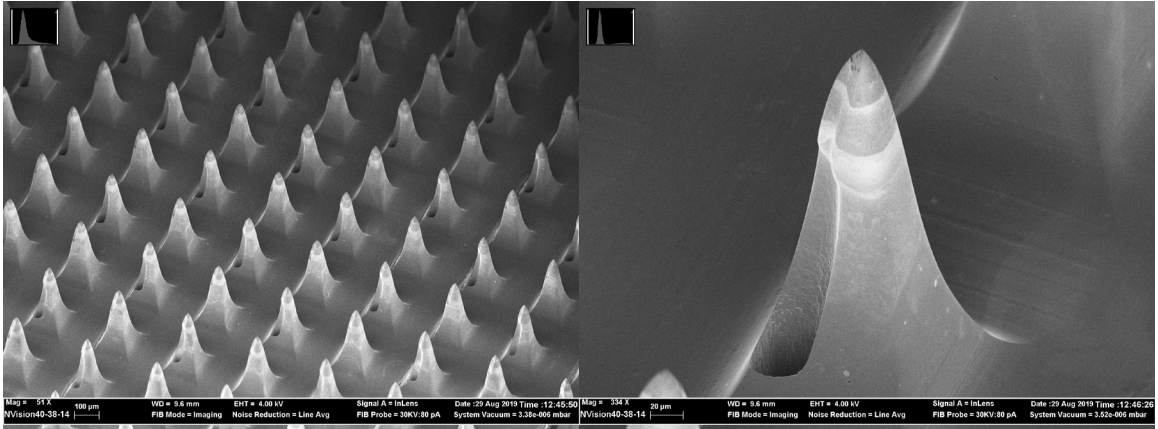


Figure 4.26 – Results from the first round of sharpening of the DISCO-fabricated wafer.

The first round of sharpening tests immediately showed that the tips could look much better with different placement of the 10 μ m hole (Figure 4.26). These were not sharp enough, which required some tinkering with the sharpening recipe. By using more time on the initial thinning step, the needles sharpened up sufficiently to pierce skin, and they successfully extracted ISF from human skin (Figure 4.27).

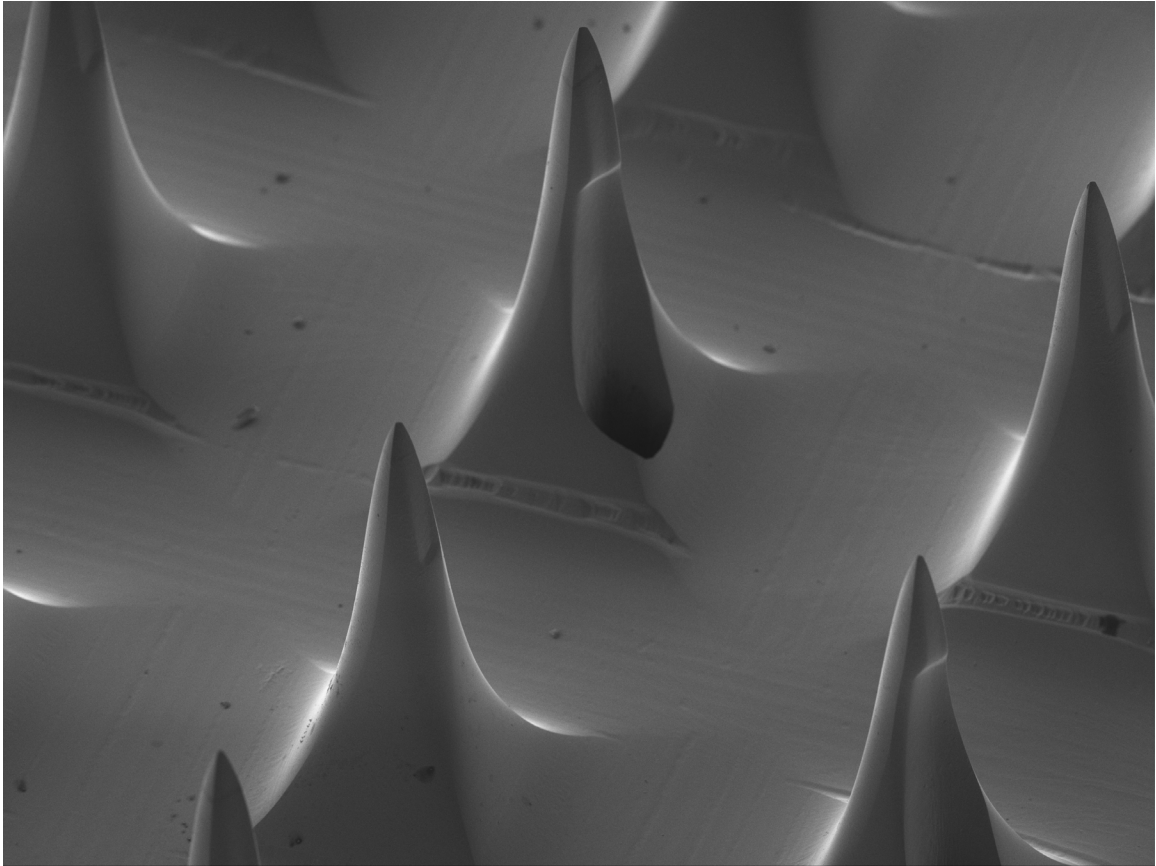


Figure 4.27 – SEM image of sharp needles, which extract ISF

4.4 Dicing from wafer to individual chips

After anodic bonding the glass to the silicon wafer (§ 4.1.2), the wafer is diced into individual microneedle array chips, using the UMaine dicing saw (Kulicke & Soffa). Wafer tape is first applied to the glass side of the bonded wafer, and the chips are cut all the way through both the silicon and the glass. Tape is removed by exposure to UV light for roughly 30s in sunlight. This also works on a cloudy day, but requires longer exposure times. At night, the tape can be cured with UV light from the lamp of a mask aligner. With the current design, a single 4-inch wafer will produce 36 individual chips.

4.5 Microneedle sharpening and oxidation

After the wafer has been diced into chips, the columns are sharpened into needles. This uses a biphasic etch process with a wet etchant called HNA, designed to etch silicon.³⁸ The acronym stands for hydrofluoric acid (HF), nitric acid (HNO₃), and acetic acid (AcOH). The etch rate of the

silicon is dependent on the ratios of the three acids (see § B.2); the mixture used in this process is 1:8:1 by volume of HF:HNO₃:AcOH, respectively (see Table G-1 for bottle concentrations). The mixture etches silicon due to the formation of an oxide layer (SiO₂) on the surface by the nitric acid, and subsequent removal of the oxide layer by the hydrofluoric acid. The acetic acid acts as a surfactant.

The “biphasic” nature of the etch comes from the need to first thin the columns as evenly as possible, rounding them from square columns to a more cylindrical shape, before sharpening them into sharp cones. The extent of both of these steps is important – too much thinning and the resulting needles are overly thin and may break during insertion; too little thinning and the resulting needles are thick and may not be sharp enough to pierce skin, or the interior boreholes may not open up. To gauge how much etching is required, many different etch times were investigated and resulting the chips were observed under a SEM.

4.5.1 Thinning

The first step is to thin the columns. The step takes place in a Teflon beaker of HNA (Figure 4.28).

The beaker cannot be glass, which would be attacked by the HF. Any polymer which can withstand nitric and hydrofluoric acids will do. The temperature of the mixture is raised to 50 °C by heating a water bath around the beaker containing the HNA. A larger glass beaker is fit around the HNA beaker, and some water is added to facilitate the heat transfer. Heating increases the etch rate, and helps limit effects of day-to-day room temperature variations in the lab, which could cause different etch rates, affecting timing.

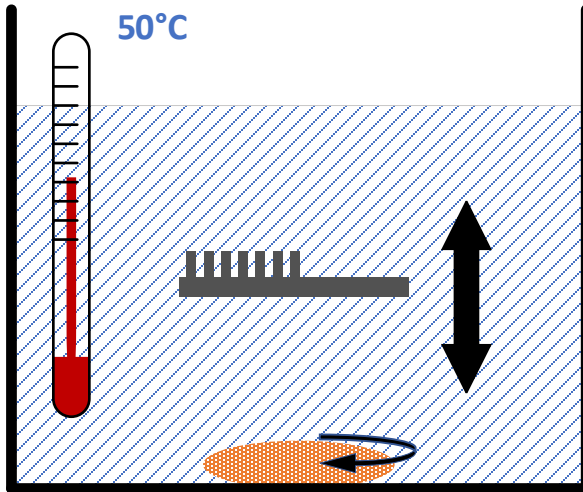


Figure 4.28 – Columns are thinned in a beaker of HNA.

In order to limit the effects of diffusion as much as possible, reactants must be allowed to reach all surfaces equally. This is accomplished by stirring the solution with a magnetic stir bar which rotates at roughly 2-Hz. The exact speed is not critical, but the solution should not be stirred too rapidly, as a small amount of diffusion will help keep the columns thick at the base due to the natural masking effect of being at the bottom of the silicon chip, farthest from the etchant bulk and surrounded by the columns. In addition to the stir bar, the chip is moved up and down in the solution with a pair of tweezers to enhance delivery of reactants to the base of the columns. The silicon nitride caps on each column act as an etch mask, preventing the height from shortening (Figure 4.29).

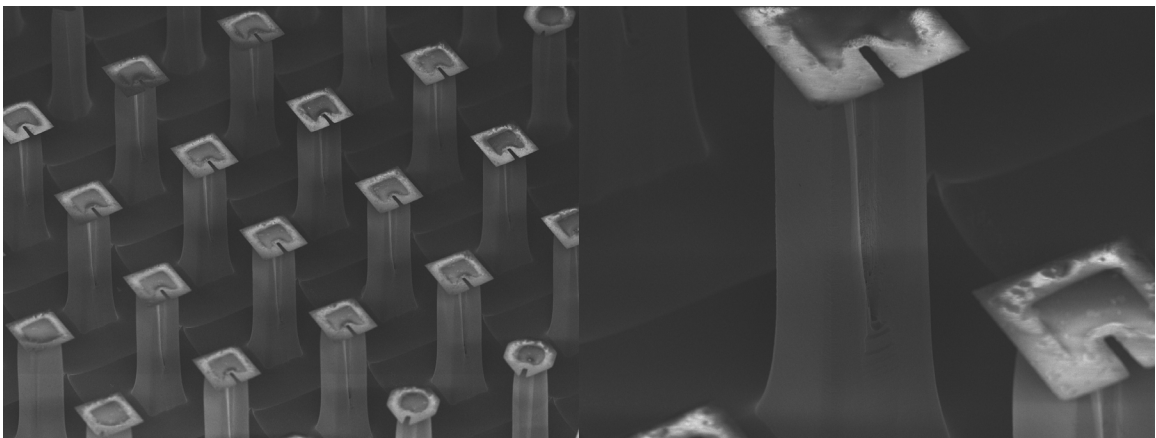


Figure 4.29 – An example of what some columns look like mid-thinning. This is from the round of shape testing described in § 4.2.2. These columns do not have backside holes, which typically open up in this step.

4.5.2 Sharpening

The second step of the etch sharpens the thinned columns into needles. The procedure takes place at room temperature and uses the same ratio of acids as the thinning step (§ 4.5.1). This time, however, the stir bar is removed. The chip is flipped upside down in the etchant and is held stagnant (Figure 4.30). This etching process naturally produces gas, which collects at the base of the columns, since the chip is upside down. The gas therefore inhibits liquid etchant from reaching the base of the columns, reducing the etch rate there. The liquid readily reaches the tips, resulting in a quicker etch rate at the tips compared to the base. This is allowed to persist until the tips are so sharp that the nitride caps have nothing to adhere to and fall off. The needles are, at this point, adequately sharp enough to pierce skin.

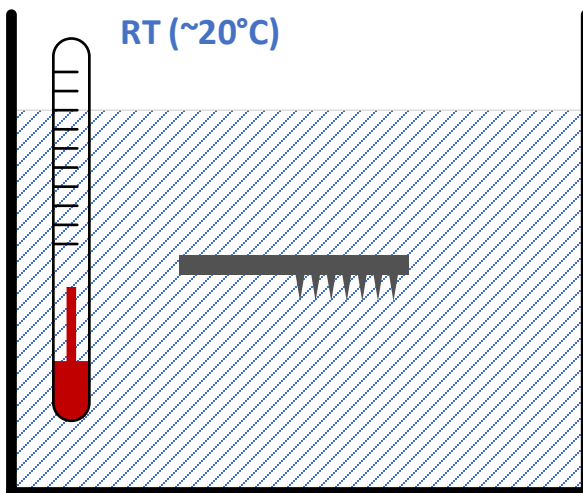


Figure 4.30 – Columns are sharpened in a beaker of HNA.

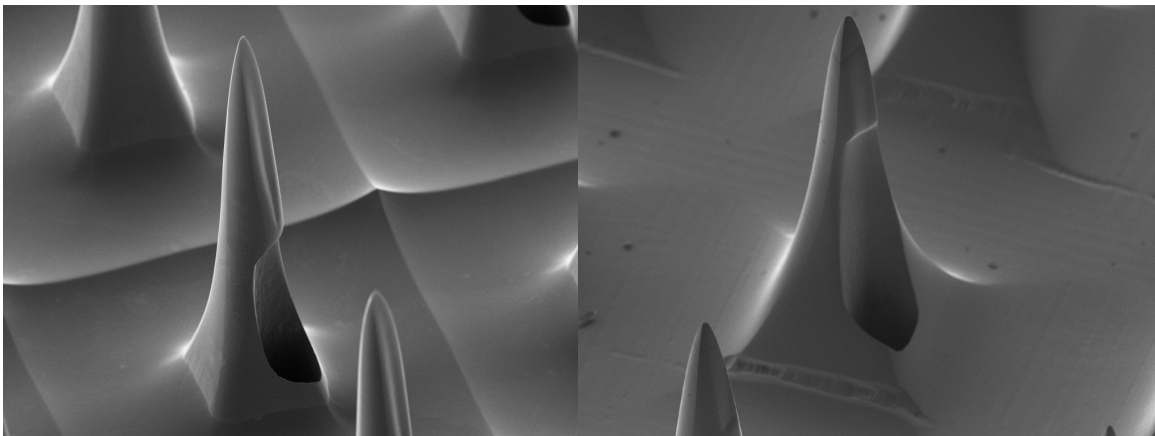


Figure 4.31 – Columns after sharpening for both designs – DRIE (left) and dicing-saw (right).

4.5.3 Oxidation

The HNA etch leaves the silicon surface bare (free of oxide), which is extremely hydrophobic. As ISF contains a high percentage of water, a hydrophobic surface is undesirable and will act to repel the fluid. Luckily, silicon dioxide is remarkably hydrophilic, and is relatively easy to create on silicon by a chemical oxidation process. The needles are submerged in nearly-boiling (70-80 °C) nitric acid for several hours. The acid enters the microchannels as well, oxidizing their silicon surfaces. Most of the time, the solution will not enter the channels without the help of a slight vacuum. The entire beaker, containing the nitric acid and chips, is placed inside a vacuum chamber. The vacuum encourages bubbles to leave the channels, allowing the acid to enter.

4.6 Cost analysis

A relative cost analysis was performed, comparing the DRIE and saw methods of column fabrication. A true, manufacturing cost analysis is at this point impossible, due to the process development status, and reliance on external service for the dicing saw. However, it is useful as it gives some insight into the mass-production viability for each method.

There are several things to note pertaining to scaling up for production. The fabrication currently uses 4-inch wafers, producing 36 chips each. If production was scaled up to 12-inch wafers, 7-9x more chips could be placed on each wafer, yielding somewhere between 250-325 chips per wafer, depending on wafer uniformity limitations of the processing equipment. This would be the single greatest cost-reduction strategy for the DRIE method, as timing for all steps should not change. Less cost-reduction (per chip) would be achieved with the saw method, as dicing saw time for column creation would increase by approximately 3x (3x larger in both x and y directions).

The actual rates are not that important, as they change frequently, and differ greatly between different facilities, and between internal, external-academic, and industry users. For example, Table 4-2 shows hourly rates in USD for six different universities. Additionally, most academic

facilities pose a monthly or annual cap on billing, and all usage beyond that cap is charged at a lesser rate, or free. Hence, it makes more sense to report the cost analysis as a ratio of cost between the two methods, rather than absolute cost. Relative ratios between rates of different processes will experience less variation over time, unless major advances in cost are made for a particular process. It is likely this cost comparison will become significantly outdated within just a few years from now, but nonetheless it is useful insight into the current cost climate for both dicing and DRIE.

Table 4-2 – Process rates from a variety of universities

	DRIE			Dicing		
	<i>Internal</i>	<i>Ext. Acad</i>	<i>Industry</i>	<i>Internal</i>	<i>Ext. Acad</i>	<i>Industry</i>
Harvard ³⁹	55	71.50	325	30	39	130
UMaine ⁴⁰	70	140	140	35	70	70
Utah ⁴¹	100	153	200	47	71	94
Illinois ⁴²	480	480	900	--	--	--
CUNY ⁴³	45	45	135/225	23	23	115
Washington ⁴⁴	70	70	210	50	50	150

Table 4-3 shows a rough, relative cost-comparison table for 4-inch wafers using published external-academic process rates from Harvard University. Harvard was ultimately chosen for the analysis because their rates are reasonably inexpensive, and they are located in a hot-spot of biomedical research.

Table 4-3 – Cost analysis

	DRIE	Saw
Number of Photomasks Required	1	1
Number of Photolithography steps required	1	1
DRIE Process Steps, time in etch chamber	55+, 9.2 hours	30, 5 hours
Dicing saw process steps	0	2 steps, ~3 hours total
Raw cost	$(9.2 \text{ hrs} * \$71.50/\text{hr}) = \657.80	$(5 \text{ hrs} * \$71.50/\text{hr}) + (3 \text{ hrs} * \$39/\text{hr}) = \$474.50$
Relative cost ratio	1.4	1

Current relative costs make the DRIE method around 1.4x the cost of the dicing saw method.

Table 4-4 – Cost analysis, hypothetical 12-inch scaleup

	DRIE	Saw
Number of Masks Required	1	1
Number of Photolithography steps required	1	1
DRIE Process Steps, time in etch chamber	55+, 9.2 hours	30, 5 hours
Dicing saw process steps	0	2 steps, ~9 hours total
Raw cost	$(9.2 \text{ hrs} * \$71.50/\text{hr}) = \657.80	$(5 \text{ hrs} * \$71.50/\text{hr}) + (9 \text{ hrs} * \$39/\text{hr}) = \$708.50$
Relative cost ratio	1	1.1

With a 12-inch scaleup, DRIE becomes cost-comparable to the dicing saw.

Table 4-5 – Cost analysis, hypothetical 12-inch scaleup with 2x faster DRIE

	DRIE	Saw
Number of Masks Required	1	1
Number of Photolithography steps required	1	1
DRIE Process Steps, time in etch chamber	55+, 4.6 hours	30, 2.5 hours
Dicing saw process steps	0	2 steps, ~9 hours total
Raw cost	$(4.6 \text{ hrs} * \$71.50/\text{hr}) = \328.90	$(2.5 \text{ hrs} * \$71.50/\text{hr}) + (9 \text{ hrs} * \$39/\text{hr}) = \$529.75$
Relative cost ratio	1	1.6

Significant advances in DRIE technology have occurred since the release of the STS DRIE at the University of Maine, which was manufactured in the early 2000s. The advances have enabled far faster etch rates. If a newer DRIE was used, with the recipe modified to be faster, a 2x faster etch rate would be a conservative estimate. And this is where one would see major reductions in cost; the DRIE method quickly becomes cheaper than the dicing saw.

Clearly, the analysis presented here takes some major shortcuts and simplifications, and much more optimization may be performed if these devices were to be manufactured on an industrial scale. However, costs are very volatile and company-specific; internal data would be needed to assess.

CHAPTER 5 – TESTING METHODS & RESULTS

5.1 Water draw

The microneedle arrays rapidly draw water into the microchannels via capillary action alone. The chips take only a fraction of a second to fill completely. Figure 5.1 shows six still frames from a 24fps video. After touching the microneedle side of the chip to a dish of water, the channels are nearly filled in four frames (167 ms), completely filling by frame 6 (250 ms). Air bubbles are trapped by the channels, an unfortunate side-effect of having multiple needles connected to a single microchannel. Current developments are underway to decrease the volume of air trapped in the chip (§ 6.2). This includes application of a slight vacuum to the back of the chip during collection, and potential microchannel collection redesign.

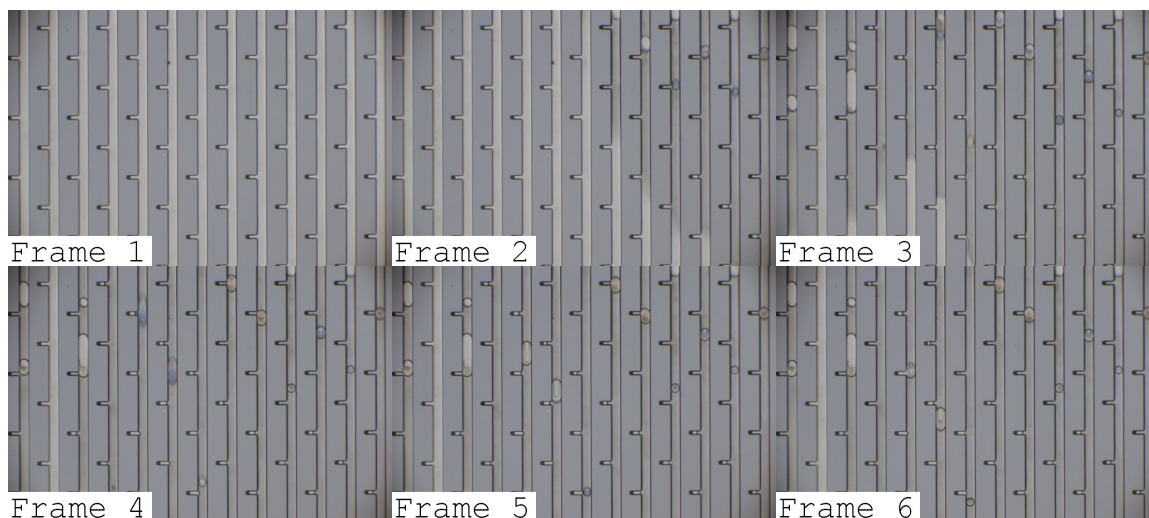


Figure 5.1 – Six still frames from a 24 fps video showing water filling the microfluidic channels.

5.2 ISF collection from human subjects

Both needle arrays have been shown to reliably collect small amounts (appx. 0.3 μ L) of ISF from human subjects (myself and R. L. Smith). This volume is far too small for RNA profiling, but only a few microliters are required for off-chip protein analysis. The volume of ISF required for on-chip detection of specific biomarkers depends on concentration. Some analytes, e.g. glucose, can be quantified in $\leq 0.1 \mu$ L. With the current design, multiple chips could be used on the same subject to collect the required volume. However, there are currently chips in fabrication which employ

deeper microchannels and a smaller drilled hole in the glass, increasing the on-chip collection capacity volume to 1 microliter. Assuming the skin's local available volume of dermal ISF is $\geq 1 \mu\text{L}$, these chips could enable the collection of enough ISF for off-chip analysis using just a few chips. This redesign is discussed in the future development section, § 6.2.

Microneedle chips were tested on the hand, earlobe, and forearm; ISF collection was successful at all sites. Needles require very little pressure for insertion, but pressure must be kept on the chip during sampling to ensure maximum collected volume. On average, the microchannels and reservoir take 15-30 minutes to fill completely with ISF, but this time varied significantly between trials. ISF would not cross the air interface at the border of the drilled via-hole in the glass. This could be due to depletion of ISF in the skin, but it is also likely that the forces needed to overcome the boundary layer are too great for capillary action alone. Evaporative loss of water at the air interface is likely to also be a significant factor. When the hole is covered with a film of silicone rubber, evaporation is reduced. However, there was too much variability between test results (each done with a different chip) to verify if hole coverage alone enhanced collection volume or if chip-to-chip or skin location variation was responsible. Future trials will employ a slight vacuum to the via-hole immediately after insertion, in an attempt to remove air from the channels and thereby assist with quicker collection at greater volumes. Also, devices currently in process will have smaller holes (1 mm instead of 2 mm) in the glass, which will both increase the reservoir collection capacity and reduce evaporative losses.



Figure 5.2 – Top and bottom left: A chip being applied to a human hand. Bottom right: needle holes are visible for a few minutes after they are removed from the skin. Some small spots of blood are also present, a rare occasion.

Larger ISF volumes were collected, at a quicker pace, when a priming step was first performed on the area of skin to be collected. In this method, solid silicon microneedles were inserted and removed five to ten times before the hollow needle chip was applied. The priming appeared to cause an edemic reaction, with subjects showing slight redness and a small amount of swelling. As this is a type of wound response, it is unclear at this time whether the ISF composition collected via this method will be the same as when priming is not used.

Once the needles are removed, holes are visible on the skin which persist for around five minutes, and redness persists for fifteen minutes to a few hours, depending on the skin sensitivity of the subject and location. Occasionally, small amounts of blood enter the channels and residue is observed after removal (Figure 5.2). Subjects reported no pain throughout the procedure, but sensed the pressure applied, sometimes accompanied by a “prickly” sensation, and mild tugging upon removal.

We have been able to remove the collected ISF from the chip by placing it in a centrifuge tube and spinning. Centrifugal forces draw the fluid out of the chip through the needles and ISF collects at the bottom of the tube. Undoubtedly, some residual fluid and/or constituents (e.g. protein) remains inside the chip. Application of 0.5 μL of fluid, either just water, or analytical preparation solution (such as trypsin for protein analysis via mass spectrometry), can be pipetted into the chip, and centrifugation repeated to flush the channels, noting the consequential dilution of the sample contents. The tube can then be frozen for future analysis.

5.3 Depth of penetration

A company called Optiscan, Melbourne, Australia (<https://www.optiscan.com>), has an endomicroscopic confocal imaging probe which can be focused with micron accuracy at different depths inside living tissue, and captures an image of anything that fluoresces. We sent them several microneedle devices to see if needle penetration depth could be quantified. Here, the hollow microneedles' tips were dipped into 10% fluorescein (in water), and after removing excess liquid from the tips, the needles were pressed into the skin on the back of the hand. After removal from the skin, mineral oil was immediately applied to the skin, in an attempt to fill the holes, as fluorescein quickly diffused away into the interstitial space. This is why the holes appear dark (no fluorescence) whereas the area surrounding the holes are light (fluorescing). The skin area was then imaged at increasing depths. The results (Figure 5.3) clearly show the holes left by the microneedles at depths of 30, 50, and 100 microns. After applying contrast enhancement (also called stretching, or normalization) to the images, holes could be seen at greater depths, up to 164 μm (Figure 5.4). There is a change in texture in the images surrounding the holes, attributed to cells, at depths $\geq 100 \mu\text{m}$, which could be indicative of the change in tissue type from epidermis to dermis. Further tests are needed to verify this, but these images confirm that the microneedle tips penetrate to depths $\geq 164 \mu\text{m}$.

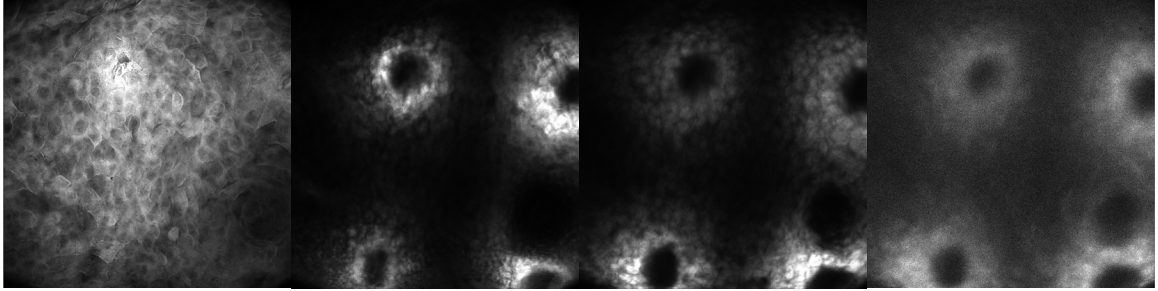


Figure 5.3 – Image results showing the needles' penetration into the skin at (L to R) 0, 30, 50, and 100 microns. Images courtesy of Dr. Lindsay Bussau, Optiscan Pty Ltd, Melbourne, Australia.

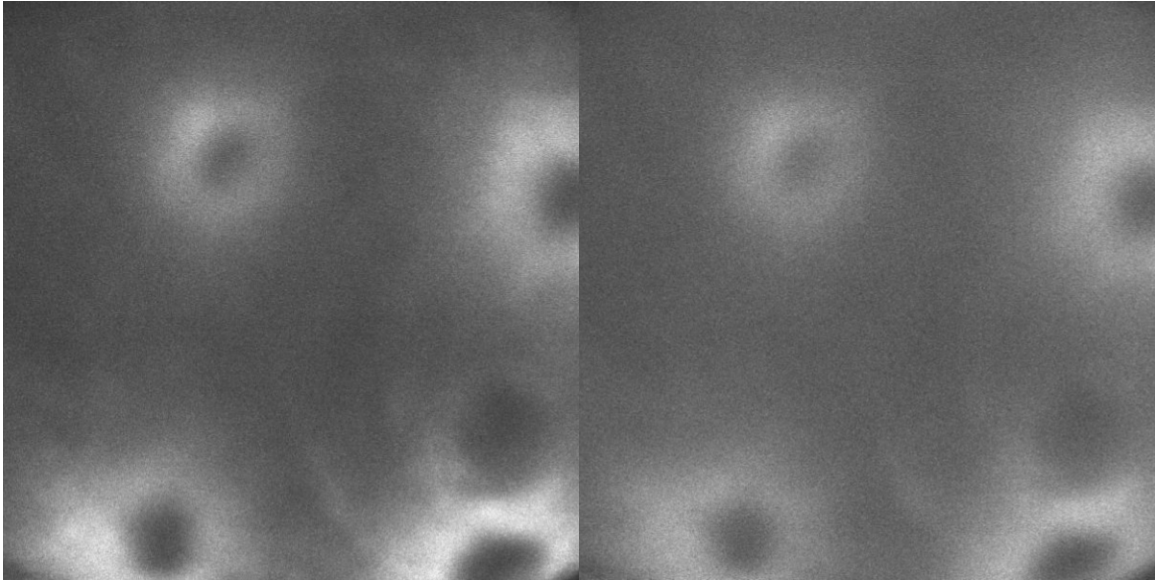


Figure 5.4 – Image results showing the needles' penetration, after contrast stretching, into the skin at (L to R) 132, and 164 microns. Images courtesy of Dr. Lindsay Bussau, Optiscan Pty Ltd, Melbourne, Australia.

CHAPTER 6 – CONCLUSIONS & FUTURE WORK

6.1 Conclusions

A microfabricated instrument was proposed, fabricated and tested. Significant improvements were made over prior art:

- Chip collection capacity volume was increased from ≈ 200 nanoliters to ≈ 1 microliter. This was made possible by increasing the number and depth of the microchannels on the back of the chip.
- The number of collecting needles was increased from 18 needles to 162, with expectation that increasing the number of collecting needles will increase the rate and volume of ISF collection.
- Production time was decreased, resulting in a dramatic increase of throughput. The improved process flow substantially increased yield of functioning devices. The previous (Mukerjee *et al.*) chip fabrication method is estimated to require ≥ 120 process hours to create just a couple of working devices, while now it takes roughly 40 process hours to produce a wafer containing 36 working devices.
- I designed a new column geometry, that is created using one DRIE step, which after sharpening produces the requisite microneedle shape for successful ISF extraction. This method of fabrication is currently costlier than using an automated dicing saw, but several optimizations can be made which would make this DRIE method cheaper, the most significant being the use of larger diameter wafers.

- I was able to increase the thickness of the wafers used to 550 μm for the dicing saw design, and 625 μm for the DRIE design, up from 500 μm published by Mukerjee *et al.* This increase in wafer thickness allows for an increase in microneedle height from 250-350 μm in Mukerjee's chips to 400-420 μm , without sacrificing yield due to wafer fragility. The taller needles penetrate deeper into the dermis layer of skin, potentially increasing the volume of ISF available for collection.

ISF extraction capability was consistent and repeatable, although the performance, in terms of extraction volume and rate, was highly variable. Because a different chip had to be used for each trial, as well as other variables, including different subject, location on skin, skin preparation protocol, the amount of pressure applied, and evaporative loss; the cause for collection volume variation cannot be determined at this time.

The microneedle device is both mechanically robust and small enough to consider it completely portable and ultimately "wearable." Thirty-six chips of the current size can fit on a single 4-inch silicon wafer. If the design were to go to mass production, throughput could be significantly increased if 8-inch or 12-inch wafers were employed. Currently, needles are sharpened on a per-chip basis. A wafer-scale sharpening etch could be implemented, further reducing manufacturing time, and chip-to-chip variability.

The needles themselves are strong enough to withstand multiple skin penetrations, and devices could potentially be cleaned, sterilized and reused.

6.2 Future considerations

The largest, most immediate concern for future development is to increase the volume of ISF collected by the chip. Channel depth has been increased to double the collected volume, but there is a limit: ISF must reach the extremely-hydrophilic glass backing to be sucked into the channels

via capillary action. The needles are oxidized in nitric acid after sharpening to increase hydrophilicity, but glass is believed to be the main source of capillary forces drawing the ISF into the chamber. Significant microchannel redesign is necessary to achieve single-chip capacity volumes necessary for RNA sequencing and other volume-intensive tasks. This may be accomplished by a microchannel redesign to prevent air bubbles from collecting and being trapped in the channels. A vertical approach could prove possible, with drilled glass or silicon containing arrays of small holes instead of a single collection point. However, it also may be that collection is limited by the accessible volume of dermal ISF. In that case, the only way to increase collected volume is to increase the area of skin from which collection is performed. This may be done using multiple chips, larger chips, and/or by increasing needle height to access a larger volume of dermal tissue. The latter will be difficult to achieve with the current out-of-plane silicon microneedle design using DRIE for borehole formation, but other methods and/or materials are available, albeit with limitations.⁴⁵

Alternatively, diagnostic techniques could be incorporated into the chips themselves as a lab-on-a-chip (LoC). If these devices are to be used in austere environments, it will be of great importance for them to be a single point of analysis, requiring nothing else but the chips themselves. Additionally, this may alleviate the volume issue, as LoCs can handle extremely small fluid volumes, down to picoliters, depending on the analyte and method of measurement. Certain aspects such as RNA sequencing would require major breakthroughs in sequencing technology to be able to perform that as a LoC; however, many other aspects like targeted-biomarker detection, including specific RNA sequences, could be achieved with selective sensor technology incorporated onto the chips.

REFERENCES

1. Centers for Disease Control and Prevention, *Principles of epidemiology*. 2nd ed. 1992, Atlanta: U.S. Department of Health and Human Services.
2. Tortora, G. J. and N. P. Anagnostakos, *Principles of anatomy and physiology*. 1987, New York, NY: Harper & Row.
3. Pocock, G. and C.D. Richards, *Human physiology : the basis of medicine*. 2006, Oxford: Oxford University Press.
4. Brandis, Kerry, *Fluid Physiology*. 2003.
5. Stout, P. J., N. Peled, B. J. Erickson, M. E. Hilgersm, J. R. Racchini, and T. B. Hoegh, *Comparison of Glucose Levels in Dermal Interstitial Fluid and Finger Capillary Blood*. *Diabetes Technol. & Ther.*, 2004. **3**(1): p. 81-90.
6. Müller, André C., Florian P. Breitwieser, Heinz Fischer, Christopher Schuster, Oliver Brandt, Jacques Colinge, . . . Keiryn L. Bennett, *A comparative proteomic study of human skin suction blister fluid from healthy individuals using immunodepletion and iTRAQ labeling*. *Journal of proteome research*, 2012. **11**(7): p. 3715-3727. DOI: 10.1021/pr3002035.
7. Smith, Tracey J., Marques Wilson, J. Philip Karl, Jeb Orr, Carl Smith, Adam Cooper, . . . Scott J. Montain, *Impact of sleep restriction on local immune response and skin barrier restoration with and without "multinutrient" nutrition intervention*. *Journal of Applied Physiology*, 2018. **124**(1): p. 190-200. DOI: 10.1152/jappphysiol.00547.2017.
8. Kool, Jeroen, Léon Reubsaet, Feikje Wesseldijk, Raquel T. Maravilha, Martijn W. Pinkse, Clive S. D'Santos, . . . Albert J. R. Heck, *Suction blister fluid as potential body fluid for biomarker proteins*. *Proteomics*, 2007. **7**(20): p. 3638-3650.
9. US-Gov, *Anatomy of the Skin*, illu_skin01.jpg, Editor. 2005-2009.
10. Donnelly, Ryan F, Thakur Raghu Raj Singh, Martin J Garland, Katarzyna Migalska, Rita Majithiya, Cian M McCrudden, . . . A David Woolfson, *Hydrogel-Forming Microneedle Arrays for Enhanced Transdermal Drug Delivery*. *Advanced Functional Materials*, 2012. **22**(23): p. 4879-4890.
11. Gardeniers, Han J. G. E., Regina Luttge, Erwin J. W. Berenschot, Meint J. de Boer, Shuki Y. Yeshurun, Meir Hefetz, . . . Albert van den Berg, *Silicon Micromachined Hollow Microneedles for Transdermal Liquid Transport*. *Journal of Microelectromechanical Systems*, 2003. **12**(6): p. 855-862.
12. Miller, Philip, Matthew Moorman, Ron Manginell, Carlee Ashlee, Igal Brener, David Wheeler, . . . Ronen Polsky, *Towards an Integrated Microneedle Total Analysis Chip for Protein Detection*. *Electroanalysis*, 2016. **28**(6): p. 1305-1310. DOI: 10.1002/elan.201600063.

13. Mukerjee, E. V., S. D. Collins, R. R. Isseroff, and R. L. Smith, *Microneedle array for transdermal biological fluid extraction and in situ analysis*. Sensors and Actuators A: Physical, 2004. **114**(2): p. 267-275. DOI: 10.1016/j.sna.2003.11.008.
14. Samant, Pradnya P. and Mark R. Prausnitz, *Mechanisms of sampling interstitial fluid from skin using a microneedle patch*. Proceedings of the National Academy of Sciences, 2018. **115**(18): p. 4583-4588. DOI: 10.1073/pnas.1716772115.
15. Campbell, Patrick K., Kelly E. Jones, Robert J. Huber, Kenneth W. Horch, and Richard A. Normann, *A Silicon-Based, Three-Dimensional Neural Interface: Manufacturing Processes for an Intracortical Electrode Array*. IEEE Transactions on Biomedical Engineering, 1991. **38**(8): p. 758-768.
16. Mukerjee, Erik Vivek, *Design, Fabrication and Testing of Silicon Microneedle-Based Microfabricated Biomedical Devices*, in *Biomedical Engineering*. 2003, University of California, Davis: Davis, CA. p. 209.
17. Liu, G.-S., Y. Kong, Y. Wang, Y. Luo, X. Fan, X. Xie, . . . M. X. Wu, *Microneedles for transdermal diagnostics: Recent advances and new horizons*. Biomaterials, 2019. **232**.
18. Sagoe-Moses, C., R.D. Pearson, J. Perry, and J. Jagger, *Risks to health care workers in developing countries*. The New England Journal of Medicine, 2001. **345**: p. 538-541.
19. Ayala, Erica S, Alicia E Meuret, and Thomas Ritz, *Treatments for blood-injury-injection phobia: a critical review of current evidence*. Journal of psychiatric research, 2009. **43**(15): p. 1235-1242.
20. Miller, Philip R., Roger J. Narayan, and Ronen Polsky, *Microneedle-based sensors for medical diagnosis*. Journal of Materials Chemistry B, 2016: p. 1379-1383.
21. Kaushik, Shilpa, PhD, Allen H. Hord, MD, Donald D. Denson, PhD, Devin V. McAllister, PhD, Sudhasinee Smitra, MS, Mark G. Allen, PhD, and Mark R. Prausnitz, PhD, *Lack of Pain Associated with Microfabricated Microneedles*. Anesthesia and Analgesia, 2001: p. 502-504.
22. Henry, Sebastien, Devin V. McAllister, Mark G. Allen, and Mark R. Prausnitz, *Microfabricated microneedles: a novel approach to transdermal drug delivery*. Journal of Pharmaceutical Sciences, 1998: p. 922-925.
23. Mukerjee, E.V., S.D. Collins, and R.L. Smith, *Microinstrument for transdermal, wound potential measurements*. Hilton Head Solid-State Sensor & Actuator Workshop, 2000.
24. Smart, Wilson H. and Kumar Subramanian, *The Use of Silicon Microfabrication Technology in Painless Blood Glucose Monitoring*. Diabetes Technology & Therapeutics, 2000. **2**(4): p. 549-559.
25. Prausnitz, Mark R., John A. Mikszta, Michel Cormier, and Alexander K. Andrianov, *Microneedle-based vaccines*. Current topics in microbiology and immunology, 2009. **333**: p. 369-393. DOI: 10.1007/978-3-540-92165-3_18.

26. Vandervoort, Jo and Annick Ludwig, *Microneedles for transdermal drug delivery: a minireview*. Frontiers in Bioscience: a journal and virtual library, 2008. **13**: p. 1711-1715. DOI: 10.2741/2794.
27. Li, Junwei, Zeng Mingtau, Hu Shan, and Tong Chunyi, *Microneedle Patches as Drug and Vaccine Delivery Platform*. Current medicinal chemistry, 2017. **24**(22): p. 2413-2422. DOI: 10.2174/0929867324666170526124053.
28. Griss, Patrick and Goran Stemme, *Side-Opened Out-of-Plane Microneedles for Microfluidic Transdermal Liquid Transfer*. Journal of Microelectromechanical Systems, 2003. **12**(3): p. 296-301.
29. Zhang, Peiyu, Colin Dalton, and Graham A. Jullien, *Design and fabrication of MEMS-based microneedle arrays for medical applications*. Microsystem Technologies, 2009. **15**(7): p. 1073-1082. DOI: 10.1007/s00542-009-0883-5.
30. Zhang, Rumi, Peiyu Zhang, Colin Dalton, and Graham A. Jullien, *Modeling of drug delivery into tissues with a microneedle array using mixture theory*. Biomechanics and Modeling in Mechanobiology, 2010. **9**(1): p. 77-86. DOI: 10.1007/s10237-009-0160-7.
31. Tang, Y., A. Sandoughsaz, and K. Najafi. *Ultra high aspect-ratio and thick deep silicon etching (UDRIE)*. in *2017 IEEE 30th International Conference on Micro Electro Mechanical Systems (MEMS)*. 2017.
32. Cozma, A and B Puers, *Characterization of the electrostatic bonding of silicon and Pyrex glass*. Journal of Micromechanics and Microengineering, 1995. **5**(2): p. 98-102.
33. Lee, Thomas M.H., Debbie H.Y. Lee, Connie Y.N. Liaw, Alex I.K. Lao, and I-Ming Hsing, *Detailed characterization of anodic bonding process between glass and thin-film coated silicon substrates*. Sensors and Actuators A, 2000. **86**(1-2): p. 103-107.
34. Berry, C. A., Z. R. Smith, S. D. Collins, and R. L. Smith. *Dermal ISF Collection Using a Si Microneedle Array*. in *2020 IEEE 33rd International Conference on Micro Electro Mechanical Systems (MEMS)*. 2020.
35. Shipley Company, L.L.C., *MEGAPOSIT® SPR® 220 Series Photoresist*. 1999.
36. van Drienuizen, Bert P., *Advances in MEMS using SFB and DRIE technology*. Micromachined Devices and Components V, 1999. DOI: 10.1117/12.360510.
37. Guan, Taotao, Fang Yang, Wei Wang, Peng Liu, Zexin Fan, Leijian Cheng, . . . Dacheng Zhang, *A High-Selectivity HNA Etching System for Bulk Micromachined Deep Holes with High Roundness [Abstract]*. 2018 IEEE 13th Annual International Conference on Nano/Micro Engineered and Molecular Systems (NEMS), 2018. DOI: 10.1109/nems.2018.8556953.
38. Robbins, H., & Schwartz, B., *Chemical Etching of Silicon*. Journal of The Electrochemical Society, 1960. **107**(2). DOI: 10.1149/1.2427617.

39. Harvard. *CNS Consolidated Rate Sheet 2020*. 07/01/2020 [cited 2020 07/28]; Available from: <https://cns1.rc.fas.harvard.edu/documents/2018/06/cns-consolidated-rate-sheet.pdf>.
40. UMaine. *Cleanroom Rates*. [cited 2020 07/28]; Available from: <https://umaine.edu/core/processing/>.
41. Utah. *Utah Nanofab Cleanroom Rates*. 07/01/2019 [cited 2020 07/28]; Available from: <https://www.nanofab.utah.edu/billing-rates/>.
42. Illinois. *MNMS Lab Rate Details*. [cited 2020 07/28]; Available from: https://www.s.mechse.uiuc.edu/cleanroom/equipment/rates_details.php.
43. CUNY. *Academic, Start-up and Industry Rates (subject to change)*. [cited 2020 07/28]; Available from: <https://asrc.gc.cuny.edu/nanofab/become-a-member/equipment-rates/>.
44. UWashington. *Washington Nanofabrication Facility Rate Structure for 2017–2019 (Effective 11/1/17)*. [cited 2020 07/28]; Available from: <https://www.wnf.washington.edu/docs/WNF-Rates.pdf>.
45. Miller, Philip R., Robert M. Taylor, Bao Quoc Tran, Gabrielle Boyd, Trevor Glaros, Victor H. Chavez, . . . Ronen Polsky, *Extraction and biomolecular analysis of dermal interstitial fluid collected with hollow microneedles*. *Communications Biology*, 2018. **1**(1): p. 173. DOI: 10.1038/s42003-018-0170-z.

APPENDIX A – COMPLETE FABRICATION PROCESS FLOW

Major steps are given a number, i.e. “Step 1.” The explanation and procedure of the step follows in a bulleted list format. It should be assumed the bulleted list was followed sequentially, unless otherwise indicated.

A.1 Backside fabrication

Both designs begin by fabricating the backside microchannels, reservoir, and 30 μ m holes. The procedure for both designs is the same.

Step 1 – RCA clean

- Prepare base bath – 4 liters deionized water + 600 mL ammonium hydroxide + 500 mL hydrogen peroxide – heat to 75 °C
- Prepare acid bath – 4 liters deionized water + 600 mL hydrochloric acid + 500 mL hydrogen peroxide – heat to 75 °C
- Place wafers in wafer carrier, and lower into base bath. Leave for 10 minutes, and then rinse in deionized water bath.
- Lower wafer carrier into the acid bath. Leave for 10 minutes, and then rinse in deionized water bath.
- Blow dry with nitrogen gun. Be extremely thorough, as any leftover water will leave a visible streak in the wafer post-oxidation.

Step 2 – Thermal oxidation furnace, 500 nm (1050 °C, wet oxidation, 1 hour)

- Verify and record final oxidation thickness with ellipsometer

Step 3 – Photolithography for channel-side oxide etch

- HMDS vapor prime wafer at 115 °C hotplate temperature in HMDS vacuum hotplate system
- Spin 5.5 mL AZ1512 photoresist using table spinner
 - Spread: ramp to 400 RPM in 5 seconds, hold for 10 seconds
 - Spin: ramp to 3500 RPM in 2.5 seconds, hold for 40 seconds
 - Final: ramp to 1000 RPM in 4 seconds, then ramp to 0 RPM in 10 seconds
 - Rest on spinner 30 seconds before bake
- Soft bake on vacuum hotplate for 90 seconds at 100 °C, using vacuum cycle
- Expose wafer to MASK A – channels, 85 mJ dose, Karl Suss MA6
 - Mask images can be found in Appendix B: mask images

- Develop in MIF300 for 60 seconds
 - MIF300 contains TMAH, a potent neurotoxin. Exercise extreme caution.
- Rinse in deionized water, dry with N2 gun, and inspect print
- Hard bake on hotplate for 60 seconds at 100 °C

Step 4 – Channel oxide etch

- Apply UV-release dicing tape to the column side (opposite)
 - This is to act as a mask for BOE, protecting the oxide layer on that side for now. Having an oxide layer protects the wafer silicon surface from scratching while it is being processed.
- Place in teflon dish with 6:1 BOE solution for 8 minutes
 - BOE etches glass, so glass cannot be used.
 - When the etch has finished, the surface that was etched away will be bare silicon, and will be hydrophobic. This information can be used to determine when the etch has finished.
- Remove dicing tape by exposing to UV with the aligner for 30 seconds
- Strip photoresist with PG remover, or Acetone/IPA/MeOH/DIW
- Clean in piranha solution

Step 5 – Photolithography for channel-side 30µm hole arrays

- HMDS vapor prime wafer at 115 °C hotplate temperature in HMDS vacuum hotplate system
- Spin 6 mL SPR220 photoresist using table spinner
 - Spread: ramp to 500 RPM in 10 seconds, hold for 10 seconds
 - Spin: ramp to 1800 RPM in 10 seconds, hold for 30 seconds
 - Final: ramp to 0 RPM in 15 seconds
 - Rest on spinner 30 seconds before bake
- Soft bake on hotplate for 300 seconds at 115 °C
 - Ramp temperature by placing wafer on the pins first, then slowly retract the pins until the wafer touches the hotplate surface. Start the timer when the wafer touches the hotplate surface. Use the chuck vacuum for tight hotplate contact.
 - After the soft bake, it is important to avoid thermal shock. Ramp the temperature down by slowly raising the pins after disabling the vacuum. Raise the pins all the way and then leave for several minutes to ensure a slow temperature ramp down.

Failure to do so may result in many cracks in the resist over the wafer. Place on a cleanroom wipe after cool down.

- Expose wafer to MASK B – 30µm hole, 385 mJ dose, Karl Suss MA6
 - Use multiple exposure option, 4 cycles with 30 second hold time between cycles
- Hold time – wait at least 30 minutes before developing. This step is crucial, as it allows time for the photoactive compound (PAC) to break down in the thick resist.
- Develop in MIF300 for 300 seconds, with manual agitation
 - MIF300 contains TMAH, a potent neurotoxin. Exercise extreme caution.
- Rinse in deionized water, dry with N2 gun, and inspect print

Step 6 – DRIE 30µm hole arrays 400µm deep

- Etch in STS DRIE using 48 runs of recipe “Maine2” (see Appendix B – recipes)
- Strip photoresist with (sequentially) Acetone, IPA, MeOH, DIW
- Clean wafer with piranha solution

Step 7 – DRIE channels 40µm deep, using SiO₂ patterned in steps 3/4 as mask

- Etch in STS DRIE using 4 runs of recipe “Maine2” (see Appendix B – recipes)

Step 8 – Column side oxide etch

- Apply UV-release dicing tape to the **channel** side (opposite)
 - The column side oxide now needs to be removed, as the bare silicon surface is needed for PECVD. Again, the tape is to act as a mask for BOE, now protecting the remaining oxide layer on the channel side. As mentioned previously, having an oxide layer protects the wafer silicon surface from scratches while it is being processed.
- Place in teflon dish with 6:1 BOE solution for 8 minutes
 - BOE etches glass, so a glass dish cannot be used.
 - When the etch has finished, the surface that was etched away will be bare silicon, and will be hydrophobic. This information can be used to determine when the etch has finished.
- Remove dicing tape by exposing to UV with the aligner for 30 seconds

A.2 Frontside fabrication, DRIE design

The after completion of the backside, each design has its own process flow for the front, or needle-side. The DRIE procedure is as follows:

Step 9 – Nitride deposition (PECVD) on column side

- Have the hotplate chuck set at 390 °C
- Open the chamber and place the wafer on the chuck
- Close and pump down the chamber
- Run recipe “MSC SiN-Hi Qual” (see Appendix B – Recipes)
- Verify thickness using the ellipsometer. It should be around 8200Å.

Step 10 - Photolithography for columns

- HMDS vapor prime wafer at 115 °C hotplate temperature in HMDS vacuum hotplate system
- Spin 6 mL SPR220 photoresist using table spinner
 - Spread: ramp to 500 RPM in 10 seconds, hold for 10 seconds
 - Spin: ramp to 1800 RPM in 10 seconds, hold for 30 seconds
 - Final: ramp to 0 RPM in 15 seconds
 - Rest on spinner 30 seconds before bake
- Soft bake on hotplate for 300 seconds at 115 °C
 - Ramp temperature by placing wafer on the pins first, then slowly retract the pins until the wafer touches the hotplate surface. Start the timer when the wafer touches the hotplate surface. Use the chuck vacuum for tight hotplate contact.
 - After the soft bake, it is important to avoid thermal shock. Ramp the temperature down by slowly raising the pins after disabling the vacuum. Raise the pins all the way and then leave for several minutes to ensure a slow temperature ramp down. Failure to do so may result in many cracks in the resist over the wafer. Place on a lint-free wipe after cool down.
- Expose wafer to MASK D – columns, 385 mJ dose, Karl Suss MA6
 - Use multiple exposure option, 4 cycles with 30 second hold time between cycles
- Hold time – wait at least 30 minutes before developing. This step is crucial, as it allows time for the photoactive compound (PAC) to break down in the thick resist.
- Develop in MIF300 for 300 seconds, with manual agitation
 - MIF300 contains TMAH, a potent neurotoxin. Exercise extreme caution.

- Rinse in deionized water, dry with N2 gun, and inspect print

Step 11 – DRIE columns 400µm deep

- Etch in STS DRIE using 48 runs of recipe “Maine2” (see Appendix B – recipes)
- Check depth
- Etch further as needed, using a shorter run
 - Repeat until 400µm depth is reached
- Strip photoresist with (sequentially) Acetone, IPA, MeOH, DIW
- Clean wafer with piranha solution

Step 12 – Channel-side oxide etch

- Apply UV-release dicing tape to the **column**-side (opposite)
 - The remaining channel-side oxide now needs to be removed, as the bare silicon surface is needed for anodic bonding to glass. The tape is to act as a mask for BOE, protecting the PECVD nitride on the column-side.
- Place in teflon dish with 6:1 BOE solution for 8 minutes
 - BOE etches glass, so a glass dish cannot be used.
 - When the etch has finished, the surface that was etched away will be bare silicon, and will be hydrophobic. This information can be used to determine when the etch has finished.
- Remove dicing tape by exposing to UV with the aligner for 30 seconds

Step 13 – Anodic bond to glass

- Set hotplate temperature to 420 °C
- Place wafer on chuck, column-side down
- Place 4-inch Pyrex 7740 (or equivalent) wafer on top of the silicon wafer
 - This glass wafer has had via holes pre-drilled, for ISF access
- Align pre-drilled holes (see schematic)
- Place electrode on Pyrex wafer
- Apply 1100V and wait for bonding

Step 14 – Dicing saw, cut individual die

- Align saw angle to columns
- Find walls between chips, cut along wall

- Repeat for entire wafer
- Rotate 90 degrees
- Find walls between chips, cut along wall
- Repeat for entire wafer

Step 15 – Cover via holes on the backs of chips with tape that can stand HNA

- I used Kapton tape, which held up satisfactorily. There are probably some tapes that will work better.

Step 16 – Thinning columns

- Prepare a solution of HNA (hydrofluoric acid : nitric acid : acetic acid) 1:8:1 by volume
- Heat solution to 50 °C in water bath
 - Polymer beaker that can withstand HNA at 50 °C (e.g. Teflon), inside larger glass dish with hot water, sitting on hotplate
- Add stir bar to HNA solution, set to ~2 revolutions per second
- Gripping chip with tweezers, column-side up, submerge in HNA, and move slowly up and down (chip remaining in solution the whole time) at a rate of ~2 per second
- Continue for 90 seconds
- Remove, rinse in hot water, dry, and inspect column tips with optical microscope

Step 17 – Sharpening columns

- Pour 40 mL HNA (1:8:1 vol) solution into a plastic beaker that can stand HNA, e.g. Teflon
 - Room temperature, no stir bar
- Gripping chip with tweezers, column-side down, submerge in HNA, and do not move
 - The goal is to get this step as quiescent as possible. Bubbles produced by the HNA reaction will collect at the column base, enhancing etching at the tip. Result will be sharpened needles
- Every 30 seconds, take the chip out, rinse in hot water, dry, and inspect the tips with optical microscope.
 - The tips will get smaller and smaller, until you cannot see a tip. This is when they are sharpened. Stop sharpening as soon as this happens, as shank length will be reduced dramatically if sharpening continues.
 - When finished, work can be verified with SEM.

A.3 Frontside fabrication, dicing saw design

The dicing saw needle-side procedure is as follows:

Step 9 - Photolithography for column-side 10 μ m hole

- HMDS vapor prime wafer at 115 °C hotplate temperature in HMDS vacuum hotplate system
- Spin 6 mL SPR220 photoresist using table spinner
 - Spread: ramp to 500 RPM in 10 seconds, hold for 10 seconds
 - Spin: ramp to 1800 RPM in 10 seconds, hold for 30 seconds
 - Final: ramp to 0 RPM in 15 seconds
 - Rest on spinner 30 seconds before bake
- Soft bake on hotplate for 300 seconds at 115 °C
 - Ramp temperature by placing wafer on the pins first, then slowly retract the pins until the wafer touches the hotplate surface. Start the timer when the wafer touches the hotplate surface. Use the chuck vacuum for tight hotplate contact.
 - After the soft bake, it is important to avoid thermal shock. Ramp the temperature down by slowly raising the pins after disabling the vacuum. Raise the pins all the way and then leave for several minutes to ensure a slow temperature ramp down. Failure to do so may result in many cracks in the resist over the wafer. Place on a lint-free wipe after cool down.
- Expose wafer to MASK C – 10 μ m hole, 385 mJ dose, Karl Suss MA6
 - Use multiple exposure option, 4 cycles with 30 second hold time between cycles
- Hold time – wait at least 30 minutes before developing. This step is crucial, as it allows time for the photoactive compound (PAC) to break down in the thick resist.
- Develop in MIF300 for 300 seconds, with manual agitation
 - MIF300 contains TMAH, a potent neurotoxin. Exercise extreme caution.
- Rinse in deionized water, dry with N₂ gun, and inspect print

Step 10 – DRIE 10 μ m hole arrays until they meet 30 μ m hole

- Etch in STS DRIE using 48 runs of recipe “Maine2” (see Appendix B – recipes)
- Etch will automatically stop when holes are broken through, as the helium leakup rate will rise higher than the cutoff
- Strip photoresist with (sequentially) Acetone, IPA, MeOH, DIW
- Clean wafer with piranha solution

Step 11 – Nitride deposition (PECVD) on column side

- Have the hotplate chuck set at 390 °C
- Open the chamber and place the wafer on the chuck
- Close and pump down the chamber
- Run recipe “MSC SiN-Hi Qual” (see Appendix B – Recipes)
- Verify thickness using the ellipsometer. It should be around 8200Å.

Step 12 – Channel-side oxide etch

- Apply UV-release dicing tape to the **column**-side (opposite)
 - The remaining channel-side oxide now needs to be removed, as the bare silicon surface is needed for anodic bonding to glass. The tape is to act as a mask for BOE, protecting the PECVD nitride on the column-side.
- Place in teflon dish with 6:1 BOE solution for 8 minutes
 - BOE etches glass, so a glass dish cannot be used.
 - When the etch has finished, the surface that was etched away will be bare silicon, and will be hydrophobic. This information can be used to determine when the etch has finished.
- Remove dicing tape by exposing to UV with the aligner for 30 seconds

Step 13 – Anodic bond to glass

- Set hotplate temperature to 420 °C
- Place wafer on chuck, column-side down
- Place 4-inch Pyrex 7740 (or equivalent) wafer on top of the silicon wafer
 - This glass wafer has had via holes pre-drilled, for ISF access
- Align pre-drilled holes (see schematic)
- Place electrode on Pyrex wafer
- Apply 1100V and wait for bonding

Step 14 – Dicing saw, columns

- Align saw angle to 10µm hole arrays
- Starting at the bottom row of 10µm hole arrays, make 23 full cuts, 400µm deep (measured from wafer top surface), 300µm center-to-center spacing between cuts
 - See schematic for more detailed alignment information

- Move the saw blade up to the next row of 10 μ m hole arrays and repeat the same 23 cuts
- Repeat for remaining rows of 10 μ m hole arrays
- Rotate chuck 90 degrees
- Repeat the 23 cuts, move, 23 cuts, etc. for the 8 columns of 10 μ m hole arrays

Step 15 – Dicing saw, clear field

- Align saw angle to columns
- Using a wide blade, make stepwise cuts at the same depth as the columns (400 μ m), clearing all of the silicon between the column arrays

Step 16 – Dicing saw, cut individual die

- Align saw angle to columns
- Find midpoint between arrays, cut along midpoint
- Repeat for entire wafer
- Rotate 90 degrees
- Find midpoint between arrays, cut along midpoint
- Repeat for entire wafer

Step 17 – Cover via holes on the backs of chips with tape that can stand HNA

- I used Kapton tape, which held up satisfactorily. There are probably some tapes that will work better.

Step 18 – Thinning columns

- Prepare a solution of HNA (hydrofluoric acid : nitric acid : acetic acid) 1:8:1 by volume
- Heat solution to 50 °C in water bath
 - Polymer beaker that can withstand HNA at 50 °C (e.g. Teflon), inside larger glass dish with hot water, sitting on hotplate
- Add stir bar to HNA solution, set to ~2 revolutions per second
- Gripping chip with tweezers, column-side up, submerge in HNA, and move slowly up and down (chip remaining in solution the whole time) at a rate of ~2 per second
- Continue for 90 seconds
- Remove, rinse in hot water, dry, and inspect column tips with optical microscope

Step 19 – Sharpening columns

- Pour 40 mL HNA (1:8:1 vol) solution into a plastic beaker that can stand HNA, e.g. Teflon
 - Room temperature, no stir bar
- Gripping chip with tweezers, column-side down, submerge in HNA, and do not move
 - The goal is to get this step as quiescent as possible. Bubbles produced by the HNA reaction will collect at the column base, enhancing etching at the tip. Result will be sharpened needles
- Every 30 seconds, take the chip out, rinse in hot water, dry, and inspect the tips with optical microscope.
 - The tips will get smaller and smaller, until you cannot see a tip. This is when they are sharpened. Stop sharpening as soon as this happens, as shank length will be reduced dramatically if sharpening continues.
 - When finished, work can be verified with SEM.

APPENDIX B – RECIPES

Following are recipes for each of the machine-automated steps in the fabrication process.

B.1 STS DRIE

Recipe: Process for 3 minutes, then hold for 10 minutes to allow for better heat management.

Start on passivate, end on etch.

	Etch	Passivate
C4F8 flow rate (sccm)	0	110
SF6 flow rate (sccm)	130	0
RF Power, 13.56MHz, Coil	900 W, ramp rate 0 W/min	800 W, ramp rate 0 W/min
	auto matching, match load 30%, match tune 53%	
RF Power, 13.56MHz, Platen	16 W, ramp rate 0.1 W/min	0 W, ramp rate 0 W/min
	auto matching, match load 42%, match tune 61%	
Time	13s	7s

Helium backside cooling

Pressure: 9500 mTorr

Tolerance: 99%

Max flow: 40 sccm; Min flow: 10 sccm

Leak-up rate test time: 15s; max leak: 15 mTorr/min

B.2 HNA ETCH

The HNA etch used to sharpen the columns into needles is a biphasic procedure which combines an actively stirred thinning etch step with a quiescent sharpening step. It is currently on the chip level, although instruments could be designed to bring the process to wafer-scale.

Below is an example of how etch rate changes by composition of HNA. The ratio of acids used in this fabrication is 1:8:1 HF:HNO₃:AcOH, resulting in a moderately slow etch rate.

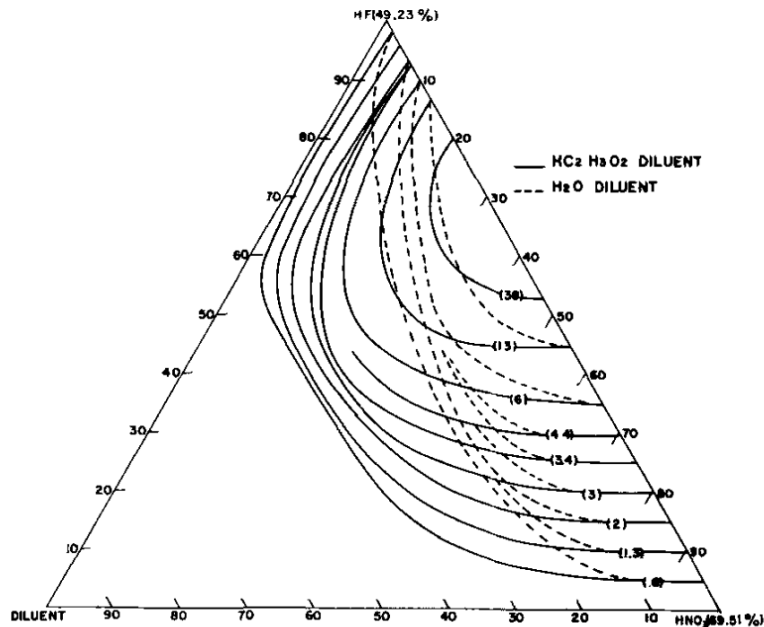


Figure B.1 – Curves of constant rate of change of die thickness (mils/min) as a function of etchant composition in the system 49% HF, 70% HNO₃ and diluent.³⁸

B.2.1 Thinning

The thinning step is performed at 50 °C. Etchant can be heated in a water bath. Solution is stirred with magnetic stir bar rotating at roughly 2-Hz. The chip is moved up and down in the solution with a pair of tweezers.

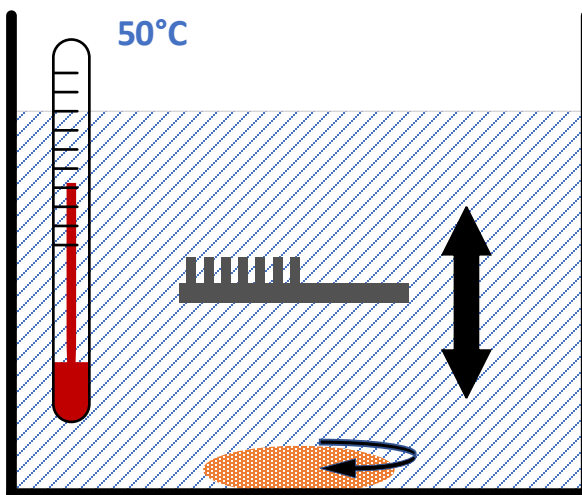


Figure B.2 – The thinning procedure utilizes an up/down motion of the chip and a stir bar to minimize the effects of diffusion.

B.2.2 Sharpening

The sharpening step is performed at room temperature. The chip is placed upside down in the solution and held stagnant. Bubbles, produced by the reaction, collect at the base of the columns, halting the etching there.

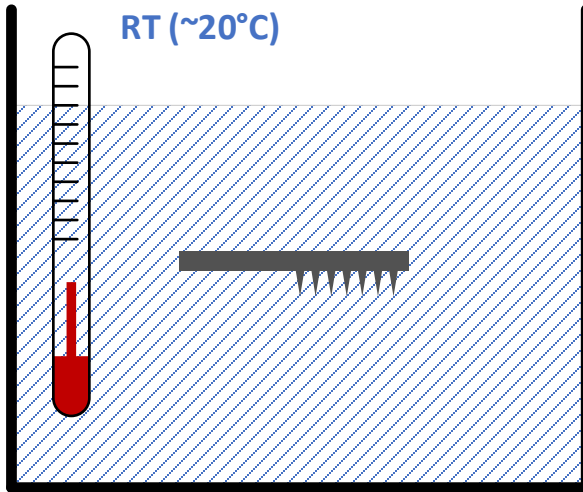


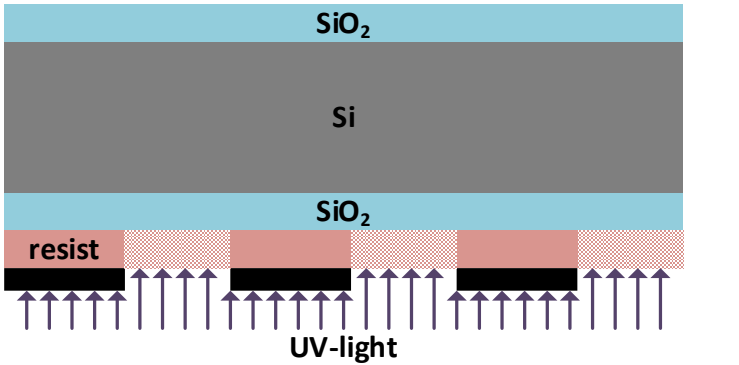
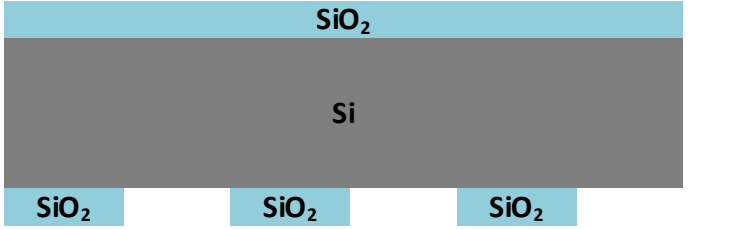




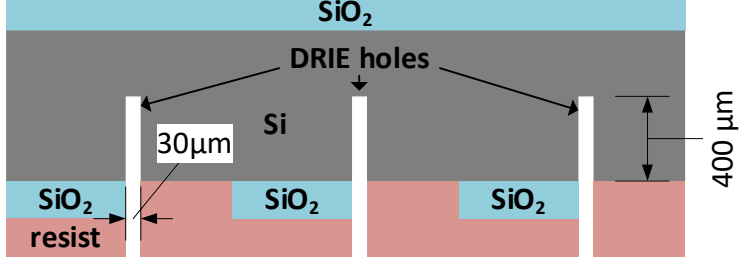
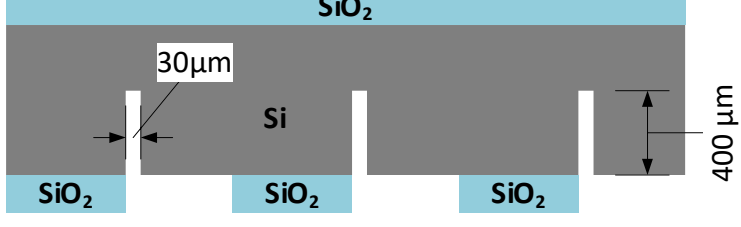
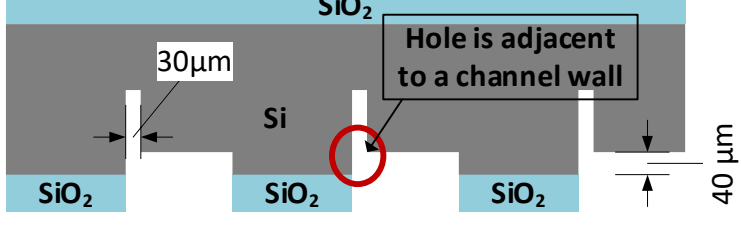
Figure B.3 – The sharpening procedure is quiescent.


APPENDIX C – DEVICE FABRICATION SCHEMATIC

The following pages show a pictorial representation of the fabrication steps described in APPENDIX A. The dimensions have been significantly modified for ideal special formatting in this document, so thicknesses are explicitly noted where required. All materials (i.e. Si, SiO₂, resist, etc.) are labeled at least once and have consistent coloring.

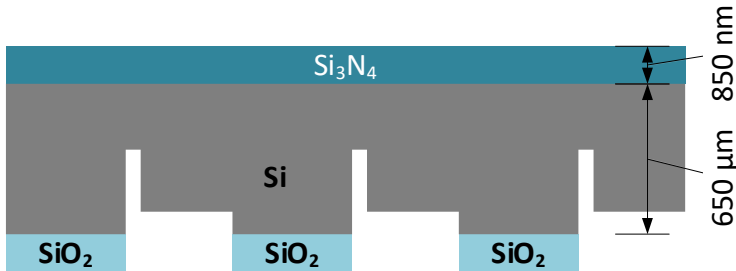
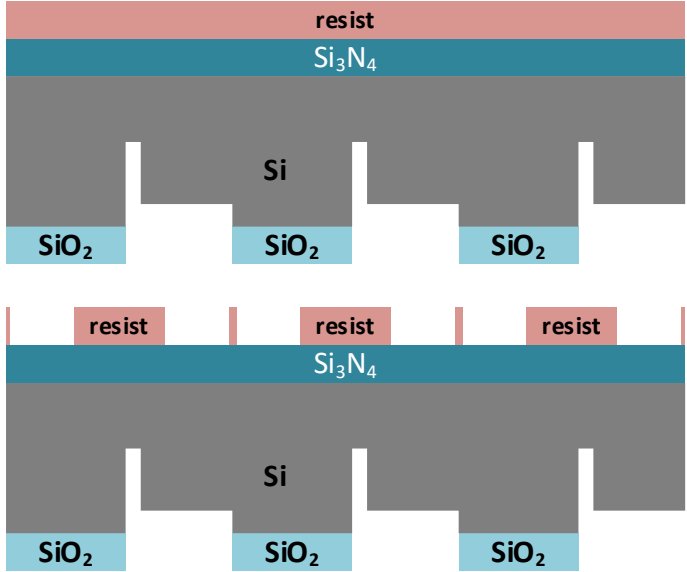
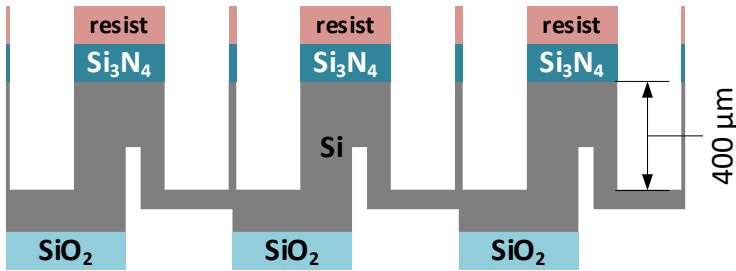
C.1 BACKSIDE FABRICATION, BOTH DESIGNS

Step 1 – RCA clean	
Step 2 – Thermal steam oxidation, 500nm thickness	
Step 3 – Photolithography for channel-side oxide etch	
Step 4 – Channel oxide etch	

<p>Step 5a – Spin thick photoresist, covering oxide pattern</p>	 <p>Diagram showing a cross-section of a silicon substrate (Si) with a thick SiO_2 layer. A resist layer is spun on top of the SiO_2. The resist is 10 μm thick. The SiO_2 layer is also 10 μm thick.</p>
<p>Step 5b – Expose to 30μm hole arrays, develop</p>	 <p>Diagram showing the resist layer after exposure and development. The resist is now patterned into a series of rectangular blocks, each 30 μm wide. The SiO_2 layer is still 10 μm thick.</p>
<p>Step 6a – DRIE 30μm hole arrays 400μm deep</p>	 <p>Diagram showing the result of a Deep Reactive Ion Etch (DRIE) process. The resist blocks are still present, and deep holes (DRIE holes) have been etched into the silicon substrate to a depth of 400 μm. The SiO_2 layer is 10 μm thick.</p>
<p>Step 6b – Remove photoresist, revealing the oxide patterned earlier</p>	 <p>Diagram showing the result of removing the photoresist. The resist blocks have been removed, leaving a series of rectangular pits in the silicon substrate. The SiO_2 layer is 10 μm thick.</p>
<p>Step 7 – DRIE channels 40μm deep using SiO_2 as etch mask</p>	 <p>Diagram showing the result of a second DRIE process. The SiO_2 layer is now used as an etch mask to create channels in the silicon substrate. The channels are 40 μm deep. A red circle highlights a hole adjacent to a channel wall.</p>

Step 8 – Column-side oxide etch	
---------------------------------	--

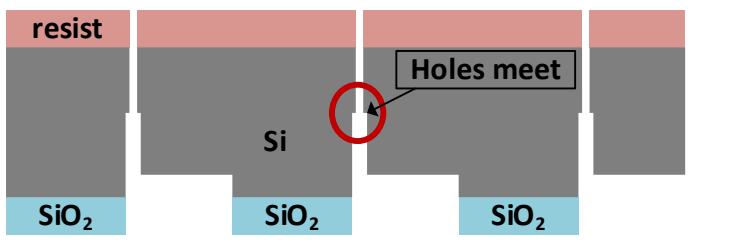

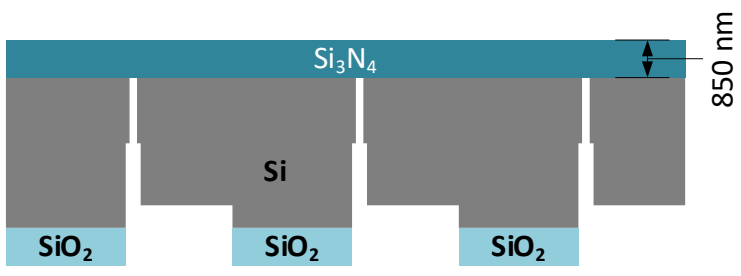

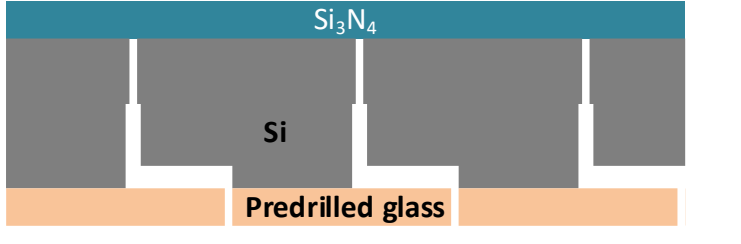
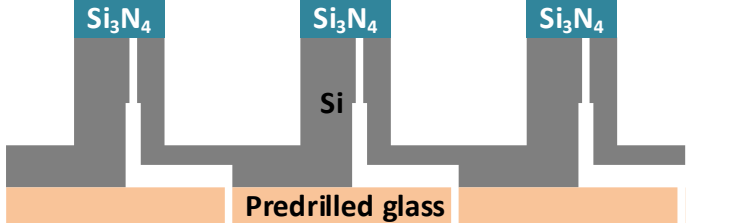
C.2 DRIE COLUMN FABRICATION PROCESS

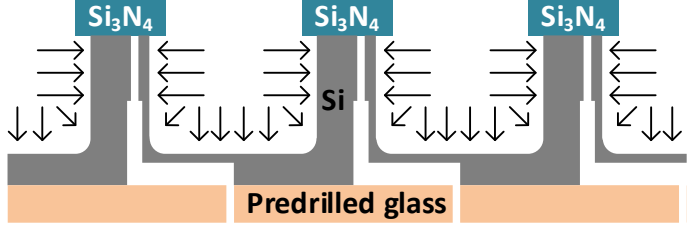
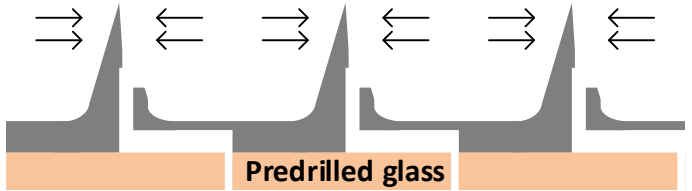
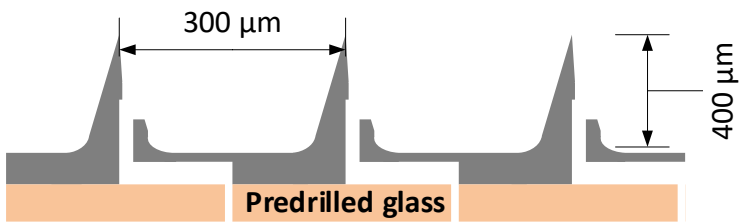
DRIE step 9 – PECVD nitride on column side. Saw wafers are 650 microns thick.	
DRIE step 10 – Photolithography for columns	
DRIE step 11 – DRIE columns 400 microns deep	

DRIE step 12 – Remove resist, and channel-side oxide	
DRIE step 13 – Anodic bond to glass	
DRIE step 16 – Thin columns	
DRIE step 17 – Sharpen columns	
Final dimensions	

C.3 SAW COLUMN FABRICATION PROCESS

Saw step 9 – Photolithography for column-side 10μm hole arrays	
--	--

<p>Saw step 10 – DRIE 10μm hole arrays until they meet 30μm hole</p>	
<p>Saw step 11 – Channel-side oxide etch</p>	
<p>Saw step 12 – PECVD nitride</p>	
<p>Saw step 13a – Remove oxide layer</p>	
<p>Saw step 13b – Anodic bond to glass</p>	
<p>Saw step 14, 15, 16 – Cut columns with dicing saw</p>	

<p>Saw step 17, 18 – Thin columns</p>	
<p>Saw step 19 – Sharpen columns, nitride caps fall off</p>	
<p>Final dimensions</p>	

APPENDIX D – PHOTOMASKS

There are four photomasks in total for this project. Each column formation process (DRIE vs. dicing saw) only uses three each, and they are named as follows:

- USED FOR BOTH: Mask #1 – Channels. This mask is used for patterning the microfluidic channels and reservoir. In the photos, this mask is colored blue.
- USED FOR BOTH: Mask #2 – 30 μ m Borehole. This mask is used for patterning the 30 μ m borehole on the channel-side of the wafer. The borehole is DRIE'd to a depth of 400 μ m and is what allows the ISF to reach the microfluidic channels, traveling straight through the wafer. In the photos, this mask is colored red, or purple if overlapping another mask.
- SAW PROCESS ONLY: Mask #3 – 10 μ m Borehole. This mask is used for patterning the 10 μ m borehole on the needle-side of the wafer. The borehole is DRIE'd until it meets the 30 μ m hole patterned with mask #2. In the photos, this mask is colored dark purple.
- DRIE PROCESS ONLY: Mask #4 – Columns. This mask is used for patterning the columns, when using DRIE to form them. A 14- μ m wide frame surrounds each column, protecting it from “footing,” which happens when using DRIE to great depths.

D.1 Backside: Channels, Mask #1

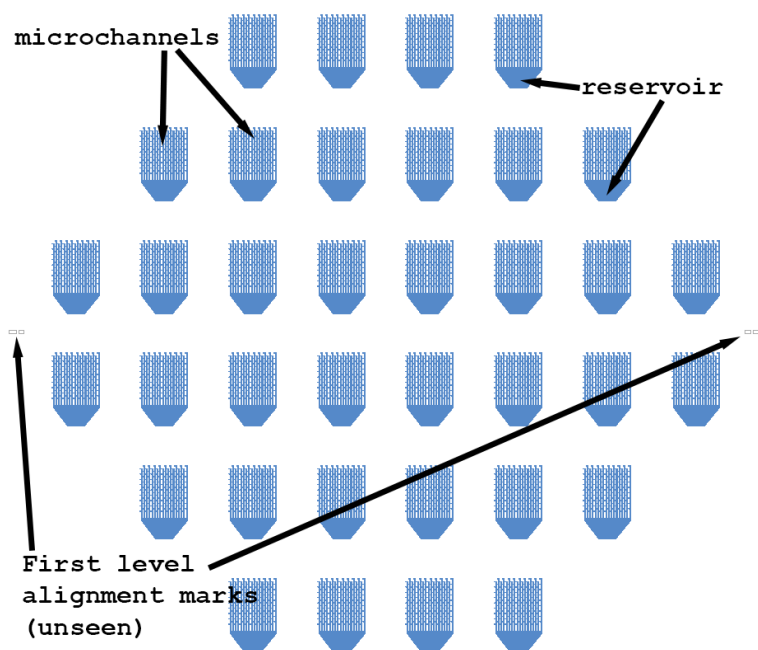


Figure D.1 – The first mask level patterns the microchannels, reservoirs and first level alignment marks.

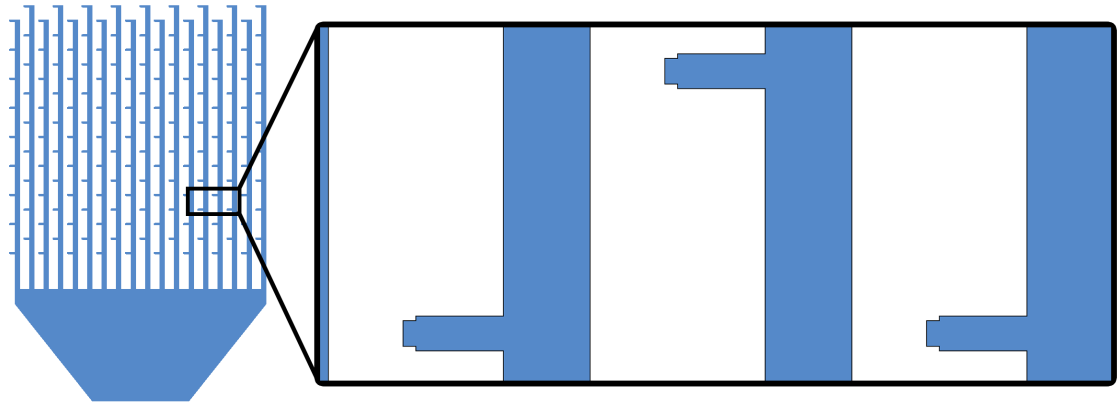


Figure D.2 – Closeup of a single chip, with a further closeup of some individual channels.

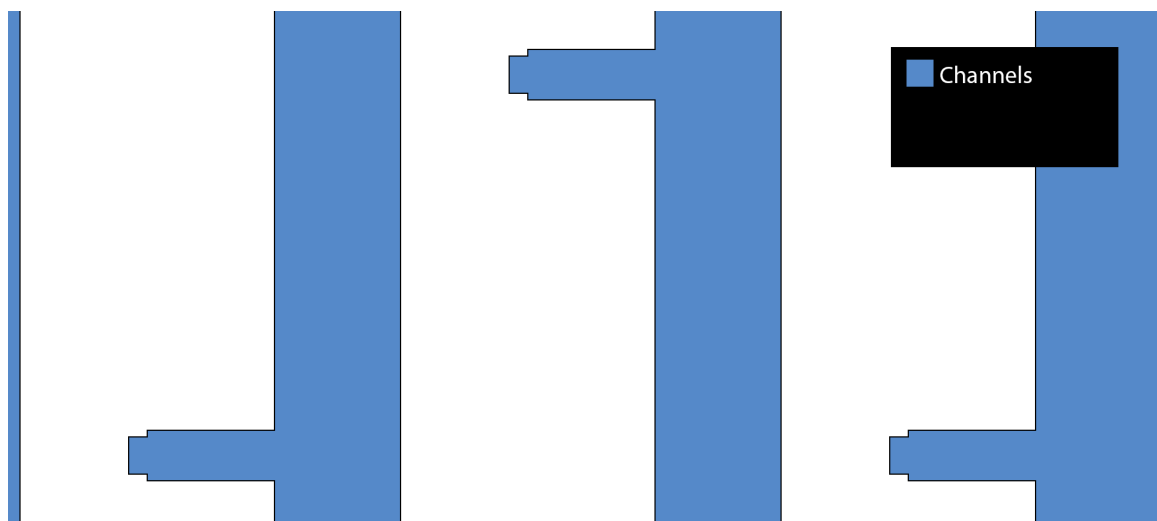


Figure D.3 – closeup of microchannels, from Figure D.2.

D.2 Backside: 30-micron holes, mask #2

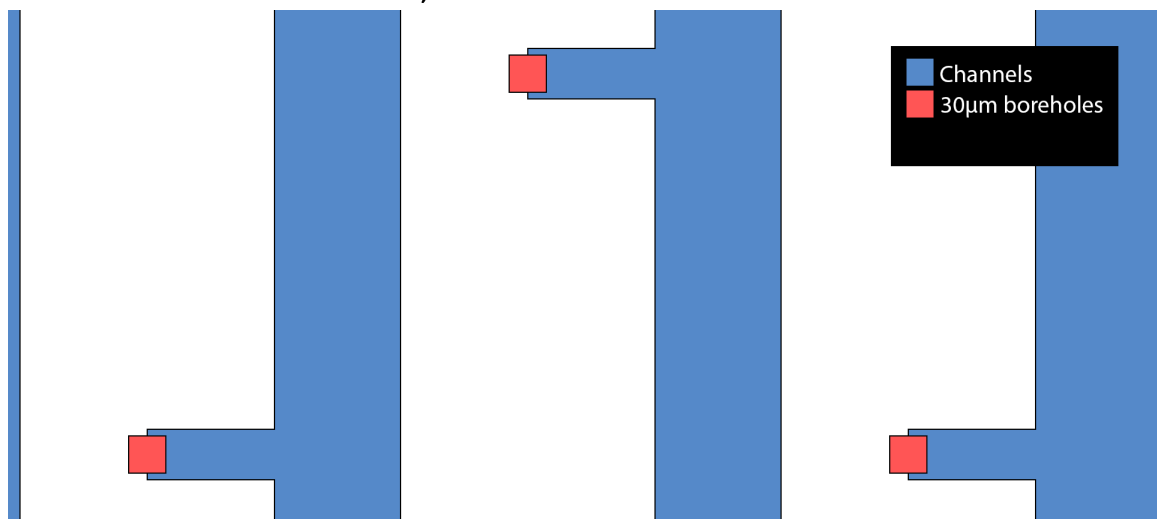


Figure D.4 – The 30-micron boreholes are aligned to the microchannels.

D.3 Frontside – Saw: 10-micron holes, mask #3

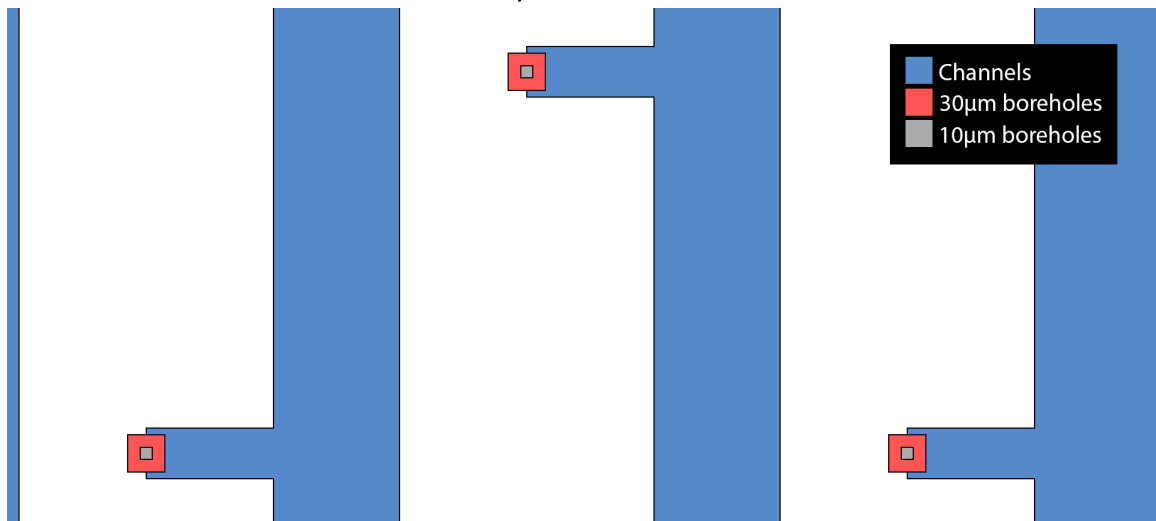


Figure D.5 – 10-micron holes

D.4 Frontside – DRIE: columns, mask #4

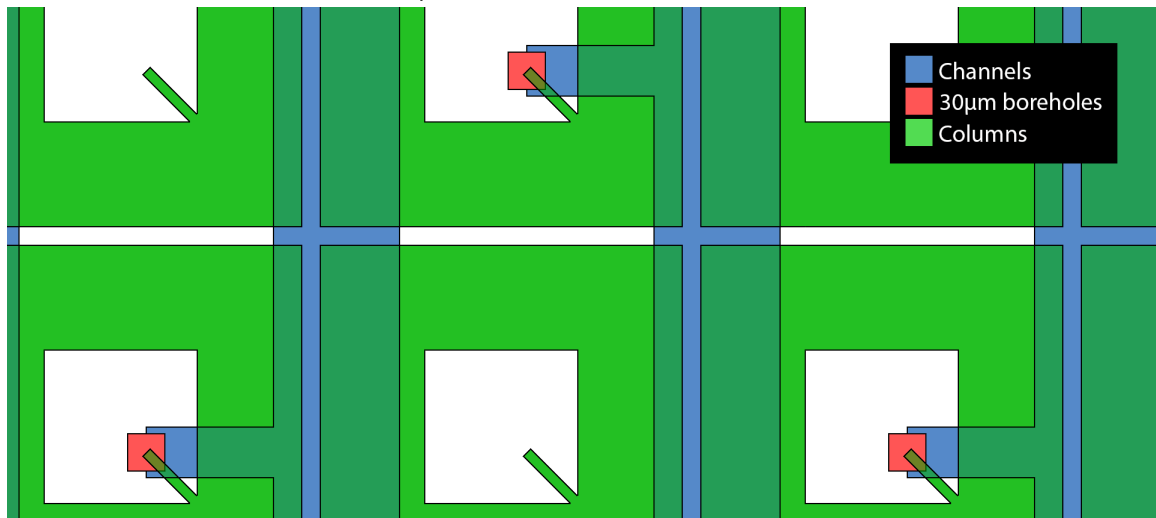


Figure D.6 – DRIE columns

D.5 Alignment marks

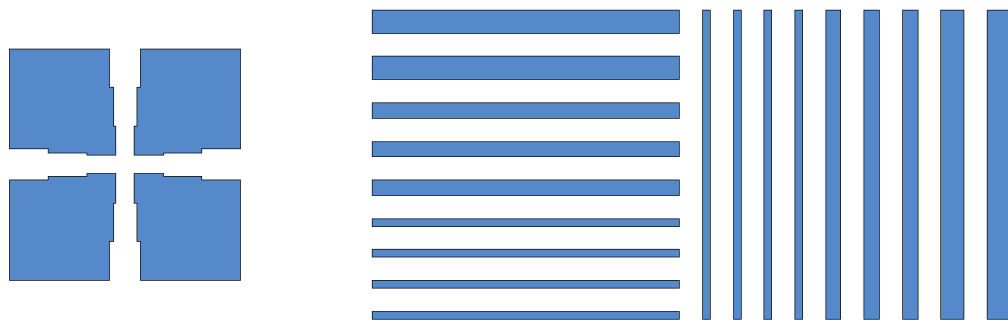


Figure D.7 – Mask #1 alignment marks

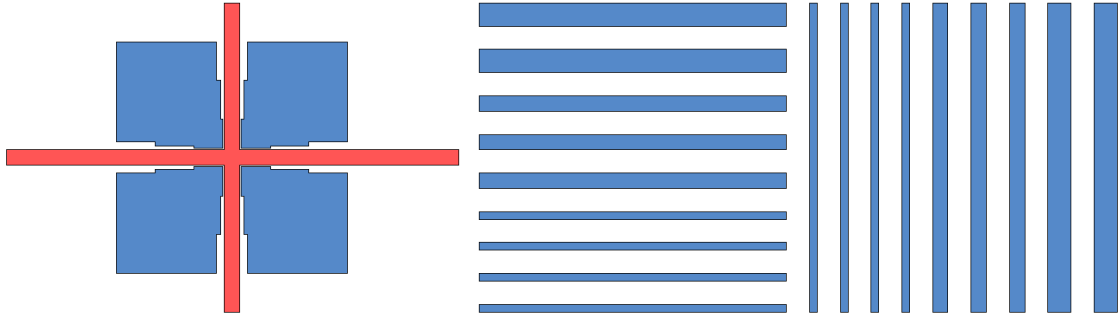


Figure D.8 – Mask #2 aligns to marks left by mask #1

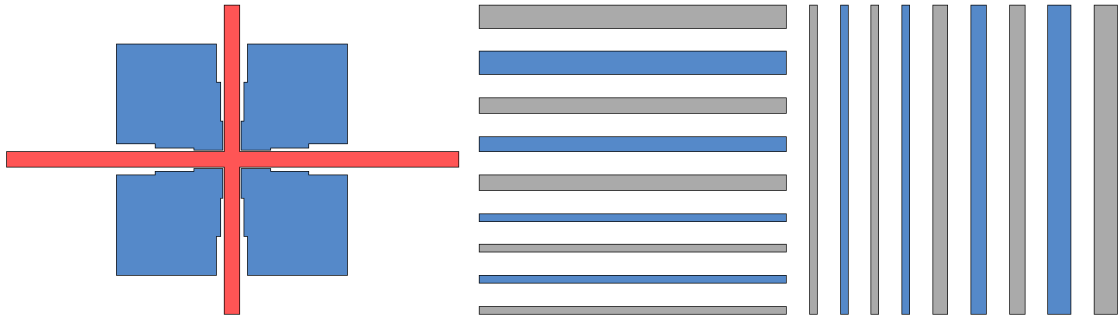


Figure D.9 – Mask #3 (saw only) aligns to marks left by mask #1

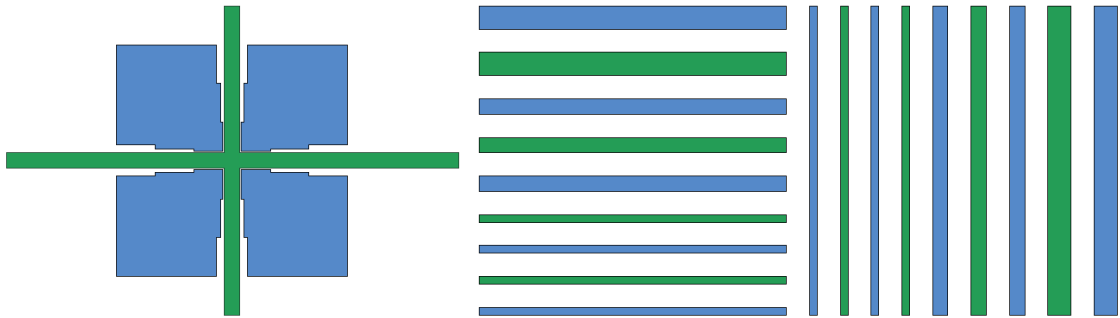


Figure D.10 – Mask #4 (DRIE only) aligns to marks left by mask #1

APPENDIX E – WAFER SPECIFICATIONS

Table E-1 – Dicing saw wafer specifications

Diameter	100.0 ± 0.5 mm
Lot number	FM4714
Type/Dopant	Silicon, P/B
Orientation	<100>
Thickness	550 ± 15 µm
Total thickness variation (TTV)	< 15 µm
Resistivity*	0.01 - 0.2 Ω-cm, 0.01 - 0.02 Ω-cm

* Resistivity range 0.01-0.2 Ω-cm was due to a purchasing order error and was corrected on a future order. However, four-point probe measurements showed that resistivity values from both orders were comparable to each other.

Table E-2 – DRIE-only wafer specifications

Diameter	100.0 ± 0.5 mm
Lot number	Unk.
Type/Dopant	Silicon, P/B
Orientation	<100>
Thickness	650 ± 10 µm
Total thickness variation (TTV)	< 10 µm
Resistivity	0.01 - 0.05 Ω-cm

Table E-3 – Extra-thick test wafer specifications

Diameter	100.0 ± 0.5 mm
Lot number	Unk.
Type/Dopant	Silicon, P/B
Orientation	<100>
Thickness	750 ± [[xx]] µm
Total thickness variation (TTV)	Unk.
Resistivity	0.01 0.02 Ω-cm

APPENDIX F – EQUIPMENT

Table F-1 – Equipment

Equipment Name	Manufacturer	Model
Anodic bond power supply	Stanford Research Systems, Inc.	PS325 / 2500V 25W
Anodic bond temperature controller	OMEGA Engineering	CN76000
Camera – DSLR	Canon	EOS 6D
Camera – Zeiss Axioplan 2	Zeiss	AxioCam HRc
Camera equipment – DSLR microscope adapter system	VariMag	VariMag II V2 3BBL
Contact profilometer	KLA Tencor	Alpha-Step 500
Deep-reactive ion etch (DRIE)	STS	Multiplex
Dicing saw – in house	Kulicke & Soffa	775
Dicing saw – remote	DISCO Hi-Tec	DAD3240
Dicing saw blades – in house	Thermocarbon DiceMaster	2.187-8A-9R7-3 & 2.187-6A-9R7-3
Drill – for glass	Dremel	395 Type 5
Drill bits	Lasco Diamond Products	1.5 & 2.0 mm diamond
Ellipsometer	J. A. Woollam Co., Inc	M-2000V
Four-point probe	Keithley	2400 SourceMeter
HMDS / vacuum hotplate	Solitec Wafer Processing	VBS-200
Hot plate (wet lab)	Corning	PC-420/PC-420D
Mask aligner	Karl Suss	MA6
Optical microscope (cleanroom)	Leitz	020-448.026
Optical microscope 1 (wet lab)	Zeiss	Stemi 2000-C
Optical microscope 1 (wet lab) light source	Chiu Technical Corporation	Lumina FO-150
Optical microscope 2 (wet lab)	Zeiss	Axioplan 2
Optical microscope 2 (wet lab) light source	Zeiss	HAL 100
Optical profilometer	FRT	MicroProf 100
Oven – cleanroom	Fisher Scientific	506G
Oven – wet lab	Quincy Lab, Inc.	10GC
Oxidation furnace	Tylan	Tytan
Photomask pattern generator	GCA	MANN 3600
Plasma-enhanced chemical vapor deposition system (PECVD)	Oxford Instruments	Plasmalab80Plus
Reflectometer	Filmetrics	230-0243
Scanning electron microscope (SEM)	Zeiss	NVision 40
Table spin coater and controller	Bidtec	SP-100

APPENDIX G – STOCK SOLUTIONS

The following information explains the chemicals used in the process. The grade and concentration for all chemicals referenced in this thesis are listed in Table G-1. Relevant dangers and other information are elaborated in sections G.1-G.4.

Table G-1 – Chemical Concentration Table

Chemical	Grade	Concentration	Lookup code
Acetic acid, glacial	ACS Plus	100.0%	A38s-212
Acetone	ACS	≥99.5%	A18-4
Ammonium hydroxide	TraceMetal	20-22%	A512-4
AZ MIF 300 developer	Unspecified	2.38%-wt tetramethylammonium hydroxide in water	GHSBBG70N4
Buffered oxide etchant	Unspecified	6:1 ammonium fluoride : hydrofluoric acid	Not specified
Chromium mask etchant	Unspecified	< 5% perchloric acid < 10% ceric ammonium nitrate > 85% water	CE-5M
HNA etchant	Not applicable	1:8:1 by volume (stock) HF : Nitric : Acetic	Not applicable
Hydrochloric acid (HCl)	ACS Plus	36.5-38.0%	A144S-212
Hydrofluoric acid (HF)	Unspecified	48-51%	AC223335000
Hydrogen peroxide	ACS	30%	H325-500
Isopropyl alcohol (IPA)	ACS Plus	≥99.5%	A416-4
Methanol (MeOH)	ACS	≥99.8%	A412-4
Nitric acid	TraceMetal	68.0-71.0%	A509SK-212
Sulfuric acid	ACS Plus	95.0-98.0%	A300-212

G.1 Chemicals

Hydrofluoric acid

Hydrofluoric acid is a powerful contact poison. There is no antidote for internal HF toxicity. HF has the ability to penetrate tissue, and poisoning can occur readily through the skin or eyes, or when inhaled or swallowed. Symptoms of exposure typically are not immediately evident, which can provide false reassurance causing victims to delay medical treatment. Hydrofluoric acid exposure requires immediate specialized medical attention! Calcium gluconate gel, which binds to the fluoride ion, is used for skin burns. However, HF attacks very rapidly, and tissue will need to be removed, and/or deep injections made to access the area where the HF has reached. Amputation is not uncommon.

G.2 Developers

AZ-MIF-300 (MIF300)

AZ-MIF-300 is a solution of 2.38%-wt high purity tetramethylammonium hydroxide (TMAH) in water. The solution is colorless, or slightly yellow. TMAH has virtually no odor

when pure, but often has a strongly fishy smell when trimethylamine is present as an impurity.

Exposure to TMAH affects nerves and muscles, causing difficulties in breathing, muscular paralysis and death. There is no antidote. The tetramethylammonium ion is structurally related to acetylcholine, and binds and activates the nicotinic acetylcholine receptors. There is evidence that poisoning can occur through skin-contact with concentrated solutions of TMAH.

G.3 Etchants

Buffered Oxide Etch (BOE)

The BOE used for this project is a 6:1 solution of ammonium fluoride and hydrofluoric acid. It is manufactured by Transene. Hydrofluoric acid is a powerful contact poison.

Chromium Mask Etchant CE-5M

From the manufacturer (Transene): Chrome Mask Etchant CE-5M is a ceric ammonium nitrate and perchloric acid etching solution for all types of chrome plates. Etch rate will depend upon substrate chrome density and process conditions. In general, the etch time usually ranges from 15 to 55 seconds at room temperature (25 C). Chrome Mask Etchant CE-5M is suitable for sub-micron photolithography applications.

G.4 Photoresists

Megaposit SPR220-7.0

From the manufacturer: SPR220 i-Line photoresist is a general purpose, multi-wavelength resist designed to cover a wide range of film thicknesses, 1-10 μ m, with a single coat process.

Nominal thickness for my process: 10 μ m

AZ 1512

From the manufacturer: The AZ 1500 series yields an improved adhesion for all common wet etching processes. AZ 1512 has a very high photo active compound concentration, maximizing resist contrast (very high development rate, minimized dark erosion). Resist film thickness varies between 1.0 – 1.8 μ m, depending on spin speed.

Nominal thickness for my process: 1.2 μ m

BIOGRAPHY OF THE AUTHOR

Caleb Berry was born in Farmington, Maine on April 9, 1996. He was raised in Livermore, Maine and graduated from Livermore Falls High School in 2013. He attended the University of Maine and graduated in 2017 with a Bachelor's degree in Chemical Engineering. He then entered the Chemical Engineering graduate program in the spring of 2018. After receiving his degree, Caleb looks forward to a lifelong career in microfabrication. Caleb is a candidate for the Master of Science in Chemical Engineering from the University of Maine in August 2020.